Endogenous Lunar Volatiles

Francis M. McCubbin[1], Jessica J. Barnes[2], Peng Ni[3], Hejiu Hui[4], Rachel L. Klima[5], David Burney[6], James M. D. Day[7], Tomáš Magna[8], Jeremy W. Boyce[1], Romain Tartèse[9], Kathleen E. Vander Kaaden[10], Edgar Steenstra[3], Stephen M. Elardo[11], Ryan A. Zeigler[1], Mahesh Anand[12], Yang Liu[13]

[1]NASA Johnson Space Center, 2101 NASA Parkway, mail code XI, Houston TX 77058, USA
[2]Lunar and Planetary Laboratory, University of Arizona, 1629 E University Blvd, Tucson AZ 85721
[3]Earth and Planets Laboratory, Carnegie Institution of Washington, 5251 Broad Branch Rd. NW Washington DC 20015, USA
[4]State Key Laboratory for Mineral Deposits Research & Lunar and Planetary Science Institute, School of Earth Sciences and Engineering, Nanjing University, Nanjing 210023, China
[5]Planetary Exploration Group, Space Department, Johns Hopkins University Applied Physics Lab, Laurel, Maryland 20723, USA
[6]Department of Civil & Environmental Engineering & Earth Sciences, University of Notre Dame, Notre Dame, Indiana 46556, USA
[7]Geosciences Research Division, Scripps Institution of Oceanography, La Jolla, CA 92093-0244, USA
[8]Czech Geological Survey, Klárov 3, CZ-118 21 Prague 1, Czech Republic
[9]The University of Manchester, Department of Earth and Environmental Sciences, Oxford Road, Manchester M13 9PL, UK
[10]Jacobs, NASA Johnson Space Center, 2101 NASA Parkway, mail code XI3, Houston TX 77058, USA
[11]Department of Geological Sciences, University of Florida, Gainesville, FL 32611, USA
[12]Planetary and Space Sciences, The Open University, Walton Hall, Milton Keynes, MK7 6AA, UK
[13]Jet Propulsion Laboratory, California Institute of Technology, Pasadena, California 91109, USA

francis.m.mccubbin@nasa.gov; jjbarnes@arizona.edu; yang.liu@jpl.nasa.gov

1. INTRODUCTION

The intrinsic properties of the elements and their resulting behavior in natural systems represent the underpinnings of geochemistry as a scientific discipline (Goldschmidt 1937). One of the most valuable intrinsic properties of an element is its volatility. The volatility of an element is most commonly expressed as a 50% condensation temperature, which corresponds to the temperature at which 50% of an element would have condensed from a gas of solar composition at nebular total pressure of 10^{-4} bars (e.g., Lodders 2003). Refractory elements are characterized by high condensation temperatures with the inverse being true for more volatile elements. Although condensation temperatures are widely used to understand elemental depletions in planetary materials, condensation from a nebular gas may not be the most relevant system for understanding volatile loss from planetary bodies or from the protolunar disk. The silicate-dominant compositions of planetary bodies are a mismatch for nebular gas and form at a range of

pressures and oxygen fugacities that are not representative of nebular conditions (e.g., Albarede et al. 2015; Norris and Wood 2017; Ni et al. 2019). Instead, alternative expressions of element volatility have arisen for understanding planetary volatile-element depletion, specifically within the Earth-Moon system, including a volatility scale based on bond energy of an element to a particular ligand (Albarede et al. 2015), a volatility scale based on melt-vapor partitioning of elements at magmatic temperatures as a function of oxygen fugacity (O'Neill and Palme 2008; Norris and Wood 2017; Siebert et al. 2018; Sossi et al. 2019), or a volatility scale based on compositions of degassed lunar glass beads and undegassed olivine-hosted melt inclusions from the same magma source (Ni et al. 2019). All of these volatility scales have broad similarities to the volatility scale based on condensation temperatures with a few exceptions (e.g., Albarede et al. 2015; Norris and Wood 2017; Ni et al. 2019). Nevertheless, we use condensation temperatures in this work to enable direct comparisons with previous work, although we note here that volatility scales are an active area of study at present.

All terrestrial planetary bodies are depleted in volatile elements relative to carbonaceous Ivuna-type (CI) chondrites (volatile elements are defined here as elements with 50% condensation temperatures less than 1300 K). These depletions in volatiles are thought to be linked, at least in part, to the high-temperature formation processes of planetary accretion. Consequently, the inventory of volatile elements in a planetary body records important clues as to the formation history and subsequent thermochemical evolution of that body. The Moon is highly depleted in volatile elements compared with CI chondrites and further, it is volatile-depleted relative to the terrestrial planets (Fig. 1). This volatile depletion is thought to be due to a combination of the cataclysmic circumstances under which the Moon formed (Hartmann and Davis 1975; Lock et al. 2018), a geochemical signature of the protoplanet Theia (thought to be the impactor that collided with the proto-Earth; Canup and Asphaug 2001), and the process of planetary differentiation. The abundances, distributions, and isotopic compositions of volatile elements in and on the Moon have been intensely scrutinized since the publication of the first *New Views of the Moon* volume (referred to hereafter as NVM 1) in 2006. Since that time, tremendous insights have been gained into the roles that volatiles have played in the origin, formation, and subsequent thermochemical evolution of the Moon. In fact, many of the updated models in the present volume regarding lunar formation and evolution have been modified and/or transformed by the new insights gained in the last decade on endogenous lunar volatiles (Canup et al. 2021, this volume; Elardo et al. 2021, this volume; Gaffney et al. 2021, this volume; Joy et al. 2021, this volume; Shearer et al. 2021, this volume). The presence of volatile species not only changes the way scientists view the geological history of the Moon but opens new possibilities for future lunar exploration in the form of resource utilization. Although not the focus of this chapter, volatiles on the Moon will play a key role in long-term space exploration and habitation (Crawford et al. 2021, this volume).

Although the study of lunar volatiles began as soon as the Apollo samples were returned, the primary motivation behind the lunar volatile studies of the last decade stems from the discovery of indigenous hydrogen in lunar samples (Saal et al. 2008; Boyce et al. 2010; McCubbin et al. 2010a; McCubbin et al. 2010b; Hauri et al. 2011), the remote detection of H, OH^-, or H_2O on the lunar surface (Feldman et al. 1998; Clark 2009; Pieters et al. 2009; Sunshine et al. 2009), and the discovery that stable isotopic compositions of moderately volatile and volatile elements are fractionated in lunar samples relative to terrestrial values (Moynier et al. 2006; Herzog et al. 2009; Sharp et al. 2010; Greenwood et al. 2011; Paniello et al. 2012). Prior to these studies, the Moon was commonly referred to as “bone dry”, and was thought to host less than 1 part per billion (ppb) H_2O in its interior (e.g., Taylor et al. 2006a). These studies initiated a complete reassessment

of the abundances of volatiles within the Moon as well as of the isotopic compositions of volatile and moderately volatile elements in lunar samples. This chapter will discuss the status of endogenous lunar volatiles and set the stage for subsequent chapters on various aspects of lunar evolution that consider the effects of endogenous volatiles, which we define as volatiles originating from the interior of the Moon that have played a role in its thermal and magmatic evolution. Volatiles on the surface of the Moon and within the lunar regolith are discussed in a separate chapter in this volume dedicated to the topic of lunar surface volatiles and exogenous lunar volatiles (Hurley et al. 2021, this volume).

We have defined volatile elements in this chapter as elements with 50% condensation temperatures less than 1300 K, which is the approximate condensation temperature at which elements are consistently depleted in Earth relative to CI chondrites (McDonough and Sun 1995). However, much of the effort to constrain the inventory of lunar volatiles in the last decade has been focused on a subset of volatile elements referred to as magmatic volatiles, which include the elements H, C, N, F, S, and Cl. Magmatic volatiles affect a wide range of important physicochemical processes including the thermal stabilities of minerals and melts, the transport and eruption of magma and lava, and the formation of fluid phases in silicate-melt systems. In fact, magmatic volatiles comprise the major constituents of hydrothermal fluid phases that are key to mass transport within the crusts and mantles of planetary bodies. Although the Moon is volatile-depleted, there has been long-standing evidence indicating that magmatic volatiles are present in sufficiently high concentrations to have had a pronounced effect on numerous geologic processes within and on the Moon. Specifically, magmatic volatiles purportedly drove fire-fountain eruptions, which produced the pyroclastic glass beads encountered at each of the Apollo landing sites and at the Luna 20 and 24 landing sites (Sato 1979; Shearer et al. 2006). The volcanic glass beads are coated by thin films that are highly enriched in volatile elements, including Zn, Ga, S, F, and Cl, which have been proposed to have condensed as sublimates on the glass surfaces during fire-fountain eruptions (e.g., Heiken and McKay 1977). Furthermore, highly vesiculated basalts, analogous to those produced during eruption of volatile-bearing terrestrial lavas, were encountered on the Moon and subsequently recovered during several of the Apollo missions. For example, Apollo mare basalt 15556 contains 33 ± 1 % vesicles by volume (Fig. 2). Additionally, the volatile-bearing mineral apatite, which has magmatic volatiles as essential structural constituents, was initially reported in numerous lunar rocks (Griffin et al. 1972).

The recent progress in our understanding of endogenous lunar volatiles also comes largely through the study of lunar samples. In particular, the abundances of the volatile elements F, Cl, S, C and H have been studied extensively in lunar apatite, glass beads and mesostasis glasses, olivine-hosted melt inclusions, and within nominally anhydrous mineral (NAM) phases. In addition to elemental abundances, the H- and Cl-isotopic compositions of apatite, glasses, and NAMs have been determined from a large variety of lunar rock types, and some bulk rock N-, Cl-, and S-isotopic data have also been determined. Finally, there has been substantial progress in evaluating the abundances and isotopic compositions of a number of other volatile to moderately volatile elements in lunar samples, including Li, Cu, K, Ga, B, Ge, Rb, Cs, Pb, Sn, Se, and Zn.

The volatile-depleted nature of the Moon was well documented in previous studies, including NVM 1 (Jolliff 2006) and the Lunar Source Book (Heiken et al. 1991). We do not wish to duplicate either of those efforts, so in this contribution we will summarize the recent results on endogenous lunar volatiles since the publication of NVM 1 over a decade ago. Furthermore, we will use those new results, as well as pre-2006 published data on the abundances of volatile elements in lunar samples, to provide a revised view on the abundances of volatiles in the lunar

interior. Additionally, we seek to provide insights into how those volatiles are distributed between the mantle, crust, and/or other geochemical reservoirs. We will also discuss the isotopic compositions of volatiles within various lunar source regions, providing potential insights into the processes that established those reservoirs. Finally, we will summarize the gaps in our current understanding on the topic of endogenous lunar volatiles as well as identify some of the important remaining questions that need to be addressed through future studies.

2. METHODS AND DATA: ABUNDANCES

Studies of Apollo, Luna, and lunar meteorite samples have yielded tremendous insights into the abundances and distributions of endogenous lunar volatiles. These samples host numerous volatile-bearing phases, with each having their utilities and drawbacks as faithful recorders of volatiles in lunar magmatic systems. Advancement in our understanding of the abundances of endogenous lunar volatiles in the previous decade has been acquired, partly, through the study of magmatic volatiles in apatite, glasses, olivine-hosted melt inclusions, bulk rock samples, and NAM phases. The utilities and drawbacks of each of these materials as recorders of volatile abundances will be discussed.

2.1 Apatite

2.1.1 Apatite as a tool to monitor volatile elements in the Moon. Apatite is a calcium phosphate mineral [$Ca_5(PO_4)_3$(OH, F, Cl)] that has F^-, Cl^-, and OH^- as essential structural constituents (ESC). To date, apatite is the only igneous mineral with OH^- as an ESC that has been identified and analyzed in lunar samples (McCubbin and Jones 2015). Apatite is nearly ubiquitous within lunar samples, occurring in all lunar sample types with the exception of ferroan anorthosites and pyroclastic glass beads (McCubbin et al. 2015b). However, apatite occurs in only trace abundances in most lunar rocks, making up less than 1% of the mode (McCubbin et al. 2015b). The wide-spread occurrence of apatite in lunar samples is an attractive attribute for its use as a monitor of volatiles in lunar systems because a wide array of sample types can be investigated with what is ostensibly the same tool. However, the use of apatite as a recorder of magmatic volatiles is not without complicating factors that have motivated numerous avenues of research, many of which are still ongoing. These complicating factors include: (1) determining appropriate apatite–melt partitioning relationships for F^-, Cl^-, and OH^- in lunar systems to quantify melt volatile abundances, (2) accounting for secondary processes that could have modified pristine volatile or isotopic ratios in melt prior to being recorded in apatite, and (3) accounting for secondary processes that could have modified pristine volatile or isotopic ratios in apatite after crystallization from lunar magmas and/or lavas.

Concerning factor (1), numerous modeling and experimental studies have reported that apatite–melt and apatite–fluid partitioning relationships for F^-, Cl^-, and OH^- are variable, and they appear to vary as a function of pressure, temperature, melt composition, apatite composition, and possibly oxygen fugacity (e.g., Boyce et al. 2014; McCubbin et al. 2015a; Webster and Piccoli 2015; McCubbin and Ustunisik 2018; Riker et al. 2018). Despite reports of large variations in apatite–melt partitioning behavior of F^-, Cl^-, and OH^-, all of these studies have noted that fluoride is preferred in apatite over chloride, and chloride is preferred in apatite over hydroxyl. Importantly, this systematic behavior in anion preference in apatite does not result in constant apatite–melt or apatite–fluid partition coefficients for F^-, Cl^-, and OH^- because the combined

abundances of F^-, Cl^-, and OH^- in apatite are fixed by stoichiometry, and the combined abundances of F^-, Cl^-, and OH^- in melt or fluid at apatite saturation are constrained only by their respective solubilities in silicate melt and the vapor composition with which they are in equilibrium if the melt is fluid-saturated (Boyce et al. 2014; McCubbin et al. 2015a). These same studies have described the partitioning of volatiles between apatite and melt as exchange equilibria involving each of the three anion pairs in apatite (i.e., F–OH, Cl–OH, F–Cl), similar to the treatment of Fe–Mg partitioning between olivine and silicate melt (e.g., Roeder and Emslie 1970). This formalism largely cancels out the effects of large variations in melt F^-, Cl^-, and OH^- abundances on apatite–melt partition coefficients, which allows for a clearer evaluation of the partitioning behavior across disparate systems. Although this new approach to apatite–melt partitioning has yielded promising results, substantial efforts remain to be invested before apatite will become a reliable quantitative tool for extracting melt volatile abundances over a wide range of pressures, temperatures, melt compositions, apatite compositions, and oxygen fugacities. Although none of these studies have specifically investigated chemical systems directly relevant to the Moon, McCubbin et al. (2015a) investigated an Fe-rich basaltic melt composition with apatite compositions, oxygen fugacity, and temperatures relevant to apatite crystallization in lunar systems. Consequently, we use the apatite–melt exchange coefficients reported by McCubbin et al. (2015a) in this review to estimate lunar magmatic volatile abundances from apatite, where appropriate.

Regarding factors (2) and (3), apatite forms late in the crystallization sequence of lunar magmas, and hence it provides a record of the volatile abundances and isotopic compositions of late-stage lunar magmas. Although the aim of many lunar volatile studies is to characterize the volatile abundances and isotopic composition of the magmatic source region from which a magma is derived, numerous secondary processes (e.g., degassing, assimilation, metasomatism, and fractional crystallization) could have perturbed initial volatile and isotopic ratios in the late-stage magmas before the onset of apatite crystallization. Additionally, some of these same secondary processes could have affected apatite after crystallization from an igneous system. In either case, the apatite compositions would not be representative of the magmatic source from which their parental liquids were derived. These complications can be mitigated, in part, by conducting detailed textural analysis of apatite to place their chemical compositions into petrographic context. In particular, many samples exhibit intrasample variation in apatite volatile compositions that can be manifested as intracrystal zoning or intercrystal variations. Textural characterizations of apatite in such samples can be used to piece together relative timing of crystallization between crystals or crystal zones in the case of zoned apatite crystals. This timing is important because each secondary process will impart distinct evolutionary paths for F, Cl, and H records in apatite (e.g., Boyce et al. 2014; McCubbin et al. 2016). In fact, substantial efforts have been put forth to better understand and characterize how volatile abundances and isotopic compositions in apatite evolve as a function of specific secondary processes, and we are now able to use the intrasample variations in apatite volatile chemistry from an individual sample to deduce what secondary processes, if any, has affected that sample (e.g., Boyce et al. 2014; Tartèse et al. 2014b; McCubbin et al. 2016; Treiman et al. 2016). When applied properly, these methods can be used to select the most appropriate samples for estimating volatile abundances in magmatic source regions using apatite (e.g., McCubbin et al. 2015b).

2.1.2 Occurrences of apatite in lunar samples and their volatile compositions. The abundances of volatiles (F^-, Cl^-, OH^-, and S^{2-}) in lunar apatite have been reported from both

secondary ion mass spectrometry (SIMS) and electron probe microanalysis (EPMA) of numerous lunar rock types. Apatite has been reported and analyzed in all major lunar rock types exclusive of the ferroan anorthosites (McCubbin et al. 2015b). Apatite ranges in crystal habit from anhedral to euhedral in lunar samples (McCubbin et al. 2015b), and crystal size (longest reported dimension) ranges from submicron to rare examples of millimeter-sized crystals in Apollo 17 granulite 79215 (Treiman et al. 2014). The apatite grains in highlands plutonic rocks are typically larger than those in mare basalts, whose typical apatite crystal sizes are less than 20 micrometers in the long axis (McCubbin et al. 2011). In general, lunar apatite is fluorine-dominant (i.e., fluorapatite); however, there are rare examples of chlorine-dominant (i.e., chlorapatite) and hydroxyl-dominant (i.e., hydroxylapatite) apatite in some samples (Fig. 3; Table S1). Comparisons of apatite volatile compositions among lunar rock types reveal important distinctions in volatile chemistry that have been interpreted as indicating a heterogeneous distribution of volatiles in the lunar interior (McCubbin et al. 2011; Robinson and Taylor 2014). Volatile compositions of apatite in each lunar rock type analyzed to date are provided in Table S1.

Low-Ti mare basalts host apatite that span much of the fluor-hydroxyl apatite join, with less variation in the chlorapatite component (Fig. 3; Table S1). High-Ti mare basalts contain apatite with similar F^- and Cl^- contents as the low-Ti basalts, but they generally have less OH^- (Fig. 3; Table S1). There are much less data available on high-Al mare basalts, VHK mare basalts, and VLT mare basalts in comparison to low-Ti and high-Ti mare basalts, but apatite in these samples are generally F-rich (Fig. 3; Table S1). KREEP basalts have apatite with a large range in volatile abundances compared to typical mare basalts (Fig. 3; Table S1). Apatite within magnesian-suite rocks are typically more Cl-rich than those in mare basalts, and their range encompasses much lower OH^- abundances (Fig. 3; Table S1). Apatite within alkali-suite rocks are also more Cl-rich than those in mare basalts and have much lower OH^- abundances than apatite in mare basalts (Fig. 3; Table S1). Apatite grains within impact-melt rocks, granulites, and the matrices of regolith breccias have also been reported and analyzed, but we do not use those data to determine volatile abundance estimates for the bulk silicate Moon. However, apatite from these samples can be used to understand the range of apatite compositions in lunar samples, and they can help to constrain effects of secondary processes, particularly those associated with impacts.

2.2 Nominally anhydrous minerals (NAMs)

2.2.1 NAMs as a tool to monitor volatiles in the Moon. Nominally anhydrous minerals (NAMs), including olivine, feldspar, and pyroxene, do not incorporate hydrogen as an essential structural constituent. Furthermore, these minerals are also nominally devoid of many other volatile elements. However, nominally anhydrous minerals can store minor to trace abundances of H and other volatile elements in their respective crystal lattices through a number of coupled crystal-chemical substitutions and/or lattice-defect accommodations (e.g., Bell and Rossman 1992; Mosenfelder et al. 2006). Studies of NAMs have resulted in substantial upward revisions and modifications to estimates of the bulk H_2O content of Earth's interior (Peslier et al. 2017 and references therein). All of the efforts to understand NAMs in terrestrial systems have offered the opportunity to use them to help assess volatile inventories in other planetary magmatic systems (Peslier 2010 and references therein). With the exception of apatite, all of the igneous minerals within lunar rocks reported to date are nominally anhydrous. Consequently, NAMs could be a

very useful tool for assessing the volatile abundances of lunar magmas. Moreover, the ubiquitous nature of NAMs in lunar samples would allow for a large number of lunar sample types to be assessed. Similarly to apatite, the use of NAMs as a recorder of volatiles is not without some complicating factors, including (1) accounting for secondary processes that could have modified pristine volatile abundances or isotopic ratios in a melt prior to being recorded in NAMs; (2) consideration of secondary processes that could have modified pristine volatile abundances or isotopic ratios in NAMs after their formation; and (3) determining appropriate mineral–melt partitioning relationships for trace and minor volatile elements in lunar systems.

Concerning factors (1) and (2), NAMs form throughout the crystallization sequence of lunar magmas, and hence there is a potential for providing a record of the melt volatile abundances and isotopic compositions of magmas throughout their crystallization history. However, secondary processes during and/or after magma crystallization could have disturbed H distributions within NAMs. This complication could be mitigated, at least partly, through detailed petrographic analyses and combined trace-element studies. If the samples were altered without loss of volatiles during secondary processes (e.g., partial melting, metasomatism, or assimilation), H_2O could have coevolved with other trace elements (Peslier et al. 2012; Hui et al. 2015). Therefore, it may be possible to recalculate H_2O contents in melt from which NAMs crystallized utilizing the correlations between H_2O and other trace elements with different partitioning behavior. If degassing occurred, however, the evolution of H_2O and other trace elements in NAMs could be decoupled. Diffusion of H in NAMs is rapid and on timescales consistent with ascent and crystallization of magmas (e.g., Peslier 2010; Johnson and Rossman 2013), and hence the diffusive loss of H or H_2O could reset H distributions within NAMs. Olivine is particularly susceptible to resetting of its H abundances, but pyroxene and plagioclase are potentially more reliable than olivine at high temperatures (Peslier 2010; Johnson and Rossman 2013). If H_2O abundances in NAMs are in equilibrium among different phases in a given sample, it signals that these phases could have preserved their H_2O contents before the onset of degassing (Peslier et al. 2012; Warren and Hauri 2014). While diffusive loss of H skews initial volatile content calculations, the resulting diffusion profiles preserved in NAMs may be used to piece together the volatile history of a sample.

Regarding factor (3) (i.e., determination of appropriate mineral–melt partition coefficients), substantial efforts have been put forth to quantify the storage capacities of H in nominally anhydrous minerals as well as establish the mineral–melt partitioning relationships for H and other volatiles under terrestrial conditions (e.g., Hauri et al. 2006; Tenner et al. 2009; O'Leary et al. 2010). These studies have reported that mineral–melt exchange equilibria for each mineral change as a function of pressure, temperature, oxygen fugacity, melt composition, and various crystallographic constraints. At present, there is a paucity of mineral–melt partitioning data for NAMs pertaining to lunar systems and/or conducted under lunar-relevant conditions. In particular, only a few experiments have been run at lunar-appropriate oxygen fugacity or under mineral–melt compositions that are directly relevant to the Moon. Partition coefficients for H_2O between plagioclase and melt (up to 0.046) have been recently determined under lunar conditions (Lin et al. 2019), which are generally higher than those (0.002 to 0.006) determined previously under terrestrial conditions (Johnson 2006; Hamada et al. 2013). This result demonstrates the need for additional experimental work before NAMs can be established as a reliable tool to quantify magmatic volatile abundances in lunar systems.

2.2.2 Volatile abundances of NAMs in lunar samples. Lunar sample studies to understand the volatile budget of the Moon from NAMs have focused almost exclusively on H abundances (reported here as H_2O abundances) and H-isotopic compositions of feldspar (Hui et al. 2013; Hui et al. 2017; Mills et al. 2017; Simon et al. 2020), although H_2O abundances in pyroxenes and an "SiO_2 phases" have also been reported (Mills et al. 2017; Simon et al. 2020). The abundances of H_2O in NAMs from lunar samples have been quantified by Fourier Transform Infrared Spectroscopy (FTIR) (Hui et al. 2013) and SIMS (Hui et al. 2017; Mills et al. 2017). Although NAMs occur in all lunar samples, studies of volatiles in lunar NAMs are limited to crustal samples, all of which may have experienced complicated and poorly constrained geologic histories (McCallum and Obrien 1996; Borg et al. 2015; Shearer et al. 2015; Borg et al. 2017). Consequently, the interpretations of H_2O abundances in the lunar interior cannot be well constrained using only NAMs.

Plagioclase has been analyzed for H_2O in ferroan anorthosites 60015,787 and 15415,238. Plagioclase in ferroan anorthosite 60015,787 is reported to contain 3.4 ± 1.7 ppm H_2O by micro-FTIR (Hui et al. 2013; Hui et al. 2017) and 5 ± 1 ppm H_2O by SIMS (Hui et al. 2017). The values determined by micro-FTIR differ from those originally reported by Hui et al. (2013) because molecular absorption coefficients for anorthitic plagioclase, which are used to convert OH^- absorbance from polarized micro-FTIR spectra into H_2O abundance, have been updated (i.e., Mosenfelder et al. 2015) since the initial reports of H_2O in lunar plagioclase (Hui et al. 2013). The SIMS and updated micro-FTIR abundances of H_2O in ferroan anorthosite 60015 are in mutual agreement within the reported analytical uncertainties. Only the lower bound of H_2O contents in plagioclase from ferroan anorthosite 15415,238 could be determined based on polarized infrared spectra because only two orthogonal directions were measured (Hui et al. 2013). However, SIMS analysis of ferroan anorthosite 15415,238 indicates 4 ± 1 ppm H_2O in plagioclase.

Plagioclase from the magnesian-suite troctolite 76535 has been analyzed for H_2O. Similar to 15415,238, only the lower bound of H_2O contents could be determined based on polarized infrared spectra because only two orthogonal directions were measured (Hui et al. 2013). However, SIMS analysis of plagioclase in 76535 indicates an H_2O abundance of 5 ± 1 ppm (Hui et al. 2017).

Plagioclase, alkali feldspar and "SiO_2 phases" within an alkali-suite clasts in brecciated samples 15405,255, 14321,1062, and 12013,141 were analyzed for H_2O using NanoSIMS (Mills et al. 2017; Simon et al. 2020). Plagioclase in these samples contain between 2.4 and 8.1 ppm H_2O (Simon et al. 2020), alkali feldspar between 1.5 and 14.7 ppm H_2O (Simon et al. 2020), and SiO_2 2.4 ± 0.3 ppm H_2O (Mills et al. 2017). Feldspathic glass in 15405,78 was reported to contain 21.6 ± 1.3 ppm H_2O (Mills et al. 2017). Simon et al. (2020) also measured between 3.0 and 4.0 ppm H_2O in clinopyroxene in 15405,255 and between 5.5 and 6.1 ppm H_2O in orthopyroxene in 14303,363. In addition, Simon et al. (2020) reported trace amounts of F, S, Cl and C in feldspars, SiO_2, and pyroxene.

2.3 Mineral-hosted melt inclusions

2.3.1 Mineral-hosted melt inclusions as a tool to monitor volatiles in the Moon. Mineral-hosted melt inclusions are pockets of silicate melt that are trapped within a mineral as it crystallizes (Roedder 1979). Once trapped, these melt pockets are largely isolated from the parent magma and protected by the mineral host, hence they may capture a snapshot of the melt composition, including volatile abundances, at the time of crystallization of the mineral host.

Consequently, melt inclusions in volcanic rocks represent a powerful petrologic tool with which to reconstruct volatile abundances and the volatile history of a magma (e.g., Anderson 1974; Wallace 2005). The use of melt inclusions is well developed for volcanic rocks, but less so for intrusive rocks (Webster 2006).

In addition to terrestrial systems, melt inclusions have been used to estimate volatile abundances and volatile element isotopic compositions of parental melts in extraterrestrial systems, including the Moon (Hauri et al. 2011; Saal et al. 2013; Chen et al. 2015; Wetzel et al. 2015; Ni et al. 2017; Singer et al. 2017; Ni et al. 2019; McCubbin and Barnes 2020). Although melt inclusions occur in many minerals, it is well recognized that mineral hosts with good mechanical strength and free of cleavage (e.g., olivine, quartz, ite) can best protect and isolate melt pockets. In particular, olivine-hosted melt inclusions are useful to infer terrestrial mantle volatile abundances because olivine is usually the liquidus phase of basaltic magma at low pressure, making it possible to capture melt with primary compositions. Although melt inclusions have been reported in multiple mineral phases in lunar rocks (e.g. olivine, pyroxene, ilmenite), volatile data for lunar melt inclusions reported in the literature are exclusively for olivine-hosted melt inclusions. Similar to apatite and NAMs, there are several complications in the interpretation of melt inclusion data: (1) melt inclusions commonly undergo chemical reactions with the host mineral after entrapment; (2) many melt inclusions in lunar samples are partially or completely crystallized; and (3) several processes can cause the initial melt compositions of melt inclusions to differ from those of the bulk melt at the time of entrapment. For olivine-hosted melt inclusions, however, mature mitigation methods are available for most of the complications, and we address each of these caveats below.

The chemical evolution of melt inclusions can differ substantially from those of the greater magmatic system because the composition of the melt inclusion can be affected by the composition of the hosting phase (e.g., Danyushevsky et al. 2002). The interactions between the melt inclusion and its host include diffusive exchange between the two phases (e.g., Danyushevsky et al. 2000; Gaetani and Watson 2000) or crystallization of the host mineral as an overgrowth on the walls of the melt inclusion due to the low nucleation energy at the phase boundary (e.g., Danyushevsky et al. 2002). In olivine, these processes involve Fe–Mg exchange, which results in Fe-loss from the melt to the olivine and inhibits the expected Fe-enrichment of crystallizing ferromagnesian phases with dropping temperature (e.g., Gaetani and Watson 2002). When using volatile abundances in melt inclusions to estimate volatile abundances in melt at the time of entrapment, it is important to estimate the amount of host crystallization on the walls of the inclusion that occurred, otherwise volatile abundances will be overestimated. For olivine-hosted melt inclusions, well-established methods are available to correct for post-entrapment crystallization (PEC) by iteratively adding equilibrium olivine back into the melt inclusion until the melt inclusion is in Fe–Mg exchange equilibrium with the olivine host. The increase of volatile concentrations caused by PEC can therefore be corrected based on the amount of olivine added (e.g., Hauri et al. 2011). The complication of post-entrapment crystallization can also be mitigated when ratios of volatile elements over refractory trace elements of similar incompatibility are used. These ratios have been used to estimate volatile abundances in magmatic source regions on Earth, Moon, and Mars (e.g., Saal et al. 2002; Chen et al. 2015; Filiberto et al. 2016). Specifically, the H_2O/Ce, Cl/K, F/P, CO_2/Nb, and S/Dy ratios are used to determine source region abundances of volatiles in terrestrial systems, as each element in these ratios has a similar incompatibility during mantle melting (Saal et al. 2002), and F/Nd and Cl/Ba have proven useful for lunar systems (Chen et al. 2015).

Melt inclusions that cool rapidly undergo minimal crystallization that is typically limited to the walls of the mineral host; however, melt inclusions in rocks from slowly-cooled volcanic settings or in plutonic settings tend to be partially or completely crystallized. If some melt of measurable size (e.g., >10 × 10 μm in size) remains in these inclusions, the concentrations of volatiles can still be measured and then used to infer their abundances at the time of entrapment based on appropriate volatile/refractory element ratios (e.g., H_2O/Ce or F/Nd). As measured by Chen et al. (2015) and Ni et al. (2019), H_2O/Ce ratios in partially crystalline melt inclusions from lunar ilmenite basalt 10020 remained roughly constant after ~70% crystallization, supporting the use of these ratios after correction for post-entrapment crystallization. Theoretically, if the modal abundance of residual melt relative to the initially entrapped volume can be accurately determined (including the amount of host crystallization on the melt inclusion walls), the volatile abundances measured in the remaining melt can be corrected for the amount of crystallization. However, accurate determination of modal abundance is not straightforward and requires three-dimensional analysis of melt inclusions given the variation in modal estimates from two-dimensional analyses. When the melt inclusions are highly crystalline, homogenization experiments are usually necessary to form homogeneous glassy phases for reliable micro-beam analysis (e.g., Danyushevsky et al. 2000; Gaetani and Watson 2000). This method is applicable to partially crystalline melt inclusions as well. Great care must be exercised during the re-homogenization process to minimize loss of H, such as rapid heating and cooling rates without causing host-mineral breach or heating under appropriate oxygen fugacity without significantly changing the oxidation state of Fe. Even with these mitigation strategies, the loss of H from cracks in the host mineral cannot be avoided (e.g., Chen et al., 2015). There are also micro-beam methods, such as NanoSIMS or the use of scanning complimentary metal-oxide-semiconductor- (CMOS) type activated pixel sensors (SCAPS) with ion microprobes, that have been used to measure crystalline melt inclusions in lunar samples (e.g., Hauri et al. 2011; Singer et al. 2017).

Although melt inclusions are physically isolated from the melt interstitial to the mineral host, they are not closed systems with respect to H. Diffusive exchange between the melt-inclusion melt and the melt interstitial to the mineral host can occur through the mineral host for elements that diffuse rapidly, and H is particularly vulnerable. Numerous studies have attempted to quantify the diffusion rates for H in olivine hosts, and all of these studies indicate that H diffusion is rapid (e.g., Kohlstedt and Mackwell 1998; Portnyagin et al. 2008; Chen et al. 2011; Gaetani et al. 2012). Consequently, knowing the thermal histories (inclusive of eruptive style) of rocks containing olivine-hosted melt inclusions is critical to determining whether the abundances and isotopic composition of H_2O in the melt inclusions can be related to parental magmas or their source. Other volatile elements, including F, Cl, and S are less susceptible to diffusive exchange through olivine hosts (Bucholz et al. 2013; Le Voyer et al. 2014; Ni et al. 2017), although S can exsolve to the vapor phase on the time scale of approximately 24 hours (Bucholz et al. 2013). With the exception of Ni et al. (2017), much of the work on H diffusion in olivine has not been conducted under low oxygen fugacity relevant to lunar systems. Oxygen fugacity may play an important role in H exchange through mineral hosts because the abundance of structural defects in olivine changes as a function of oxygen fugacity (Dohmen et al. 2007). Fewer structural defects in the surrounding olivine at lower oxygen fugacities would result in lower diffusivities of H. In contrast, H_2:H_2O fugacity ratios increase with decreasing oxygen fugacity (e.g., Hirschmann et al. 2012), which could result in faster diffusivities of H through a mineral host at lower oxygen fugacity. Finally, in the future, in-depth studies of other mineral hosts, analogous to the extensive

work done on olivine, will help evaluate the reliability of those hosts for retaining the abundances of volatiles under lunar conditions.

At the interface between a growing mineral and the melt from which it crystallizes, there exists a boundary layer that is depleted in melt components that comprise the mineral and enriched in melt components that are incompatible in the mineral (e.g., Harrison and Watson 1984). In cases where the mineral growth rate outpaces the rates of diffusive re-equilibration within the surrounding melt, the growth of the mineral phase will become limited by diffusion of an equilibrium-determining component (e.g. MgO for the growth of olivine; Chen and Zhang 2008). The rate of diffusive re-equilibration adjacent to the growing mineral phase has the capability of deviating the bulk composition of this boundary layer melt from the composition of the bulk magma (Harrison and Watson 1984; Bacon 1989; Baker 2008), particularly for elements that diffuse significantly slower than the equilibrium-determining component of the growing mineral phase (Zhang 2008). Although the diffusivities of volatile elements in basaltic melts could vary significantly as a function of H_2O concentration and oxygen fugacity, available data in the literature show that H_2O usually diffuses much faster than Mg (Zhang and Ni 2010; Zhang et al. 2010), while diffusivities of F, Cl and S are only marginally slower than that of Mg in anhydrous basaltic melts (Freda et al. 2005; Alletti et al. 2007; Zhang and Ni 2010; Zhang et al. 2010). Rare earth elements (REE) and P, on the other hand, diffuse at a much slower rate relative to Mg (Watson 1994; Baker 2008; Zhang et al. 2010), resulting in an enhanced probability of their enrichment in the silicate boundary layers. There are two methods by which boundary layer enrichment of volatiles in melt inclusions can be assessed, including utilization of Cl/P_2O_5 ratios and by examining the relationship between melt inclusion size and volatile concentrations (Metrich and Wallace 2008). If the melt inclusions are affected by boundary layer enrichment, the same effect is expected to be more significant for smaller melt inclusions compared to larger inclusions in the same sample. Despite the theoretical prediction of possible enrichment of slowly diffusing elements in the melt inclusions during rapid growth, such an effect is rarely observed in terrestrial melt inclusion studies (Metrich and Wallace 2008). As the most well studied lunar sample with melt inclusions, the orange pyroclastic glass 74220 also exhibits no correlation between the melt inclusion size and their F, Cl, S, REE, and P concentrations (Chen et al. 2015; Ni et al. 2017), mitigating such a concern in lunar melt inclusion studies.

2.3.2 Volatile abundances of olivine-hosted melt inclusions in lunar samples. The abundances of volatiles in olivine-hosted melt inclusions from lunar samples have been instrumental in constraining the abundances and distributions of volatiles in the lunar interior. Studies of volatiles in lunar melt inclusions have focused mainly on H, C, F, S, and Cl abundances and H-isotopic compositions (Hauri et al. 2011; Saal et al. 2013; Chen et al. 2015; Wetzel et al. 2015; Singer et al. 2017; Ni et al. 2019); although Cl isotopic data has been reported (Stephant et al. 2019), and abundances of a number of other moderately volatile elements have also been reported (i.e., Li, Cu, K, Ga, B, Ge, Rb, Cs, Pb, and Zn; Hauri et al. 2011; Chen et al. 2015; Hauri et al. 2015; Ni et al. 2019). The abundances of volatile elements and their isotopic ratios in these studies have been determined by SIMS, EPMA, laser-ablation inductively-coupled plasma mass spectrometry (LA-ICP-MS), and multi-collector inductively-coupled plasma mass spectrometry (MC-ICP-MS). Melt inclusions in lunar samples have been reported in mare basalts, KREEP basalts, pyroclastic glass beads, and within plutonic highlands rocks (Roedder and Weiblen 1970; Shearer et al. 2001; Hauri et al. 2011; Elardo et al. 2012; Tartèse et al. 2014b; Chen et al. 2015; Singer et al. 2017). However, studies of volatiles in lunar melt inclusions have been limited to

olivine grains in the orange pyroclastic glass 74220 and olivine hosts in several mare basalt samples (10020, 12008, 12018, 12035, 12040, 15016, 15647, and 74235). Among the lunar samples studied, glassy, or partially glassy melt inclusions were only identified in 74220, 10020, and 74235 (Ni et al. 2019). Homogenized melt inclusion data were reported for 10020, 12008, 12040, 15016, 15647, 74220, and 74235 (Chen et al. 2015; Ni et al. 2017; Ni et al. 2019). For samples 12018 and 12035, only crystalline melt inclusion data are available (Singer et al. 2017). The volatile abundance data from crystalline melt inclusions will not be used to directly estimate parental melt volatile abundances because the modal abundances of melt have not been determined in those inclusions. However, ratios of volatile abundances with other incompatible elements will be used from crystalline melt inclusions where appropriate to estimate volatile abundances in magmatic source regions. A summary of volatile element abundances determined from lunar melt inclusions is provided in Table S2.

2.4 Glass beads, interstitial glass, and mesostasis glasses

2.4.1 Volcanic glasses as a tool to monitor volatiles in the Moon. Volcanic glass is the product of rapid cooling of a magma or lava and represents a snapshot of the composition of a melt at the time of quench. Given that the formation of volcanic glass is dependent on the nature of cooling of a silicate melt, volcanic glass can form at any stage of petrologic evolution from a primary melt composition to a late-stage residual melt composition. Volcanic glass provides a direct representation of a silicate melt composition; hence it is an important geochemical tool in petrogenetic studies. Volcanic glass has also been used to study the abundances of volatiles in silicate melts from terrestrial and extra-terrestrial systems (e.g., Ross and Smith 1955; Saal et al. 2008; Sarafian et al. 2017). The application of glasses to study magmatic volatiles in terrestrial volcanic systems was facilitated by the development of FTIR methods to quantify the most abundant volatiles (H_2O and CO_2) in terrestrial silicate glasses (e.g., Stolper 1982; Dixon et al. 1991), and more recently SIMS has also been developed to quantify volatile abundances in glasses (e.g., Hauri et al. 2002).

In lunar samples, volcanic glasses are best represented by the pyroclastic glass beads and interstitial glass in vitrophyric basalts, both of which are basaltic in composition and were formed by sufficiently rapid cooling (e.g., Delano 1986). In addition, highly differentiated glass can be found in the mesostasis of many basalts. Mesostasis is a term used for late-stage residues in basaltic rocks formed after prolonged cooling and fractionation of the parent basaltic magma (Kushiro et al. 1970). Glasses in mesostasis regions of lunar samples are typically enriched in Si and K, and they are commonly comingled with late-stage accessory phases such as phosphates. Similar to other methods, there are substantial limitations to the applicability of volcanic glass to studying volatiles in lunar systems: (1) un-confined silicate melt is highly susceptible to open-system processes such as degassing or assimilation; (2) volcanic glass can only record the terminal stage of these processes at the time of quench. For example, although lunar pyroclastic glass beads are sourced from depths of >250 km and erupted rapidly (e.g., Elkins-Tanton et al. 2003; Krawczynski and Grove 2012; Vander Kaaden et al. 2015), they experienced volatile loss prior to quench (e.g., Saal et al. 2008). Glass-bearing basalts represent rapidly cooled lava flows on the lunar surface and may have assimilated surface materials such as older flows or regolith. Because glass can only record the melt composition at the time of quench, the use of mesostasis glass in deconvolving H_2O abundances in the lunar interior faces additional issues. There are methods to mitigate some of these concerns. For lunar volcanic glasses, concentration profiles and ratios of

volatiles (H_2O/Cl, H_2O/F), H_2O and D/H values, and volatile/refractory element ratios can be used to assess any secondary processes that have occurred, similar to melt inclusions (Saal et al. 2008; Saal et al. 2013). Moreover, incompatible refractory trace elements in pyroclastic glass can be used in conjunction with melt inclusion data in minerals from the same magma to estimate the abundance of boundary-layer melt that was incorporated in a particular melt inclusion. Furthermore, the abundances of incompatible refractory trace elements in pyroclastic glasses can be used to constrain the trace element composition of the magmatic source region from which the melt was derived, which will also aid in quantifying volatile abundances in that magmatic source region from melt inclusion data in the same sample (e.g., Chen et al. 2015).

2.4.2 Volatile abundances of glass beads and mesostasis glasses in lunar samples. Volatile abundances and H-isotopic compositions have been reported for numerous pyroclastic glass beads from Apollo missions 15 and 17, spanning from very-low-Ti to high-Ti glasses (Saal et al. 2008; Hauri et al. 2011; Saal et al. 2013; Chen et al. 2015; Hauri et al. 2015; Wetzel et al. 2015). Furthermore, late-stage glasses in the mesostasis regions of KREEP basalts 15382, 15386, and high-Ti mare basalt 74235 have also been reported (Greenwood et al. 2017). Studies of volatiles in glass beads and mesostasis glasses in lunar samples have focused mainly on H, C, F, S, and Cl abundances and H-isotopic compositions, although abundances and isotopic compositions of a number of other moderately volatile elements have also been reported (i.e., Li, Cu, K, Ga, B, Ge, Rb, Cs, Pb, and Zn). The abundances of these moderately volatile elements have been determined by SIMS, EPMA, LA-ICP-MS, and MC-ICP-MS in volcanic glass beads. The data from pyroclastic glasses are primarily used in conjunction with melt inclusion data, where available, to constrain volatile abundances in lunar magmatic source regions. A summary of volatile abundances in lunar glass beads is provided in Tables S3-S10.

3. METHODS AND DATA: STABLE ISOTOPES

Stable isotope systems across the periodic table hold the power to elucidate both the processes and materials involved in the formation and evolution of the Moon. The following section summarizes the results of the investigations of stable isotopic systematics of moderately volatile and volatile elements made in lunar samples since NVM 1. This is largely the result of dynamic development in instrumentation (mostly SIMS and MC-ICPMS) that made lunar samples available to a broader scientific community interested in stable isotopic fractionations of major and trace elements. At the time of NVM1 publication, or shortly after, several pioneering studies of some stable isotopic systems of major and trace elements emerged (Poitrasson et al. 2004; Weyer et al. 2005; Magna et al. 2006; Moynier et al. 2006; Seitz et al. 2006), which unequivocally proved the existence of subtle but resolvable (often sub-per mil) isotopic differences between Earth and various lunar reservoirs, including mare basalts and crustal lithologies. These observations also included some peculiar features, such as strong elemental depletions (e.g., Cu, Zn) or a complete lack thereof (e.g., Li) for some moderately volatile elements. In due time, this topic became addressed in numerous studies that placed further constraints on the formation of the Moon, conditions in the post-collisional environment, magmatic evolution of the Moon, as well as the history of moderately to highly mobile elements, linked to the escape/loss of volatile species (e.g., K, Rb, Ga).

In-depth reviews of stable isotopic fractionation in nature are described elsewhere (Bigeleisen and Mayer 1947; Urey 1947; Schauble 2004), and the interested reader is directed to

these works for further details. Here, we only recap several important rules governing equilibrium isotopic fractionation. (1) With increasing temperature, equilibrium isotopic fractionations decrease roughly in $1/T^2$ proportion. It was originally assumed that at magmatic temperatures, no equilibrium isotopic fractionations would occur beyond the levels of analytical uncertainty. This would leave most stable isotopic variations at high-temperature conditions largely non-measurable, but as detailed below, this is not the case for many systems. In general, however, low-temperature isotopic fractionation is significantly larger than that occurring at high temperatures (e.g., Ca – Gussone et al. 2016; Li – Tomascak et al. 2016; Mg – Teng 2017). (2) Light elements show a larger extent of isotopic variations than heavier elements due to larger relative mass differences between light-element isotopes. For example, elements whose isotopic species have a large relative mass difference will tend to show significantly larger isotopic variations (light elements such as H, Li, S, Cl) than those where differences between isotopic masses are smaller (heavy elements such as Fe and Mo). These variations range from per mil to tens of per cent for the former isotopic systems, whereas sub-per mil variations are usually observed for the latter group. (3) Heavy isotopes of an element favor stiffer bonds (literally speaking shorter, stronger bonds) and tend to concentrate in phases where oxidation state and covalency are high, and coordination number is low. All these and other aspects (see Schauble 2004 for further details) are the key phenomena that drive stable isotopic fractionations.

In addition to equilibrium isotopic fractionations, kinetic isotopic processes (most notably diffusion and evaporation) may play a role under conditions relevant to the Moon, in particular for boiling of the LMO and associated volatile loss from the LMO or protolunar disk. Kinetic effects also appear to figure prominently at the microscale, most reliably detected using *in situ* techniques such as SIMS. These could be particularly effective in dissecting the extent and time scales of interactions of solid materials with percolating melts/fluids at sub-solidus conditions.

A general formula for calculating stable isotopic composition of an element of interest is: $\delta^{A}X_{sample}$ (‰, permil) = $({}^{A}R_{sample}/{}^{A}R_{STD})-1 \times 1000$; Where δ denotes the abundance of isotope A of element X in a sample relative to the abundance of that same isotope in an arbitrarily designated reference material (STD), or isotopic standard. ${}^{A}R$ represents the ratio of ${}^{A}X/{}^{B}X$. The commonly used stable isotopic ratios of volatile to moderately volatile elements, paralleled by their utilized reference materials, are listed in Table 1.

3.1 Hydrogen

The isotopic compositions of H have been determined for apatite, olivine-hosted melt inclusions, volcanic glasses, and NAMs. Furthermore, H isotopic data have been collected for a wide variety of lunar sample types, including VLT, low-Ti, high-Ti, high-Al, VHK, and KREEP basalts, pyroclastic glasses, magnesian-suite rocks, alkali-suite rocks, and ferroan anorthosites. Such data must also be corrected for the contribution of H and D from galactic cosmic ray spallation processes operating at the lunar surface over geological time. The first study to make such corrections to H isotopic data from lunar samples was that of Saal et al. (2013). They used the ${}^{2}H$ (D) production rate at the lunar surface (P_D) reported by Merlivat et al. (1976) and Reedy (1981), respectively of 0.92×10^{-12} mol/g/Myr, and they used a production rate for H (P_H) of 4×10^{-12} mol/g/Myr from Reedy (1981). Following the methods of Saal et al. (2013) we corrected most of the H isotopic data available for lunar samples for these effects (Table S11-S12). Only where cosmic ray exposure ages were not available (i.e., for certain brecciated meteorites, e.g., Tartèse et al. 2014a) was the original measured data considered, and only where spallation-

corrected data was published was that data used instead of our correction (i.e., Table S11-S12). It should be noted that since the initial data on H isotopic compositions from glass beads was published (Saal et al. 2013), the P_D value has been revised upward to $(2.17 \pm 0.11) \times 10^{-12}$ mol/g/Myr (Füri et al. 2017). It has been noted, however, that the standards used in Füri et al. (2017) were not directly measured for OH^- contents, and the FTIR measurements of separated pieces of the same standards showed that the OH^- contents are less than the reference values by a factor of up to ~0.5 (Liu et al. 2018). Using these directly measured OH^- contents, the P_D is still 40% higher than that of Merlivat et al. (1976) and Reedy (1981). Although the application of the revised P_D drastically affects the final δD value in samples with low abundances of H, including many of the volcanic glasses, substantial uncertainties remain in the P_D rates, so we corrected the volcanic glasses using both proposed P_D rates (Merlivat et al. 1976; Reedy 1981; Füri et al. 2017). Additionally, it is unclear how widely the revised P_D can be applied to apatite or plagioclase (Füri et al. 2017), so we only consider apatite and plagioclase data corrected using the P_D value of Merlivat et al. (1976) in the discussion section of this chapter.

3.1.1 Apatite. *In situ* hydrogen isotope data for apatite in lunar materials have been exclusively determined using SIMS techniques. To date, δD values of apatite have been reported for low- and high-Ti mare basalts, high-aluminum and KREEP-rich basalts, regolith breccias, and highlands samples (including Mg-suite and alkali suite rocks) (Fig. 4). Apatite from low-Ti basalts collected at the Apollo 12 and 15 landing sites display a range of δD values from −130 to +1430‰ (Greenwood et al. 2011; Barnes et al. 2013; Tartèse et al. 2013; Boyce et al. 2015; Treiman et al. 2016; Singer et al. 2017; Barnes et al. 2019). Apatite from the Apollo high-Ti basalts are characterized by similar δD values ranging from +530 to +1100‰ (Greenwood et al. 2011; Barnes et al. 2013; Tartèse et al. 2013; Boyce et al. 2015). Apatite from low-Ti basaltic meteorites (Miller Range (MIL) 05035 and LaPaz Icefield (LAP) 04841 are generally characterized by lower δD values ranging from +90 to +570‰ (Tartèse et al. 2013; Tartèse et al. 2014a; Wang et al. 2019b), although these values are not corrected for cosmic ray spallation (see discussion in Tartèse et al. 2014a). In high-Al basalt 14053, apatite δD values cluster between −200 and +50‰ (Greenwood et al. 2011; Pernet-Fisher et al. 2014). Apatite within the high-Al basaltic meteorite Kalahari 009 have δD values ranging from −100 to +450‰ (Tartèse et al. 2014a).

When compared to the other basalts, the KREEP basalts (15386, 72275, the olivine-cumulate lithology of NWA 773 and NWA 2977, and the KREEP basalt clast in NWA 4472) span a larger range of apatite δD values from –280 to +780‰ (Tartèse et al. 2014a; Tartèse et al. 2014b; Wang et al. 2019b). Brecciated lunar meteorites NWA 773, NWA 4472, Dhofar 458, and Sayh al Uhaymir (SaU) 169 contain apatite grains that have yielded an even larger range of δD values, between –250 to +900‰ (Tartèse et al. 2014a; Tartèse et al. 2014b; Wang et al. 2019b).

Finally, apatite in highlands samples are characterized by variable H isotopic compositions ranging from –380 to +670‰ in magnesian-suite samples and from –750 to +940‰ in alkali-suite samples (Greenwood et al. 2011; Barnes et al. 2014; Robinson et al. 2016; Fig. 4).

3.1.2 Volcanic glasses and melt inclusions. Hydrogen isotopic data have also been reported for MIs and volcanic glass beads (Saal et al. 2013; Füri et al. 2014; Chen et al. 2015). Such data must also be corrected for the contribution of H and D from galactic cosmic ray spallation processes operating on the lunar surface over geological time. Application of the original P_D value (Merlivat et al. 1976; Reedy 1981) to H isotopic data results in δD values of

+200 to +450 ‰ for 74220 high-Ti glasses and from +30 to +770 ‰ for 74002 (Saal et al. 2013; Füri et al. 2014). Application of the new P_D value (Füri et al. 2017) changes the range of δD values for high-Ti glasses from −440 to +140 ‰ for 74220 and from −20 to +470 ‰ for 74002 (Saal et al. 2013; Füri et al. 2014). The combined effect of relatively low H_2O contents (4 to 34 ppm H_2O), low D/H ratios, and long cosmic ray exposure (CRE) ages of the very-low-Ti glasses 15426/7 (Saal et al. 2013) culminates in H isotopic compositions from −780 to +4040 ‰ (P_D of Merlivat et al. 1976) and from −8590 to +2510 ‰ (P_D Füri et al. 2017). It should be noted that with all glass data there is a strong dependence of final δD value, and its associated uncertainty, on the H_2O content of the glass. For example, low-Ti glass beads with ≤ 12 ppm H_2O have δD values with prohibitively large uncertainties after correction (−782 +2385/−4996 ‰ to +2210 +1844/−3802, P_D of Merlivat et al. 1976) and are basically rendered meaningless when the P_D of Füri et al (2017) is used as these result in δD values <−1000 ‰ (−8600 to −1150 ‰). Therefore, hydrogen isotope data for glass beads with <~12 ppm H_2O should be used with extreme caution.

On the other hand, due to the protective nature of melt inclusions relative to unconfined magma and/or lava, they generally contain hundreds to thousands ppm H_2O. Once corrected for spallation (P_D of Merlivat et al. 1976), MIs in orange glass beads from 74220 are characterized by δD values between +186 ± 19 to +325 ± 37 ‰ (Saal et al. 2013), although we note that there is only a few per mil difference between the results when using the two different production rates. Melt inclusions from Apollo 12 mare basalts have H isotopic composition of –566 +334/–452 ‰ to –2 ± 185 ‰, after spallation correction (Singer et al. 2017). Additionally, Robinson et al. (2016) reported δD values between +492 +94/–96 ‰ to +657 +122/–127 ‰ for mesostasis glass in KREEPy basalt 15358.

3.1.3 Nominally anhydrous minerals. The extremely low H_2O contents in lunar NAMs make analyses of their H isotopic compositions challenging. Furthermore, such data must also be corrected for the effects of cosmic ray spallation occurring at the lunar surface (e.g., Saal et al. 2013; Füri et al. 2017), which for samples with extremely low H_2O contents and long CRE ages often mean large corrections are applied that result in huge uncertainties effectively rendering the data unsuitable for further consideration (Hui et al. 2017). Hui et al. (2017) reported the first careful H isotopic measurement of plagioclase in ferroan anorthosite 60015,787 using SIMS, and reported δD = +310 ± 110 ‰ after CRE correction (P_D of Merlivat et al. 1976).

3.2 Nitrogen

The bulk abundances and isotopic compositions of N have been determined for fragments and mineral separates of numerous mare basalts, one highland breccia (14321), and one ferroan anorthosite (15414) (Füri et al. 2015; Mortimer et al. 2015; Mortimer et al. 2016). These studies have shown that Solar-gas-free lunar samples contain up to ~0.8 ppm N and that indigenous lunar $\delta^{15}N$ values range from $\delta^{15}N$ around –0.2 ‰ and up to +26.7 ‰.

3.3 Sulfur

Bulk-rock sulfur isotopic compositions of lunar low-Ti and high-Ti basalts from Apollo 11, 12, 15, and 17 sites were reported by Wing and Farqhuar (2015). They observed relatively homogeneous S isotopic ratios of $\delta^{34}S = 0.58 \pm 0.05$ ‰, $\Delta^{33}S = 0.008 \pm 0.006$ ‰, and $\Delta^{36}S = 0.2$

± 0.2 ‰, despite differences in S abundance between the two major basaltic lithologies at 499–1028 ppm for low-Ti mare basalts versus 1174–2131 ppm S for high-Ti mare basalts.

3.4 Chlorine

The isotopic compositions of Cl have been determined for apatite, melt inclusions, and several bulk-rock samples spanning numerous lunar basalt types, including VLT, low-Ti, high-Ti, high-Al, VHK, and KREEP basalts. In addition, Cl isotopic compositions have also been determined for pyroclastic glass beads, magnesian-suite rocks, and regolith breccias.

3.4.1 Apatite. *In situ* Cl isotopic data for apatite grains in lunar materials have been exclusively determined by SIMS. To date, δ^{37}Cl values of apatite have been reported for mare, VHK, and KREEP basalts, regolith breccias, and highlands samples including impact breccias and Mg-suite rocks (Table S13; Fig. 5). In general, lunar apatite display fractionated Cl isotopic compositions that are distinct from unaltered terrestrial rocks and chondrites (δ^{37}Cl = –0.3 ± 0.5 ‰; Sharp et al. 2013b).

Apatite from low-Ti basalts show a range in δ^{37}Cl values from –4 to +19‰ (Sharp et al. 2010; Boyce et al. 2015; Barnes et al. 2016b; Barnes et al. 2019; Wang et al. 2019b). Similarly, high Ti-basalts yielded apatite δ^{37}Cl values ranging from +2 to +17‰ (Boyce et al. 2015; Barnes et al. 2016b; Barnes et al. 2019). In comparison, KREEP basalts (i.e., 15386, 72275, NWA 2977, and NWA 4472) span a range in apatite δ^{37}Cl values of approximately +9 to +31‰ (Sharp et al. 2010; Tartèse et al. 2014a; Barnes et al. 2016b). The VHK basalt 14304 and VHK clasts in SaU 169 contain apatite with elevated but similar range in δ^{37}Cl values of +11 and +32‰, respectively (Tartèse et al. 2014a; Barnes et al. 2016b). Apatite in high-Al basaltic lunar meteorite Kalahari 009 exhibit δ^{37}Cl values from +15 to +22 ‰ (Barnes et al. 2019). Apollo 14 high aluminum basalts have δ^{37}Cl values between +16 to +40 ‰ (Potts et al. 2018). The brecciated portions of lunar basaltic meteorites NWA 4472, and SaU 169 contain apatite with δ^{37}Cl values ranging from +5 to +15‰ (Tartèse et al. 2014a). Impact melt rocks, impact breccias, and granulites have apatite with δ^{37}Cl values between +15 and +81 ‰ (Treiman et al. 2014; Barnes et al. 2016b; Potts et al. 2018; Wang et al. 2019b), although the most extreme positive values are from a single sample (i.e., Dhofar 458; Wang et al. 2019b).

The Cl isotopic composition of apatite in highlands Magnesian-suite rocks (76535 and 78235) are elevated compared to basaltic lithologies and range from +28 to +34‰ (Barnes et al. 2016b; McCubbin and Barnes 2020). The Cl-isotopic composition of highlands alkali-suite samples have not been reported.

3.4.2 Melt inclusions. In addition to apatite, Cl isotopic compositions have been reported for melt inclusions in mare basalts (Stephant et al. 2019). For non-glassy olivine-hosted melt inclusions, δ^{37}Cl values range from +7 to +26 (Stephant et al. 2019). Two glassy olivine-hosted melt inclusions from 15016 yielded δ^{37}Cl values of +13 ‰. Non-glassy pyroxene-hosted melt inclusions have δ^{37}Cl values of +5 to +33 ‰ (Stephant et al. 2019).

3.4.3 Bulk-rock samples. Chlorine isotopic compositions have also been reported for bulk-rock samples by Sharp et al. (2010). These authors reported δ^{37}Cl values of –0.7 to +9.3 ‰ (leachate) for Apollo 17 orange glass beads. Bulk analyses of lunar basalts were shown to contain leachable component with δ^{37}Cl values of between 0 to +2.7 ‰ (Sharp et al. 2010). In addition,

immature soil, mature soil, regolith breccia 12034, and "Rusty Rock" 66095 have non-leachate δ^{37}Cl compositions of +14.3, +15.7, +16.0, and +15.6 ‰, respectively (Shearer et al. 2014).

Chlorine isotope compositions were measured in olivine basalt 12040 on both a bulk portion (0 ‰, Sharp et al. 2010), *in situ* in apatite (+13 to +17.2 ‰; Sharp et al. 2010; Boyce et al. 2015), and *in situ* in melt inclusions (+10 to +33 ‰; Stephant et al. 2019). A reasonable estimate of apatite modal abundance in this rock has been used to suggest that apatite can host ~80% of the total Cl in 12040, but that reproducing the bulk rock δ^{37}Cl value of Sharp et al. (2010) requires ~20% of the bulk Cl to be hosted in an unidentified phase elsewhere in the rock and have an extremely (implausibly) low δ^{37}Cl value (ca. –70 ‰, Day and Moynier 2014). We conclude that, at present, the relationship between bulk δ^{37}Cl values and apatite δ^{37}Cl values remains poorly understood.

3.5 Lithium

Lithium isotopic ratios have been reported for bulk-rock samples from Apollo 12, 15, and 17. Low-Ti and high-Ti basalts show a range in δ^{7}Li values between 3.1 and 5.6 ‰ and 4.5 to 6.6 ‰, respectively (Magna et al. 2006; Seitz et al. 2006; Day et al. 2016). The most pristine low-Ti mare basalts 15016 and 15555 have δ^{7}Li values between 3.6 and 4.5 ‰, reflecting similarities to primitive terrestrial mantle. The Li isotopic dichotomy between low-Ti and high-Ti mare basalts appears to reflect fundamental mineralogical differences of their source regions. Apollo 15 green glass 15426 and Apollo 17 orange glass 74220 have δ^{7}Li values between 4.7 and 5.8 ‰ and from 3.5 to 4.2 ‰, respectively (Magna et al. 2006; Seitz et al. 2006). The analysis of grey glass 74240 returned δ^{7}Li = 5.6 ‰ (Magna et al., 2006). It is interesting to note that no negative δ^{7}Li values have been reported for lunar rocks in contrast to chemically similar lithologies on Earth where such values are not uncommon. The negative δ^{7}Li values in terrestrial systems are typically attributed to past hydrous histories, often combined with subduction and recycling (Tomascak et al. 2016).

3.6 Copper

Copper isotope data are available for bulk-rock high-Ti basalts from the Apollo 11 and 17 missions, for Apollo 17 orange glass, and for the "Rusty Rock" 66095. High- and low-K Apollo 11 basalts have δ^{65}Cu values between 0.12 and 0.72 ‰. The δ^{65}Cu values of Apollo 17 basalts range from 0.21 to 1.4 ‰, and from −0.97 to +0.2 ‰ for the Apollo 17 orange pyroclastic glass beads (Moynier et al. 2006; Herzog et al. 2009). The impact melt breccia, 66095 has 5.4 ± 3.1 ppm Cu [range = 3–12 ppm] and average δ^{65}Cu of 0.72 ± 0.14‰ [weighted mean = 0.78‰], similar to that of mare basalts (Day et al. 2019).

3.7 Potassium

Bulk-rock potassium isotope data indicate that high-Ti basalts have δ^{41}K values between –0.15 ± 0.04 and –0.02 ± 0.04 ‰ (Wang and Jacobsen 2016a; Tian et al. 2020). Low-Ti basalts have δ^{41}K values between –0.12 ± 0.04 ‰ and –0.01 ± 0.03 ‰ (Tian et al. 2020). Green and orange pyroclastic glass beads from 15426 and 74220 soils yielded δ^{41}K values of +2.07 ± 0.03 ‰ and +0.11 ± 0.03 ‰, respectively (Tian et al. 2020). With the exception of 15426, these values

are within error of the $\delta^{41}K$ composition of several Apollo 12 and 15 basalts and orange glass 74220 (–0.2 ± 0.9 ‰) determined by Humayun and Clayton (1995a).

Non-mare samples, cataclastic anorthosite 60015, and cataclastic magnesian-suite norite 77215 yield $\delta^{41}K$ compositions of –1.16 ± 0.04 ‰ and –0.12 ± 0.03 ‰, respectively (Tian et al. 2020). Potassium isotope compositions between –0.43 and +0.12 ‰ have also been reported for brecciated non-mare lunar samples (Wang and Jacobsen 2016a; Tian et al. 2020). Non-mare impact melt breccias and breccias with glass coats have $\delta^{41}K$ values between –2.6 ‰ and –0.06 ‰, while 62255 (anorthosite with melt) yielded a $\delta^{41}K$ value of +0.01 ± 0.02 ‰. KREEP-bearing regolith breccias and KREEP-bearing impact melt breccias have $\delta^{41}K$ values of +0.21 to +0.51 ‰ (Wang and Jacobsen 2016a; Tian et al. 2020), all of which attest to a slight ^{41}K enrichment in most lunar samples relative to terrestrial igneous rocks.

3.8 Gallium

Bulk-rock gallium isotopic compositions have been reported for basalts from Apollo 11, 12, 14, 15, and 17 missions, as well as Apollo 15 green glass. The $\delta^{71}Ga$ values of low-Ti basalts and low-K, high-Ti basalts ranges from +0.15 ± 0.05 ‰ to +0.32 ± 0.02 ‰ and from –0.03 ± 0.03 ‰ to +0.57 ± 0.02 ‰, respectively. The $\delta^{71}Ga$ value of high-Al basalt 14053 is –0.17 ± 0.05 ‰, and Apollo 15 green glass 15426 is characterized by $\delta^{71}Ga$ = –0.35 ± 0.05 ‰ (Kato and Moynier 2017b).

3.9 Rubidium

Bulk-rock rubidium isotopic data for Apollo 11, 12, 15, and 17 basalts indicate a range in $\delta^{87}Rb$ values of −0.05 ± 0.08 to +0.14 ± 0.08 ‰ (Pringle and Moynier 2017; Nie and Dauphas 2019). Apollo 17 high-Ti basalt 74275 has a $\delta^{87}Rb$ value of 0.089 ± 0.058 ‰ (Nie and Dauphas 2019). Cataclastic magnesian-suite norite 77215 has a $\delta^{87}Rb$ value of between –0.149 ± 0.032 and 0.02 ± 0.08 ‰ (Pringle and Moynier 2017; Nie and Dauphas 2019).

3.10 Zinc

For bulk-rock basalts, zinc isotope data is available for basalts from each Apollo mission and spanning the range of bulk-rock chemical composition types. Olivine-normative low-Ti basalts have $\delta^{66}Zn$ values between −3.13 and +1.62 ‰, whereas the low-Ti ilmenite, pigeonite-normative, and quartz-normative basalts show a range in $\delta^{66}Zn$ from +1.15 to +1.56‰ (Paniello et al. 2012; Kato et al. 2015). Low-Ti basaltic lunar meteorites have $\delta^{66}Zn$ between +1.14 ‰ and +1.28 ‰ (Day et al. 2020a). High-K, high-Ti basalts show the largest range in $\delta^{66}Zn$ from –5.4 to +1.4 ‰, while low-K high-Ti basalts have a more restricted range of $\delta^{66}Zn$ values between +0.17 and +1.9 ‰ (Moynier et al. 2006; Herzog et al. 2009; Paniello et al. 2012; Kato et al. 2015). High-Al basalt 14053 has a $\delta^{66}Zn$ of –1 ‰ (Kato et al. 2015), but a residue of the same sample has $\delta^{66}Zn$ of +1.4 ‰ (Day et al. 2017a). Apollo 15 green glass 15426 has $\delta^{66}Zn$ of −1.0‰ (Kato et al. 2015), whereas Apollo 17 orange glass 74220 shows a range of $\delta^{66}Zn$ values from −4.2 to −2.9‰ (Moynier et al. 2006; Herzog et al. 2009; Paniello et al. 2012).

Magnesian-suite samples have $\delta^{66}Zn$ values between +3.14 and +9.27 ‰ (Day et al. 2020a). KREEP-rich impact melt breccia SaU 169 yielded an average (n=3) $\delta^{66}Zn$ value of +1.30

± 0.04 ‰. The "Rusty Rock", 66095, possesses the lowest δ^{66}Zn value of −13.7‰, paralleled by one of the highest Zn contents (100−400 ppm; Day et al. 2017a).

3.11 Tin

Wang et al. (2019a) reported Sn abundances and isotopic compositions of a suite of low-Ti and high-Ti mare basalts. Their results indicate homogeneous Sn isotopic compositions in lunar samples with δ^{124}Sn of −0.56 ± 0.04‰, which is lower in comparison to the bulk silicate Earth value of −0.08 ± 0.11‰.

3.12 Selenium

Vollstaedt et al. (2020) reported Se abundances and isotopic compositions of three lunar mare basalts and seven lunar soils. The lunar high-Ti basalts 10022 and 70215 show $\delta^{82/78}$Se values of 1.08 and 0.82‰, respectively, which are higher than terrestrial basalts. The low-Ti basalt 12021 has a $\delta^{82/78}$Se value identical to terrestrial basalts. In contrast, lunar soils are marked by significantly heavier Se isotope compositions compared to lunar basalts (Vollstaedt et al. 2020).

4. METHODS AND DATA: REMOTE SENSING

In contrast to planetary samples that allow for detailed investigations of spatially limited materials, global distributions of elements at the surface of a planet can be determined with orbital and Earth-based telescopic data. However, at present, the number of volatile elements that have been assessed with orbital and/or telescopic data on planetary surfaces (excluding atmospheric data) are limited to H, Na, Cl, S, and K (e.g., Boynton et al. 2007; Pieters et al. 2009; Nittler et al. 2011; Evans et al. 2015). Of these, H has received the most attention with respect to the Moon since the publication of NVM 1. In particular, the instruments on numerous orbital spacecraft that have observed the Moon were capable of detecting H that is bonded to O as either hydroxyl or as molecular H_2O (e.g., Clark 2009; Pieters et al. 2009; Sunshine et al. 2009). Here, we focus on lunar volatiles, but a broader summary of scientific results from lunar missions is discussed in detail in Gaddis et al. (2021, this volume).

The Moon Mineralogy Mapper (M^3) was a near-infrared imaging spectrometer that measured reflected sunlight to map lunar mineralogy, flown on India's Chandrayaan-1 spacecraft (Goswami and Annadurai 2009). Though H_2O was not expected over the majority of the Moon, M^3's wavelength range was extended to 3000 nm in order to enable detection of any H_2O on the surface of a few polar craters (Green et al. 2011). Exceeding any expectations, M^3 detected a broadly-distributed OH^- signature present across the lunar surface, with abundances increasing towards the poles (Pieters et al. 2009). This observation was confirmed by independent analyses of EPOXI (Sunshine et al. 2009) and Cassini (Clark 2009) near-infrared data that extended beyond 3000 nm, but at lower spatial resolution. As discussed in more detail in Hurley et al. (2021, this volume), the spatial distribution, coupled with evidence that the OH^- absorption band strength varied as a function of lunar daytime, led to the conclusion that the majority of OH^- had been produced *in situ* by the solar-wind hydrogen interacting with oxygen in minerals in the lunar regolith (Pieters et al. 2009; Sunshine et al. 2009; McCord et al. 2011). However, it has been

suggested that some portion of the OH^- may be endogenic (Bhattacharya et al. 2013; Klima et al. 2013; Klima and Petro 2017; Milliken and Li 2017).

Distinguishing endogenic H_2O and mapping its distribution would provide valuable global-scale constraints to complement lunar sample studies, particularly when trying to understand the relationship between OH^- and KREEP. The overprinting of solar wind-produced OH^- confounds the assessment of the distribution of endogenic OH^- from orbit. Thermal emission of the lunar regolith further complicates characterization of H_2O and OH^-. The higher the temperature of the surface, the more the short-wavelength tail of the thermal black-body emission curve distorts the apparent strength of any absorption band near 3000 nm. The equatorial temperature of the surface of the Moon varies by ~300 ˚C over the course of a lunar day (Vasavada et al. 2012), and it depends on a wide range of factors including solar illumination, time of day, albedo, rock abundance, soil particle size distribution, bulk density, thermal conductivity, and heat capacity. Although the M^3 data were corrected using an empirical thermal correction to remove a first-order thermal component from the warmest surfaces (Clark et al. 2011), it has been recognized that this method results in an incomplete removal of the thermal emission, and other thermal removal methods have been explored (Li and Milliken 2016; Wöhler et al. 2017; Bandfield et al. 2018).

Despite the uncertainties associated with both the thermal emission of the surface at the time of reflectance measurements and the global veneer of OH^- and maybe H_2O, several localized enhancements of OH^- that may be attributed to endogenic OH^- have been identified, associated with both intrusive and extrusive lithologies. Based on the geological context and multiple spectral observations of Bullialdus crater by the M^3 instrument, Klima et al. (2013) suggested that the OH^- signature detected near 2.8 microns in the central peak of the crater was due to bound, magmatic hydroxyl, present in the noritic rocks excavated from a pluton beneath Mare Nubium. Using their revised thermal correction and a parameter that relates the H_2O abundance to the strength of an absorption at three microns, Li and Milliken (2017) also identified an anomaly at Bullialdus crater.

The Compton-Belkovich volcanic complex exhibits a strong, localized OH^- signature (Bhattacharya et al. 2013; Klima and Petro 2017; Li and Milliken 2017). Like many other dome complexes on the nearside, Compton-Belkovich is comprised of extremely silicic material (Jolliff et al. 2011), and is also the location of a Th anomaly detected by the Lunar Prospector Gamma Ray Spectrometer (Lawrence et al. 2007). When examined at high resolution, the OH^- signatures correlate geologically with the individual domes in the complex. Li and Milliken (2017) also identified OH^- enrichment at the Marian and Gruithuisen domes, but not in several other prominent silicic complexes, including Hansteen.

A strong H_2O enhancement was reported in many of the lunar pyroclastic deposits by Milliken and Li (2017). Based on their analysis, they suggest H_2O abundances of around 150 ppm across several large pyroclastic deposits, with up to 400 ppm around vent locations. Among the most prominent locations are within Rima Bode, Humorum & Doppelmayer, Sulpicius Gallus and near Aristarchus crater. Milliken and Li (2017) suggest that, based on the broad geographic distribution of these anomalies there must be significant H_2O in the bulk lunar mantle.

Results based on the thermal correction of Bandfield et al. (2018) suggest that identifying endogenic lunar H_2O, at least in the 3-micron region, may not be possible from orbit. Their correction results in a prominent 3-micron band across the Moon and suggests that local anomalies are insignificant for the regions they examined, including the central peak of Bullialdus crater, the Gruithuisen domes, and the pyroclastics at Aristarchus Plateau, Sinus Aestuum, and

Sulpicius Gallus. They do conclude that the central peak of Bullialdus crater exhibits a more prominent minor absorption present near 2.8 microns, but this feature is difficult to characterize conclusively due to the coarse spectral resolution of the M^3 instrument at that wavelength range.

5. ABUNDANCE AND DISTRIBUTION OF VOLATILES

5.1 Volatile element abundances in the lunar interior

Constraining the depletion of volatiles in the Moon relative to the Earth requires determining the abundances of numerous volatile elements with a range of volatilities in the bulk Moon. The lunar interior has a heterogeneous distribution of volatiles within its mantle and crust (Robinson and Taylor 2014; McCubbin et al. 2015b), which complicates quantitative estimates of the bulk composition of the Moon. Based on the data summarized in this chapter and data available in the literature, we have attempted to quantify the abundances of Li, K, Ga, Na, Cl, B, Rb, Cs, F, Pb, Zn, S, C, and H in various lunar source regions and geochemical reservoirs using data from olivine-hosted melt inclusions, pyroclastic glasses, and the composition of apatite from mare basalts. These values are compared to previous estimates of these elemental abundances for the lunar interior. Although most of the listed elements are lithophile and primarily reside in the bulk silicate portion of the Moon, S, C, and Ga exhibit siderophile behavior under lunar conditions (O'Neill 1991; Li et al. 2015; Steenstra et al. 2017), hence they are distributed between the lunar core and bulk silicate portion of the Moon. In this review, only the abundances in the bulk silicate portion of the Moon (BSM) will be estimated.

To determine elemental abundances in the lunar interior, each volatile element is paired with another element that has similar geochemical behavior during melting and igneous differentiation. Ratios of such elemental pairs should remain relatively constant across multiple source regions and disparate rock types, even if the abundances of those elements vary across those source regions and rock types. In most cases, the element paired with each volatile element is a refractory lithophile element, the abundances of which are better constrained in the bulk Moon than those of volatile elements. In a few cases, however, volatile-volatile ratios are used where an adequate refractory-volatile pair is not available (e.g., B) or where apatite is used to determine abundances of H_2O and Cl from F abundances. The practice of using elemental ratios as described above has provided important insights into the composition of the bulk silicate portion of the Earth and Moon (Schilling et al. 1980; Hofmann and White 1983; McDonough and Sun 1995; Albarede et al. 2015). In particular, we focus on the ratios Li/Dy, Li/Yb, K/U, K/Th, Ga/Sc, Ga/Al, Na/Ti, Na/Sr, Cl/K, Cl/Ba, Cl/F, K/B, Rb/Ba, Cs/Ba, Rb/Cs, F/Dy, F/Nd, F/Zr, Pb/Th, Zn/Fe, S/Dy, CO_2/Nb, H_2O/Ce, and H_2O/F. In some cases, these ratios are highly variable in lunar samples, resulting in imprecise estimates for the bulk Moon (uncertainty for each ratio is reported as a 1-sigma standard deviation of the mean). In particular, the abundances of H span over an order of magnitude based on estimates in the literature, so we have provided a range of these estimates.

5.1.1 Lithium. Lithium abundances in the terrestrial mantle and bulk silicate Earth (BSE) have typically been estimated using Li/Dy or Li/Yb ratios (McDonough and Sun 1995; Salters and Stracke 2004). Additionally, lithium is the least volatile element discussed in this review with a 50% condensation temperature of 1142 K (Lodders 2003). In fact, previous studies of Li in lunar samples have concluded that lithium is not depleted relative to the Earth and hence does not

behave as a moderately volatile element (O'Neill 1991; Magna et al. 2006; Day et al. 2016). Lithium abundances in lunar glasses are not depleted relative to those in olivine-hosted melt inclusions (Hauri et al. 2011; Ni et al. 2019; Table S3), indicating that Li is not strongly susceptible to magmatic degassing under lunar conditions. Furthermore, the Li/Dy and Li/Yb ratios of lunar glasses (i.e., 1.7 ± 0.6 and 2.7 ± 0.9, respectively; Table S3) are enriched relative to terrestrial basalts (i.e., 1.1 ± 0.14 and 1.8 ± 0.3, respectively; Jenner and O'Neill 2012). However, Li/Dy and Li/Yb ratios exhibit substantial variation between low-Ti and high-Ti samples (Table S3), indicating these ratios may not be appropriate for estimating Li abundances in the lunar mantle. Given that the Moon does not seem to be depleted in Li relative to Earth, we use the Li/Dy of Earth (i.e., 2.37; McDonough and Sun 1995) and estimates of Dy from the bulk Moon (i.e., 0.705 ppm; Hauri et al. 2015) to estimate an Li abundance for BSM of 1.14–2.20 ppm (Table 2; Table S3), which overlaps with the value of 1.2 ppm Li for BSM estimated by Hauri et al. (2015).

5.1.2 Potassium. Potassium abundances in the terrestrial mantle and BSE have been estimated using K/U or K/Th (Jochum et al. 1983; McDonough and Sun 1995; Salters and Stracke 2004), and these ratios have also been used to estimate K abundances on the Moon (e.g., Albarede et al. 2015). In fact, all three of these elements can be measured by gamma-ray spectroscopy from orbit, so K/U and K/Th ratios are commonly used to discern the relative volatile depletion of the terrestrial planets, the Moon, and some asteroids/small bodies in our solar system (McCubbin et al. 2012 and references threin).

Lunar prospector revealed that the lunar surface has an average K/Th of 366 (Prettyman et al. 2006). In comparison, lunar pyroclastic glasses yield an average K/Th ratio of 560 ± 290 (Table S4), which is similar to other lunar rocks, which yield K/Th ratios of 220–840, with an average K/Th ratio of 339 (Gillis et al. 2004). The variation in K/Th in lunar rocks could be the result of magmatic degassing of K from lunar lavas. The low surface pressures, elevated temperature, and low oxygen fugacity typical of lunar volcanism promote the loss of alkali metals from silicate melts, including K (Gooding and Muenow 1976).

The K/Th values in lunar samples are depleted relative to MORB by a factor of approximately 9–14 (Salters and Stracke 2004; Jenner and O'Neill 2012), and they are depleted relative to BSE by a factor of 6–9 (McDonough and Sun 1995). The lunar pyroclastic glasses yield an average K/U ratio of 2200 ± 600 (Table S4), which is depleted relative to MORB by a factor of 5–9 (Salters and Stracke 2004; Jenner and O'Neill 2012) and depleted relative to BSE by a factor of 4–7 (McDonough and Sun 1995). This depletion factor translates to a BSM value for K of 33–58 ppm (Table 2; Table S4), which is in the range of, or slightly depleted relative to, values estimated previously (O'Neill 1991; Taylor and Wieczorek 2014; Albarede et al. 2015; Hauri et al. 2015).

5.1.3 Gallium. Gallium abundances in the terrestrial mantle have typically been estimated using Ga/Sc and Ga/Al ratios (McDonough and Sun 1995). However, Ga/Sc ratios in lunar samples are highly correlated with Ga concentration, so Ga/Sc ratios should be avoided to determine the Ga abundance of the bulk Moon. The Ga/Al ratios do not exhibit Ga concentration dependence, so they are used to estimate Ga. The average Ga/Al of low-Ti and VLT glasses is (8 ± 3) x 10^{-5}, and the average Ga/Al of high-Ti glasses is (9.2 ± 0.3) x 10^{-5} (Table S5). Consequently, Ga/Al ratios do not appear to be affected by the Ti content of lunar magmas. In comparison, only a single olivine-hosted melt inclusion, from sample 74220, has been analyzed for Ga and Al, and

the Ga/Al ratio of this inclusion is 8.1 x 10^{-5} (Ni et al. 2019), which is within the range of Ga/Al ratios reported for lunar pyroclastic glasses. The Ga/Al ratios of the lunar glasses are depleted relative to MORB by a factor of approximately 2–3 (Jenner and O'Neill 2012), and their depletion factor relative to BSE is 1.9–2.1 (McDonough and Sun 1995). Assuming this depletion factor is relevant globally, the BSM has 2.0–2.6 ppm Ga, which overlaps partially with the higher estimates of Ga abundances in the BSM (e.g., Hauri et al. 2015). The range we report for Ga is largely attributed to the range in reported Al abundances for the BSM used in this compilation (Table S5).

5.1.4 Sodium. Sodium is a minor element that is also an essential structural constituent in plagioclase, a major rock-forming mineral on the Moon and a major component of the primary crust. Consequently, estimating the abundance of Na in BSM is difficult to discern from volatile/refractory ratios alone. Estimates of Na from mare volcanic materials are likely lower estimates because they do not consider the distribution of Na between the primary crust and mantle, the latter of which exhibits a strong Eu anomaly indicating plagioclase extraction before the time of source formation (Weill and Drake 1973). However, the evolution of Na abundances in the LMO are further complicated by the possible presence of a pseudoazeotrope in the albite-anorthite system (Lindsley 1969), which would result in abnormal Na evolution during LMO crystallization (Nekvasil et al. 2015). Additionally, like K and other alkali metals, Na is susceptible to degassing under lunar surface conditions (Gooding and Muenow 1976), which further complicates the quantification of Na abundances from lunar rocks.

Sodium abundances in the terrestrial mantle and BSE have been estimated by Na/Ti ratios (McDonough and Sun 1995); however, it is clear that this ratio will be less meaningful on the Moon given the large variations in TiO_2 abundance of lunar magmas. If we compare only the low-Ti and VLT glasses, which are more directly comparable to typical terrestrial lavas than the high-Ti basalts, the Na_2O/TiO_2 ratio is 0.3 ± 0.1 (Table S6). This ratio is depleted relative to MORB and BSE by a factor of 4–8 (McDonough and Sun 1995; Jenner and O'Neill 2012). If we make a simplifying assumption that this depletion factor is relevant to the bulk Moon, it would imply a bulk Na abundance of 320–630 ppm (Table 2), which is within the large range of previous estimates of the Na abundance of the BSM that range from 260-890 ppm Na (O'Neill 1991; Hauri et al. 2015; Ni et al. 2019).

5.1.5 Chlorine. Chlorine abundances in the terrestrial mantle have been estimated by Cl/K ratios (Saal et al. 2002; Salters and Stracke 2004). Chlorine abundances of the Moon have been estimated with Cl/Ba and Cl/Nb ratios in olivine-hosted melt inclusions and using F/Cl ratios derived from apatite (Chen et al. 2015; Hauri et al. 2015; McCubbin et al. 2015b). We consider all four ratios for our estimate, but we note that all of these ratios for terrestrial basalts are lower than the values for BSE by factors of 3–10 (McDonough and Sun 1995; Saal et al. 2002; Salters and Stracke 2004), indicating that Cl abundances in the crust are needed to accurately constrain Cl abundances in the bulk silicate portion of a differentiated planetary body. Additionally, chlorine is susceptible to degassing under lunar surface conditions (Ustunisik et al. 2011; Ustunisik et al. 2015), so we use data from olivine-hosted melt inclusions in 74220, low-Ti mare basalts, and high-Ti mare basalts that have been analyzed for Cl, K, Ba, Nb, and F to determine the Cl content of BSM.

The average Cl/K ratio in olivine-hosted melt inclusions from both high-Ti and low-Ti samples is 0.006 ± 0.001 (Hauri et al. 2011; Chen et al. 2015; Hauri et al. 2015; Ni et al. 2017;

Ni et al. 2019). This value is indistinguishable from the Cl/K ratio of depleted MORB (Saal et al. 2002), indicating that Cl and K are similarly depleted in the terrestrial and lunar mantles. Based on the Cl/K ratios of the olivine-hosted melt inclusions, the K abundances estimated above in section 3.1.2, and the terrestrial MORB/BSE enrichment factor of 10 for Cl/K ratios (McDonough and Sun 1995; Saal et al. 2002), the Cl abundance of BSM ranges from 1.7–4.1 ppm Cl.

Both chlorine and fluorine are incompatible during mantle melting, although Cl is more incompatible than F with respect to pyroxene and olivine (Hauri et al. 2006; Tenner et al. 2009; O'Leary et al. 2010). Nevertheless, F/Cl ratios in a melt should remain nearly constant in lunar magmas until the onset of apatite crystallization (Boyce et al. 2014) or until the onset of differential degassing (Ustunisik et al. 2015). Consequently, we evaluate F/Cl ratios in olivine-hosted melt inclusions, which are typically trapped prior to apatite saturation, to glean information on the F/Cl ratio of various mare sources. These melt-inclusion F/Cl ratios are also compared to melt F/Cl ratios derived from apatite in low-Ti and high-Ti mare basalts using their respective apatite compositions and experimentally constrained F–Cl apatite-melt exchange coefficients (McCubbin et al. 2015a; McCubbin and Ustunisik 2018). The average F/Cl ratio in olivine-hosted melt inclusions from high-Ti samples is 20 ± 3 (Hauri et al. 2011; Chen et al. 2015; Hauri et al. 2015; Ni et al. 2019). The average F/Cl ratio in olivine-hosted melt inclusions from low-Ti samples is 15 ± 2 (Hauri et al. 2011; Chen et al. 2015; Hauri et al. 2015; Ni et al. 2019). The earliest crystallized apatite from high-Ti mare basalts 10058, 75055, and 10044 translate to bulk rock F/Cl ratios of 15–36 (Greenwood et al. 2011; Barnes et al. 2013; Tartèse et al. 2013; Boyce et al. 2015; Barnes et al. 2016b). The earliest crystallized apatite from low-Ti mare basalts 12039, 12064, 15058, and 15555 translate to bulk rock F/Cl ratios of 8–14 (McCubbin et al. 2010b; Sharp et al. 2010; Greenwood et al. 2011; McCubbin et al. 2011; Barnes et al. 2013; Tartèse et al. 2013; Boyce et al. 2015; Barnes et al. 2016b). All of these data demonstrate that high-Ti mare sources have a higher F/Cl ratio than low-Ti mare sources, indicating that the lunar mantle has a heterogeneous distribution of F and Cl. Notably, the estimates of bulk rock F/Cl from the earliest-formed apatite are similar to those derived from the olivine-hosted melt inclusions. Given that F/Cl ratios in the mare source are not the same as the bulk Moon (McCubbin et al. 2015b), we do not use these values to estimate Cl abundances in BSM.

Comparisons of Cl/Ba and Cl/Nb ratios among high-Ti and low-Ti samples indicate less scatter in Cl/Ba ratios than the Cl/Nb ratios, which is expected given that Nb is compatible in Fe-Ti oxides (Klemme et al. 2006). Consequently, we use Cl/Ba ratios to compute abundances in BSM, and Cl/Nb values from only the low-Ti samples are used for comparison with depleted MORB from Saal et al. (2002). The average Cl/Nb ratio in olivine-hosted melt inclusions from the low-Ti samples is 0.5 ± 0.1 (Hauri et al. 2011; Chen et al. 2015; Hauri et al. 2015; Ni et al. 2017; Ni et al. 2019), which is depleted by a factor of 5.1–7.7 relative to Cl/Nb ratios in MORB (Saal et al. 2002). The average Cl/Ba ratio in olivine-hosted melt inclusions from both high-Ti and low-Ti samples is 0.06 ± 0.01 (Hauri et al. 2011; Chen et al. 2015; Hauri et al. 2015; Ni et al. 2017). Based on the Cl/Ba ratios of the olivine-hosted melt inclusions, Ba abundance in the bulk Moon of 6.60 ppm (Hauri et al. 2015), and the terrestrial MORB/BSE enrichment factor of 3.1 for Cl/Ba ratios (McDonough and Sun 1995; Saal et al. 2002; Salters and Stracke 2004), we compute a range in Cl abundance for BSM of 1.0–1.4 ppm Cl. This estimate is slightly depleted relative to our estimate from Cl/K, and both estimates are enriched relative to estimates that use elemental ratios from mantle-derived rocks alone (e.g., Hauri et al. 2015). However, our estimates are similar to other estimates that consider Cl from both the mantle and crust (e.g., McCubbin et

al. 2015b). Our estimated BSM Cl abundances (i.e., 1.0–4.1 ppm Cl; Table 2) are depleted relative to BSE by a factor of 4–26 (McDonough and Sun 1995; Sharp and Draper 2013).

5.1.6 Boron. Boron abundances in the terrestrial mantle and bulk silicate Earth (BSE) have typically been estimated using K/B ratios (McDonough and Sun 1995; Salters and Stracke 2004), although the robustness of this ratio is dubious (Marschall et al. 2017). Two olivine-hosted melt inclusions in 74220 were analyzed for B, and the B abundances are identical to B abundances in the 74220 pyroclastic glasses (Saal et al. 2008; Hauri et al. 2015), indicating that B is not strongly susceptible to magmatic degassing. However, the K/B ratios did show distinct variation as a function of bulk TiO_2 abundance. The low-Ti lunar glasses have an average K/B ratio of 280 ± 60 (Table S7). The yellow and yellow-brown lunar glasses have an average K/B ratio of 330 ± 30 (Table S7). The orange lunar glasses have an average K/B ratio of 470 ± 40 (Table S7). On Earth, large K/B variations of 1000–2000 are exhibited in N- and E-MORB (McDonough and Sun 1995). The K/B ratio of BSE is 1100–1400 (Marschall et al. 2017), which falls in the range of values exhibited by MORB, so the K/B ratio is likely sufficient for a first order estimate of B abundances in BSM. Based on the range of K/B exhibited by lunar pyroclastic glasses and the K abundances estimated for BSM in Table 2, the abundance of B in BSM is 60–260 ppb (Table 2), which is globally consistent with the BSE B abundance of 190 ± 20 ppb (Marschall et al. 2017).

5.1.7 Rubidium. Rubidium abundances in the terrestrial mantle have typically been estimated using Rb/Ba (Hofmann and White 1983; McDonough and Sun 1995; Salters and Stracke 2004), so this ratio was recently used to constrain the Rb content of the Moon (Albarede et al. 2015). Only a single olivine-hosted melt inclusion, from sample 74220, has been analyzed for Rb and Ba abundances, and the Rb/Ba ratio of this inclusion is 0.012 (Ni et al. 2019). In comparison, the Rb/Ba ratio of lunar pyroclastic glasses exhibit substantial variation with an average Rb/Ba ratio of 0.012 ± 0.009 (Table S8). The Rb/Ba variation in the pyroclastic glasses may indicate that Rb is susceptible to degassing, similar to other alkali metals (Gooding and Muenow 1976), although additional data from olivine-hosted melt inclusions would be needed to fully evaluate this hypothesis. Assuming the Rb/Ba ratio of 0.012 is representative of the lunar interior, it indicates that lunar basalts are depleted by a factor of approximately 8 in Rb relative to MORB and BSE, both of which have nearly identical Rb/Ba (McDonough and Sun 1995; Jenner and O'Neill 2012). Our depletion factor is similar to the Earth-Moon Rb depletion factor of 7 estimated for BSM by Albarede et al. (2015). Combining these depletion factors translates to an Rb abundance of 75–86 ppb in BSM (Table 2), which is depleted by up to a factor of two relative to previous estimates of Rb in BSM (O'Neill 1991; Taylor and Wieczorek 2014; Albarede et al. 2015; Hauri et al. 2015).

5.1.8 Cesium. Cesium abundances in the terrestrial mantle have typically been estimated using Cs/Ba or Rb/Cs ratios (McDonough and Sun 1995; Salters and Stracke 2004). Only a single olivine-hosted melt inclusion, from sample 74220, has been analyzed for Cs, Rb, and Ba abundances, and the Cs/Ba and Rb/Cs ratios were reported to be 6×10^{-4} and 19, respectively (Ni et al. 2019). In comparison, the Cs/Ba and Rb/Cs ratios of lunar volcanic glasses exhibit substantial variations, with Cs/Ba of $(0.3–6) \times 10^{-3}$ with an average Cs/Ba ratio of 0.0013 ± 0.0012 (Table S9) and Rb/Cs of 6–40 with an average Rb/Cs ratio of 20 ± 10 (Table S9). The variations observed in the pyroclastic glasses may result, in part, from Cs being susceptible to degassing, similar to other alkali metals (Gooding and Muenow 1976). In fact, this could be a problem for

Rb/Cs ratios in particular given that both elements are alkali metals. However, Cs and Rb metals both have similar boiling points, so it is unclear to what extent and in what direction Rb/Cs ratios would be affected by alkali loss. The average Rb/Cs value is indistinguishable from the bulk lunar Rb/Cs of 23 estimated by McDonough et al. (1992). Using the Rb/Cs ratio of 19–23 for BSM and our BSM Rb value of 75–86 ppb, we estimate an abundance of 3.3–4.5 ppb Cs in BSM, which is depleted relative to BSE by a factor of 2.8–8.9 (Table 2). Our estimate for BSM Cs is slightly depleted relative to previous estimates of Cs in BSM (i.e., 4.8–6.7 ppb Cs in BSM; O'Neill 1991; Taylor and Wieczorek 2014; Hauri et al. 2015).

5.1.9 Fluorine. Fluorine abundances in the terrestrial mantle have typically been estimated using F/Dy ratios (Saal et al. 2002), and F/Nd ratios have been used to estimate F abundances of the Moon (Chen et al. 2015; Hauri et al. 2015). Both ratios are considered here. Fluorine is susceptible to degassing under lunar surface conditions (Ustunisik et al. 2011; Ustunisik et al. 2015), so the abundances of F cannot be accurately constrained by F abundances in pyroclastic glasses. However, olivine-hosted melt inclusions in 74220, low-Ti mare basalts, and high-Ti mare basalts have been analyzed for F, Nd, and Dy. F/Nd ratios vary less between high-Ti and low-Ti samples than F/Dy ratios, so we use F/Nd to compute abundances in BSM; while F/Dy values are used for comparison with depleted MORB from Saal et al. (2002). Olivine-hosted melt inclusions in 74220 orange glass yield average F/Nd ratios of 2.6 ± 0.9 and F/Dy ratios of 5 ± 2 (Hauri et al. 2011; Chen et al. 2015; Hauri et al. 2015; Ni et al. 2017; Ni et al. 2019). This F/Dy ratio is depleted by a factor of 4–8 relative to F/Dy ratios in depleted MORB (Saal et al. 2002). Olivine-hosted melt inclusions in low-Ti mare basalts 12008, 15016, and 15647 exhibit average F/Nd ratios of 3.5 ± 0.6 and average F/Dy ratios of 7 ± 1 (Chen et al. 2015; Ni et al. 2019). This F/Dy ratio is depleted by a factor of 3–4 relative to F/Dy ratios in depleted MORB (Saal et al. 2002). Olivine-hosted melt inclusions in high-Ti mare basalts 10020 and 74235 exhibit average F/Nd ratios of 2.5 ± 0.4 and average F/Dy ratios of 3.7 ± 0.4 (Chen et al. 2015; Ni et al. 2019). This F/Dy ratio is depleted by a factor of 6–7 relative to F/Dy ratios in depleted MORB (Saal et al. 2002).

Both the high-Ti orange glass 74220 and the high-Ti mare basalts exhibit F/Nd ratios that are slightly lower than the average F/Nd ratio exhibited by the low-Ti basalts. This difference may indicate that the low-Ti source is enriched in F relative to the high-Ti source, although all three F/Nd ratios overlap within uncertainty. In fact, the average F/Nd ratio for low-Ti and high-Ti samples is 3.0 ± 0.7. The F/Nd ratios of MORB and BSE are the same within uncertainty (McDonough and Sun 1995; Saal et al. 2002; Salters and Stracke 2004), indicating this may also be a robust ratio for estimating F in BSM. Based on estimates for the Nd abundance in the bulk Moon of 1.33 ppm (Hauri et al. 2015), we compute a range in F abundance for BSM of 3.1–4.9 ppm F (Table 2). This estimate is slightly depleted relative to previous estimates of F in BSM, which fall in the range of 4.5–7.1 ppm F (Hauri et al. 2015; McCubbin et al. 2015b). This F abundance in the BSM is depleted relative to BSE by a factor of 5–8 (McDonough and Sun 1995; Koga and Rose-Koga 2018).

5.1.10 Lead. Lead abundances in the terrestrial mantle have typically been estimated using Pb/Th ratios (Hofmann 1988), and the Pb abundance of BSE is estimated from U and Pb isotope compositions (McDonough and Sun 1995), which is enabled by a narrow range of μ ($^{238}U/^{204}Pb$) values (8–9) for terrestrial rocks (Stacey and Kramers 1975). In contrast, μ ($^{238}U/^{204}Pb$) values of lunar rocks exhibit substantial variations (Premo et al. 1999) that have been linked to lead loss

early in the Moon's history (Albarede 2009; Snape et al. 2016; Day et al. 2017a). Consequently, estimating the abundance of Pb in BSM cannot be constrained as precisely as in BSE from U and Pb isotope systematics. We thus attempt here to constrain the Pb abundance of the lunar interior from Pb/Th ratios of lunar glasses. However, there is little reliable Pb data from the lunar pyroclastic glasses. A targeted study of Pb abundances in low-Ti green glass 15426 was conducted by Tatsumoto et al. (1987), and they report an average Pb/Th ratio of 0.41 ± 0.03. Additionally, a Pb abundance of 230 ppb has been reported for a single olivine-hosted melt inclusion in orange glass 74220 (Ni et al. 2019). Based on the average Th abundance of orange glass 74220 of 390 ± 90 ppb, the average Pb/Th ratio of 74220 is 0.61 ± 0.14. These values are depleted relative to MORB by a factor of approximately 3–6. If this Earth-Moon depletion factor is relevant to the bulk Moon, it would imply 25–50 ppb Pb in BSM (Table 2). This range overlaps with and exceeds the higher end of the range of values that have been reported previously (i.e., 1.7–28 ppb Pb in BSM; O'Neill 1991; Hauri et al. 2015). We caution, however, that additional Pb data on the volcanic glasses is needed to fully assess Pb/Th values in the bulk Moon and pyroclastic glass source regions. The volatile rich coatings on the glasses can inflate measured volatile concentrations unless the sample is properly leached prior to analysis. Thus, Pb concentrations show high variability among published datasets, and care must be taken when using these analyses to calculate Pb in the BSM.

5.1.11 Zinc. Zinc abundances in the terrestrial mantle have typically been estimated using Zn/Sc ratios (Salters and Stracke 2004), but Zn/Fe ratios have also been shown to exhibit minimal variation in mafic systems on Earth (Le Roux et al. 2010). Furthermore, Zn/Fe ratios were recently used to constrain the Zn content of the Moon (Albarede et al. 2015). Zinc is susceptible to degassing under lunar conditions, which is evidenced by the presence of Zn-rich coatings on the surfaces of pyroclastic glass beads (Butler and Meyer 1976) and the range in δ^{66}Zn values exhibited by lunar samples (Moynier et al. 2006; Herzog et al. 2009; Paniello et al. 2012; Kato et al. 2015), so the abundances of Zn may not be accurately constrained by Zn abundances in volcanic glasses or bulk rocks. Nonetheless, only a single olivine-hosted melt inclusion, from sample 74220, has been analyzed for Zn and Fe, with Zn/Fe = 4.75 x 10^{-5} (Ni et al. 2019). This value falls within the range of values reported by Albarede et al. (2015), who estimated that Zn is depleted in lunar rocks by a factor of 10–200 relative to terrestrial basalts.

In the absence of additional melt inclusion data, we must consider pyroclastic glasses to glean insights into the Zn abundance of the bulk Moon. Lunar pyroclastic glasses have Zn/Fe ratios in the range of (0.0032–7.2) x 10^{-3} (Table S10); however, these data represent analyses from a wide array of analytical instrumentation, some of which resulted in overestimation of Zn abundances, as discussed in Albarede et al. (2015). Here we use only LA-ICP-MS data (i.e., Albarede et al. 2015; Ni et al. 2019) and data from glass beads for which the outer Zn-rich coatings have been removed (i.e., Chou et al. 1975; Wasson et al. 1976). From these studies, a total of 13 data points have been reported, 6 for green glass beads (i.e., Chou et al. 1975; Albarede et al. 2015; Ni et al. 2019) and 7 for orange glass beads (i.e., Wasson et al. 1976; Albarede et al. 2015; Ni et al. 2019). The Zn/Fe ratios vary from (0.023–1.1) x 10^{-4} for green glass beads and (0.32–9.3) x 10^{-5} for orange glass beads. Given the limited data available, we cannot yet discern whether the variation is due to degassing, inter-sample differences, or analytical artifacts. However, the Zn/Fe ratio of the olivine-hosted melt inclusion in 74220 is at the upper end of the reported range of the orange glass (Ni et al. 2019), which could point to degassing of Zn to explain the lower values in the reported range.

Based on the limited data available, we are unable to constrain Zn/Fe ratios in BSM to any higher degree of certainty than the depletion factor (relative to terrestrial basalts) of 10–200 that was reported previously (Albarede et al. 2015), indicating that additional data are needed to help constrain Zn abundances in lunar volcanic glasses. Assuming this wide range of Zn/Fe values for the lunar volcanic glasses are representative of the Zn/Fe ratio of BSM, the Zn abundance of BSM is in the range of 0.28–5.5 ppm Zn (Table 2).

5.1.12 Sulfur. Sulfur abundances in the terrestrial mantle have typically been estimated using S/Dy ratios (Saal et al. 2002). Sulfur is susceptible to degassing as H_2S and ZnS species in lunar systems (Colson 1992; Ustunisik et al. 2011; Bell et al. 2015; Ustunisik et al. 2015), so the abundances of S cannot be accurately constrained by S abundances in volcanic glasses. However, S and Dy have been reported from olivine-hosted melt inclusions in 74220, low-Ti mare basalts, and high-Ti mare basalts. 74220 yields average S/Dy ratios of 67 ± 19 (Hauri et al. 2011; Chen et al. 2015; Hauri et al. 2015; Ni et al. 2017), which is depleted by a factor of 3–5 relative to S/Dy ratios in MORB (Saal et al. 2002). Olivine-hosted melt inclusions in low-Ti mare basalts 12008, 12040, 15016, and 15647 exhibit a wide range in S/Dy ratios with an average value of 82 ± 72, which is depleted by a factor of 2–23 relative to S/Dy ratios in MORB (Saal et al. 2002). Olivine-hosted melt inclusions in high-Ti mare basalts 10020 and 74235 also exhibit a wide range in S/Dy ratios with an average value of 43 ± 30, which is depleted by a factor of 3–17 relative to S/Dy ratios in MORB (Saal et al. 2002).

Although the range of S/Dy values vary substantially even for inclusions from the same lunar sample, most of the variation could be attributed to the degassing loss of S from inclusions and the formation of sulfides during post-entrapment crystallization. The degassing loss of S from melt inclusions has been shown to occur experimentally after 24 hours at magmatic temperatures (Bucholz et al. 2013). Sulfur removal by sulfide crystallization has been shown by Ni et al. (2019) based on both the identified sulfide phase in melt inclusions and significant increase in S/Dy ratio after re-homogenization. By adopting the highest S/Dy ratios in each lunar sample to represent their parent magma, the low-Ti mare basalts 12008, 12040, 15016, and 15647 exhibit S/Dy ratios of 131–179, and the high-Ti basalts and pyroclastic glass 10020, 74220, and 74235 have S/Dy ratios of 78–95. Both the high-Ti orange glass 74220 and the high-Ti mare basalts exhibit S/Dy ratios that are lower than the S/Dy ratio exhibited by the low-Ti basalts. This difference may indicate that the low-Ti source is enriched in S relative to the high-Ti source. MORB S/Dy is depleted relative to BSE S/Dy by a factor of ~1.6 (McDonough and Sun 1995; Saal et al. 2002). Assuming this factor can be extrapolated to the BSM and based on the estimates of Dy abundance in the bulk Moon of 0.705 ppm (Hauri et al. 2015), we compute a range in S abundance for BSM of 88–202 ppm S (Table 2), which is either the same as BSE or depleted relative to BSE by up to a factor of 3.4 (McDonough and Sun 1995).

5.1.13 Hydrogen. Hydrogen abundances will be expressed here as the oxide component H_2O regardless of the specific molecular species in minerals, vapors, or melts in which H resides. Abundances of H_2O in the terrestrial mantle have typically been estimated using H_2O/Ce ratios (Saal et al. 2002; Salters and Stracke 2004), and H_2O/Ce ratios have also been used to estimate H_2O abundances in the lunar interior (Chen et al. 2015; Hauri et al. 2015). Abundances of H_2O in the Moon have also been estimated with F/H_2O ratios derived from apatite in mare basalts (McCubbin et al. 2015b). We consider both methods here to estimate the H_2O content of the lunar interior. H_2O is susceptible to degassing as H_2, H_2O, H_2S, and HCl under lunar surface conditions

(e.g., Ustunisik et al. 2015), so H_2O abundances cannot be accurately constrained by H_2O contents in pyroclastic glasses. However, olivine-hosted melt inclusions in orange glass 74220, low-Ti mare basalts, and high-Ti mare basalts have been analyzed for H_2O, Ce, and F.

Fluorine and H_2O are both incompatible during mantle melting, so F/H_2O ratios in a melt should remain constant in lunar magmas until the onset of apatite crystallization (Boyce et al. 2014) or differential degassing (Ustunisik et al. 2015). Consequently, we evaluate F/H_2O ratios in olivine-hosted melt inclusions, which are typically trapped prior to apatite saturation, to infer F/H_2O ratio of various mare sources. These melt-inclusion F/H_2O ratios are also compared to melt F/H_2O ratios derived from apatite in low-Ti and high-Ti mare basalts using their respective apatite compositions and experimentally constrained F–OH apatite-melt exchange coefficients (McCubbin et al. 2015a). The F/H_2O ratio in olivine-hosted melt inclusions from the orange glass 74220 are in the range 0.05–0.16 (Hauri et al. 2011; Chen et al. 2015; Hauri et al. 2015; Ni et al. 2017; Ni et al. 2019). In comparison, olivine-hosted melt inclusions in high-Ti mare basalts 10020 and 74235 exhibit a range in F/H_2O ratios of 0.25–1.3 and an average F/H_2O ratio of 0.7 ± 0.4 (Chen et al. 2015; Ni et al. 2019). The olivine-hosted melt inclusions in low-Ti mare basalts 12008, 15016, and 15647 exhibit a range in F/H_2O ratios of 0.46–6.3 and an average F/H_2O ratio of 4 ± 1 (Chen et al. 2015; Ni et al. 2019). The earliest crystallized apatite from high-Ti mare basalts 10044, 10058, and 75055 translate to bulk rock F/H_2O ratios of 0.36–0.84 (Greenwood et al. 2011; Barnes et al. 2013; Tartèse et al. 2013; Boyce et al. 2015; Barnes et al. 2016b). The earliest crystallized apatite from low-Ti mare basalts 12039, 12064, 15058, and 15555 translate to bulk rock F/H_2O ratios of 0.38–2.5 (McCubbin et al. 2010b; Sharp et al. 2010; Greenwood et al. 2011; McCubbin et al. 2011; Barnes et al. 2013; Tartèse et al. 2013; Boyce et al. 2015; Barnes et al. 2016b). All of these data indicate that high-Ti mare sources may have a lower F/H_2O ratio than low-Ti mare sources, indicating that the lunar mantle has a heterogeneous distribution of F and/or H_2O. Notably, the estimates of bulk rock F/H_2O from the earliest-formed apatite are similar to those derived from the olivine-hosted melt inclusions, although both datasets exhibit substantial scatter that could be related to degassing of H species. Based on the F/H_2O ratios and the F abundances estimated in section 3.1.9, the H_2O abundance of BSM is 0.49–98 ppm H_2O. This range of values is consistent with the wide range of estimates in the literature (Chen et al. 2015; Hauri et al. 2015; McCubbin et al. 2015b), although the lowest end of this range is likely too low because magmatic degassing of H likely affected some of the selected samples. Moreover, the upper end of this range may be too high given that it stems from a single sample (74220), and the distribution of H_2O in the lunar interior appears to be heterogeneous. If we use only the range of values from the earliest-formed apatite in the low-Ti and high-Ti mare basalts, which span a narrower range of F/H_2O ratios, it translates to a range of 1.2–14 ppm H_2O in BSM.

In addition to F/H_2O, we use H_2O/Ce ratios to compute H_2O abundances in BSM and compare these estimates with depleted MORB data from Saal et al. (2002). The average H_2O/Ce ratio in olivine-hosted melt inclusions from 74220 is 43 ± 17 (Hauri et al. 2011; Chen et al. 2015; Hauri et al. 2015; Ni et al. 2017). This average value excludes inclusions that are smaller than 30 μm in diameter, as they are more significantly affected by degassing based on reported correlations between H_2O abundances and melt inclusion size (Ni et al. 2017). The H_2O/Ce ratio of orange glass 74220 is depleted relative to depleted MORB by a factor of 3–6 (Saal et al. 2002). We have also evaluated H_2O/Ce ratios of olivine-hosted melt inclusions from low-Ti and high-Ti mare basalts, which yield a wide range of H_2O/Ce values from 0.3–9.4 (Chen et al. 2015; Ni et al. 2019). The average H_2O/Ce values range from 2.4–8.8 for high-Ti basalt samples 10020 and 74235. In contrast, average H_2O/Ce values for the low-Ti basalt samples 12008, 12040, 15016,

and 15647 fall in the range 0.8–2.4 (Chen et al. 2015; Ni et al. 2019). All of the H_2O/Ce ratios of the olivine-hosted mare basalt melt inclusions are depleted relative to olivine-hosted melt inclusions in 74220, although this could be the result of H-loss during slow cooling in the lunar crust (Chen et al. 2015). The olivine-hosted mare basalt melt inclusions are depleted relative to depleted MORB by a factor of 19–210 (Saal et al. 2002). Based on estimates for the Ce abundance in the bulk Moon of 1.728 ppm (Hauri et al. 2015), we compute H_2O abundances for BSM of 1.38–74 ppm H_2O (Table 2), using the range of average H_2O/Ce ratios of 0.8–43. This estimate is within previous estimates for the H_2O abundance of BSM (i.e., 0.064–292 ppm H_2O in BSM; McCubbin et al. 2010a; Chen et al. 2015; Hauri et al. 2015; McCubbin et al. 2015b), and it constitutes a wider range compared to our estimate from apatite in mare basalts of 1.2–14 ppm H_2O.

5.1.14 Carbon. Carbon abundances in the terrestrial mantle have typically been estimated using CO_2/Nb ratios (Saal et al. 2002). Carbon is highly susceptible to degassing as CO, CO_2, and possibly C-H species under lunar magmatic conditions (e.g., Li et al. 2017), so the abundances of C cannot be accurately constrained by carbon abundances in volcanic glasses alone. However, olivine-hosted melt inclusions in 74220 have been analyzed for C and yielded CO_2/Nb ratios of 1.05–1.35 (Hauri et al. 2015; Wetzel et al. 2015), which is depleted by a factor of ~200 relative to CO_2/Nb ratios in MORB (Saal et al. 2002). However, the differences in oxygen fugacity during melting between the MORB source and the 74220 source requires a reassessment of the CO_2/Nb relationship under lunar conditions.

If the lunar mantle retains graphite in the 74220 pyroclastic orange glass source during melting, it would imply that C is much more compatible than Nb, so we must assess the solubility of C in lunar magmas relative to the C abundance in the orange glasses. The PEC-corrected C abundances in 74220 olivine-hosted melt inclusions for which Nb data exist are 2.81–3.98 ppm C (Wetzel et al. 2015). This range in C abundance is below the solubility of C in silicate melts, even under lunar fO_2 (Li et al. 2017). Consequently, graphite likely did not remain in the source during melting, and the CO_2/Nb ratio can be used to understand C abundances in the lunar interior. The CO_2/Nb ratio of MORB is depleted by a factor of 3 relative to BSE (McDonough and Sun 1995; Saal et al. 2002), but it is unlikely that this factor can be applied to the Moon given that lower fO_2 would have a strong effect on C speciation (Li et al. 2017). Furthermore, if graphite is the primary C-bearing phase in the Moon, the distribution between the mantle and crust is further complicated by the fact that graphite is buoyant in magma ocean melts (Vander Kaaden and McCubbin 2015). Given the paucity of indigenous graphite in lunar crustal rocks (Steele et al. 2010), we assume the CO_2/Nb ratio of the melt inclusion provides an indication of the volatile depletion in the Moon relative to the Earth. Based on estimates for the Nb abundance in BSM of 0.658 ppm (Hauri et al. 2015), we compute a CO_2 abundance in BSM of 0.69–0.89 ppm CO_2 or 0.19–0.24 ppm C (Table 2), which is depleted relative to the Earth by a factor of 500–630 (McDonough and Sun 1995). Importantly, however, reliable C data in lunar samples are only available for 74220, which may not be an accurate representation of bulk lunar C abundances.

5.2 Depletion of volatile elements in the Moon

The silicate portion of the Moon is depleted in volatile elements relative to the Earth, and the Earth and Moon are both depleted in volatile elements relative to CI chondrites (Fig. 6). All of the estimated abundances of volatiles in BSM from this study are compiled in Table 2. Lithium

and possibly boron are not depleted in the Moon relative to the Earth, so they do not behave as volatile elements in the Earth-Moon system, consistent with the results of previous studies (Day et al. 2016; Sossi and Moynier 2017). In general, volatile elements with condensation temperatures between 650 K and 1050 K are depleted in the Moon relative to the Earth by up to a factor of 26, and there is not a strong correlation between the degree of depletion relative to Earth and 50% condensation temperature (Fig. 6b). These depletion factors for the moderately volatile and volatile elements match well with those reported by Hauri et al. (2015) and Ni et al. (2019), indicating that volatile depletion in the Moon relative to Earth is less extreme than previously reported (e.g., Ringwood and Kesson 1977; Albarede et al. 2015). Zinc and possibly chlorine may be notable exceptions to this trend, further reinforcing the idea that the origin and extent of volatile depletion in the Moon remains an important area of research.

The abundance of sulfur in the Moon is less depleted than would be expected from the lunar volatility trend values that are constrained by C and H (Fig. 6b). This observation indicates that the abundances of sulfur (a volatile element) are depleted relative to Earth within the same range of depletion as moderately volatile elements. In addition, the abundances of S in the silicate portions of both the Earth and the Moon are more depleted relative to CI chondrite than elements with similar 50% condensation temperatures (Fig. 6a). The strong depletions relative to CI likely result from core formation on both bodies because S is moderately siderophile and hence the bulk silicate portions of both bodies do not represent the full complement of S in the bulk Earth or Moon (McDonough and Sun 1995; McDonough 2003; Li et al. 2015; Righter et al. 2017; Steenstra et al. 2017). However, the terrestrial core comprises a higher mass fraction of the bulk Earth than the mass fraction of the lunar core in the bulk Moon (see Andrews-Hanna et al. 2021, this volume for details about the internal structure of the Moon), which could explain why S is less depleted in the lunar mantle relative to Earth's mantle compared to what would be expected based on volatility alone (Righter et al. 2017).

Of the highly volatile elements, we aimed to constrain abundances of H and C in the bulk silicate portion of the Moon. Our calculations suggest that the Moon is more depleted in H and C relative to the Earth compared to estimates from previous studies (Hauri et al. 2015; Wetzel et al. 2015), indicating that there is additional work needed to further constrain the abundances of H and C in BSM. Importantly, even the lower end of our estimated range of H_2O abundances in the lunar interior (i.e., 1.2 ppm H_2O) is enriched by a factor of >1000 relative to the estimates of bulk lunar H_2O abundances prior to 2008 (e.g., Taylor et al. 2006a; Taylor et al. 2006b). The lunar H and C abundances estimated in this work match the general trend of volatile depletion relative to CI chondrites that would be predicted based on 50% condensation temperatures, although the range in H abundances would match a large range of depletion trend slopes (Fig. 6), and the depletion of C could be the result of a higher proportion of C in the lunar core compared to Earth's core. If the C abundances estimated in this study for the bulk silicate portion of the Moon are accurate and sourced entirely from the addition of CI chondrite materials (Alexander et al. 2012; Saal et al. 2013; Sarafian et al. 2014), they indicate a CI chondrite contribution to the Moon of 4–5 $\times$ 10^{17} kg (i.e., 5.4–6.8 millionths of a lunar mass), which is substantially less than previous estimates based on volatile addition (Hauri et al. 2015; Barnes et al. 2016a) and also lower than the estimates based on highly siderophile element (HSE) abundances in the Moon (Day et al. 2007). However, based on the estimated H_2O abundances in CI chondrite (Alexander et al. 2012; Vacher et al. 2020), this mass of CI chondrite addition would account for approximately 535–940 ppb H_2O in the bulk silicate Moon, which is below the range of estimated values from this study. If we were to assume that the mass of CI chondrite addition to the Moon was best constrained by

HSE abundances (i.e., 0.0002 × CI chondrite or 1.5×10^{19} kg; Day et al. 2007), it would imply lunar mantle H_2O and C abundances of around 20–28 ppm and 7 ppm, respectively. Both estimates are intermediate between the values estimated in this study, and those reported in previous studies (Hauri et al. 2015; McCubbin et al. 2015b; Wetzel et al. 2015). All of these inconsistencies in H and C abundance estimates only further illustrate the need for additional work to constrain the H and C abundances in the bulk silicate portion of the Moon.

6. STABLE ISOTOPES: PROCESSES AND RESERVOIRS

6.1 Isotopic differences in volatile elements between the Earth and Moon

The Moon is depleted in volatiles relative to the Earth, and models to explain this depletion need to account for (1) samples that appear to be derived from mantle source regions rich in volatile elements and compounds (e.g., H_2O in orange pyroclastic glass sources), (2) the similar isotopic compositions of volatile and moderately volatile elements between the Moon and the Earth (e.g., H, N, Li), and (3) isotopic systems that show striking differences between the Earth and the Moon (e.g., K, Zn, Cl). In this section we place isotopic fractionation of volatiles into the context of the current models for the formation and magmatic evolution of the Moon.

The elements Cu, K, Ga, Cl, B, Rb, Zn, Sn, Se, and S all show significant isotopic differences between the Earth and the Moon, with sometimes little isotopic difference between lunar samples of distinct chemical compositions or petrogenesis (e.g., mare basalts vs. highlands samples), which is the case for K and Rb. In contrast, other systems such as Cl exhibit substantial isotopic differences among different lunar rock suites.

6.1.1 Mare basalts. Humayun and Clayton (1995b) obtained an average $\delta^{41}K$ value for terrestrial samples of +0.28 ± 0.21 ‰. Since then Wang and Jacobsen (2016b) and Tian et al. (2020) re-defined the $\delta^{41}K$ of the bulk silicate earth (BSE) as –0.48 ± 0.03 ‰. Tian et al. (2020) reported that K-isotopic compositions of lunar samples overlap with and exceed the range displayed by terrestrial samples. They showed that the $\delta^{41}K$ values obtained for low- and high-Ti basalts are indistinguishable, from which they determined a mare basalt average of –0.07 ± 0.09‰. Humayun and Clayton (1995a) provided the only estimate for the $\delta^{41}K$ value of a KREEP basalt at +0.8 ± 0.6 ‰, which is within error of some non-mare samples and is distinct from Earth (Wang and Jacobsen 2016b). Since K only occurs in one valence state and is predicted to form primarily ionic bonds, these characteristics prevent large equilibrium isotope effects (Schauble 2004), which agrees well with the lack of observed K isotope fractionation during igneous crystallization i.e., of the mare basalts compared to BSE (Li et al. 2016; Wang and Jacobsen 2016b).

Zinc is a moderately compatible element and Zn isotopes do not fractionate significantly during magmatic differentiation (<0.1‰, Chen et al. 2013). However, zinc isotopes can be significantly fractionated during evaporation or degassing events by >1‰, where ^{64}Zn preferentially enters the vapor phase over heavier Zn isotopes (Moynier et al. 2006; Moynier et al. 2011; Day and Moynier 2014). Together these traits make zinc isotopes extremely valuable for understanding the history of volatile depletion on the Moon. Except for the extremely negative $\delta^{66}Zn$ values reported by Herzog et al. (2009) for 10017, high-Ti lunar basalts have an average $\delta^{66}Zn$ value of +1.4 ± 0.9 ‰ (2SD, n=15, Moynier et al. 2006; Herzog et al. 2009; Kato et al. 2015). Low-Ti basalts, excluding light values from Paniello et al. (2012) for 12018, have an

average δ^{66}Zn of +1.0 ± 1.7 ‰ (2SD, n=15, Paniello et al. 2012; Kato et al. 2015). Given that different geochemical types of basalts (e.g., low-K, high-Ti and high-K, high-Ti basalts) have similar Zn isotopic signatures and that igneous differentiation does not significantly fractionate Zn isotopes (c.f., Chen et al. 2013), it is likely that the mantle sources for the mare basalts were relatively homogeneous in terms of δ^{66}Zn values. Interestingly, the lunar δ^{66}Zn values are 1 ‰ higher than those reported for terrestrial basalts (+0.3 ± 0.05 ‰, Chen et al. 2013).

The Ga isotopic composition (reported as δ^{71}Ga) of high-Ti basalts ranges from −0.03 to +0.57 ‰ and for low Ti basalts from +0.09 to +0.32 ‰ (Kato and Moynier 2017b). Consequently, most samples are fractionated towards higher values than BSE (0.00 ± 0.06 ‰, 2SD; Kato and Moynier 2017a). The Ga isotope data show overlap between the high- and low-Ti basalts, so it is reasonable to infer that the mantle cumulates were relatively homogeneous in terms of Ga isotopes, since Ga isotopes are not thought to fractionate significantly during fractional crystallization (Kato and Moynier 2017b).

Chlorine isotopic compositions have been measured on both bulk samples and *in situ* in apatite. Bulk analyses of basalts show δ^{37}Cl values ranging from 0 to +4.7 ‰ with no clear relationship between Cl concentration and Cl isotopes (Sharp et al. 2010). Overall, the small amount of bulk rock data available for lunar basalts indicates a shift towards higher δ^{37}Cl values compared to MORB (−0.7 ± 0.6 ‰, e.g, Sharp et al. 2007; Bonifacie et al. 2008). The majority of Cl isotope data for lunar basalts comes from analyses of apatite which also show a positive shift away from MORB values to δ^{37}Cl values of up to approximately +40 ‰ (Sharp et al. 2010; Tartèse et al. 2014a; Boyce et al. 2015; Barnes et al. 2016b; Potts et al. 2018). In contrast to many of the other isotope systems discussed in this section, significant differences in δ^{37}Cl values are observed within basalts and highlands samples of different bulk geochemistry, the significance of which is discussed in more detail below.

Zhai et al. (1996) reported a narrow range of boron isotope values (δ^{11}B from −5.48 ± 0.05 to −4.8 ± 0.05 ‰) of lunar basalts, with no difference between high- and low-Ti basalts. Marschall et al. (2017) recently determined that uncontaminated MORB has a δ^{11}B of −7.1 ± 0.9 ‰ (2SD). Overall, the Moon appears to be fractionated in B isotopes compared to MORB by at least ~1 to 2 ‰.

The sulfur isotopic composition of a wide range of compositionally different mare basalts is extremely homogeneous, with an average δ^{34}S of +0.57 ± 0.18 ‰ (2SD, n=9; Wing and Farquhar 2015), and these results agree well with earlier studies of Apollo samples (Chang et al. 1974; Thode and Rees 1976). Comparing this mean bulk lunar mantle value to the Earth is not trivial since (1) fractionation of S isotopes occurs during cycling of S through Earth's surface environment (e.g., Farquhar et al. 2002; Ono et al. 2012; Labidi et al. 2013); (2) S partitioning between sulfide and sulphate species in basaltic melts can lead to isotope fractionation under magmatic conditions (Sakai et al. 1984); and (3) experimental evidence has shown that core formation at relatively low pressure (1–1.5 GPa) fractionates S isotopes, leading to light isotope enrichment in the silicate mantle (Labidi et al. 2016). This has led to variations in the estimates for the S isotopic compositions of rocks derived from Earth's mantle. However, when compared to the recent estimates of δ^{34}S for the MORB source at –1.28 ± 0.33 ‰ (Labidi et al. 2013), the lunar mantle seems to be characterized by a significantly higher δ^{34}S value.

Only the high-Ti basalts have been investigated thus far for Cu isotopes. When compared to terrestrial basalts (δ^{65}Cu −0.19 to +0.82 ‰, Coplen et al. 2002; Albarede 2004; Herzog et al. 2009; Savage et al. 2015) they are consistently fractionated towards higher δ^{65}Cu values between +0.12 to +1.4 ± 0.1 ‰ (2σ uncertainties) (Moynier et al. 2006; Herzog et al. 2009).

Most lunar rocks exhibit fractionated Rb isotopic values (average +0.04 ± 0.11 ‰, 2SD n = 18) compared to terrestrial rocks that have a well-constrained average δ^{87}Rb of −0.13 ± 0.01 ‰ (Pringle and Moynier 2017; Nie and Dauphas 2019).

6.1.2 FAN and plutonic samples. Compared to lunar basalts, little isotopic data for volatile elements exists for samples of the lunar crust. Of the isotopic systematics discussed for mare basalts above, Zn, Ga, K, and Cl are the best studied for plutonic samples. Pristine, unbrecciated ferroan anorthosite 15415 and Mg-suite samples have yielded δ^{66}Zn values between +3.0 to +9.3 ‰ (Kato et al. 2015; Day et al. 2020a). Like the mare basalts, these values are significantly higher than terrestrial basalts (Chen et al. 2013). Chlorine isotopic compositions of apatite in Mg-suite samples show relatively homogeneous and extremely fractionated δ^{37}Cl values (+28.9 to +33.8 ‰, Barnes et al. 2016b; McCubbin and Barnes 2020) compared to MORB samples (Sharp et al. 2007; Bonifacie et al. 2008). In contrast to Zn and Cl, the view from Ga isotopes is not as straightforward. Ferroan anorthosite 15415 and Mg-suite norite 77215 display higher δ^{71}Ga values compared to BSE (+0.85 ± 0.05 ‰ and +0.16 ± 0.05 ‰, respectively, Kato and Moynier 2017a), yet brecciated FANs display isotopic compositions ranging from negative to positive values compared to BSE (–0.47 to +0.20 ‰, Kato et al. 2017). Non-mare anorthosite, impact melts/glass, and KREEP-rich breccias show a large range in δ^{41}K values from –2.60 to +0.51 ‰ (Tian et al. 2020).

The consistent shift towards heavier isotope ratios for most volatile elements in lunar basalts and highlands samples compared to terrestrial basalts is (1) not directly correlated with volatile element 50%-condensation temperatures (Cu = 1033 K to S = 655 K, Lodders 2003), (2) not obviously associated with any bulk chemical control, and (3) mostly unrelated to igneous differentiation processes. Therefore, the shift in isotope values may implicate a large-scale process(es) in the fractionation of the isotopes of Cu, K, Ga, Cl, B, Rb, Zn and S on the Moon that did not occur on Earth.

6.2 Volatile loss during the formation and evolution of the Moon

The widespread volatile depletion of the Moon coupled with the observed shift towards heavy isotopic signatures for a number of volatile elements in both basaltic and plutonic samples is most compatible with volatile loss during the formation of the Moon and its subsequent differentiation (see Canup et al. 2021, this volume for a detailed discussion). As discussed previously, differentiation and partial melting have limited effects on the isotopic systems of interest. However, loss or partial loss of volatiles to vacuum is an effective mechanism for fractionating volatile elements, and at this point it is important to define the effect of Rayleigh distillation on isotope ratios, which is the ideal evaporation of a liquid into a vacuum:

$$R = R_0 \times f^{(\alpha-1)} \quad (1)$$

where R = final isotope ratio, R_0 = initial isotope ratio, f = fraction of minor isotope remaining in melt, α = fractionation factor. The fractionation factor can be estimated by:

$$\alpha = \sqrt{\frac{My}{Mx}} \quad (2)$$

where My is the molecular mass of the light isotopologue and Mx represents the molecular mass of the heavy isotopologue. Rayleigh degassing of Zn, Cu, and K is unlikely to have occurred under ideal conditions because the isotopic shift from terrestrial values is much smaller than is predicted from using theoretical α values for free evaporation (c.f., discussion in Day and Moynier

2014). This has been demonstrated for large-scale nuclear detonation 'experiments' on Earth (Day et al. 2017b; Wimpenny et al. 2019; Day et al. 2020b), as well as theoretically (e.g., Young 2000; Yu et al. 2003). Rather, it is much more reasonable to consider that volatiles were only partially lost via distillation and that diffusion may have been a rate limiting factor (Day and Moynier 2014) or related to variable activity coefficients in silicate melts (Day et al. 2020b).

Volatiles may have been lost during several stages in lunar history (1) during Moon formation, including the proto-lunar disk phase (see Canup et al. 2021, this volume), (2) during cooling and crystallization of the LMO, and (3) during basalt eruption and degassing at the lunar surface (including pyroclastic eruptions; see Head et al., 2021, this volume), or any combination thereof. The timing of volatile loss may be better constrained by considering the isotopic composition of lithologies that are hypothesized to have formed at different intervals of lunar evolution (i.e. early LMO source regions vs late LMO source regions).

6.2.1 Volatile loss from the protolunar disk. The homogeneous K, Zn, Ga, and S isotopic compositions of mare basalts, regardless of geochemical grouping, that are shifted to positive values relative to MORB for each isotope system could indicate volatile loss during Moon formation (i.e., from the protolunar disk). For example, Nie and Dauphas (2019) argued that evaporation into a gaseous medium that was ~99% saturated can explain the observed isotopic fractionations of K, Ga, Rb, Cu, and Zn of lunar rocks relative to terrestrial rocks. Similarly, the difference in S isotopes between the Earth and the Moon together with the homogeneity of $\delta^{34}S$ in the source regions for the mare basalts indicates large-scale S loss from the Moon relative to Earth (Wing and Farquhar 2015). If both objects started with a MORB-like $\delta^{34}S$ value, a positive shift for the Moon could be accounted for by loss of S_2 vapor at high temperatures >1300 °C (Richet et al. 1977) from anhydrous proto-lunar disk material or from the LMO, with bulk Moon S degassing of <10% (Wing and Farquhar 2015). Note that the heavier isotopic signature of S identified in lunar rocks could also be reconciled with preferential partitioning of siderophile S into the lunar core (Mahan et al. 2017; Steenstra et al. 2017), as this could have caused fractionations of S isotopes of similar magnitudes to those measured in lunar basalts (Labidi et al. 2016).

6.2.2 Volatile loss from the LMO. Almost all of the isotopic fractionations for volatile and moderately volatile elements observed for lunar rock samples (excluding breccias) are compatible with efficient or partial loss of volatiles to the vapor phase during the cooling and crystallization of the LMO. Note that it is expected that volatiles could have been lost before the formation of a sufficiently thick crust, after which degassing into a vacuum or low-pressure environment would have been strongly inhibited. During this time frame, it is expected that an atmosphere existed around the Moon (e.g., Saxena et al. 2017). Degassing of volatiles from the LMO would have added volatiles to the atmosphere that could have (1) rained back down and been re-worked into the LMO melt or (2) could have been stripped away by atmospheric erosion for example by impacts (e.g., Schlichting and Mukhopadhyay 2018). The first pathway would lead to minimal isotopic fractionation of the remaining melt and would predict homogeneous, unfractionated isotopic compositions for mantle cumulates being formed during that time (i.e., olivine and pyroxene cumulates). The second pathway would lead to isotopic fractionation since the lighter isotopes that were lost from the melt to the vapor phase would have been completely lost from the system, and from this we would expect to see a difference in the isotopic composition of samples derived from different depths within the olivine and pyroxene mantle cumulates.

The LMO is predicted to have first crystallized olivine- and pyroxene-rich cumulates (Elardo et al. 2011; Charlier et al. 2018), followed by an anorthitic floatation crust (>60–80% solid; Charlier et al. 2018; Rapp and Draper 2018), and finally ilmenite and primitive potassium, rare earth element (REE), and phosphorous (*ur*KREEP) residues (>95% solid, e.g., Wood et al. 1970; Warren and Wasson 1979). The final 5% crystallization of ilmenite led to a gravitational instability, which is predicted to have caused heterogeneous mixing of the lunar interior as late-stage cumulates foundered through the cumulate pile (e.g., Elkins-Tanton et al. 2002). The history of LMO crystallization and subsequent hybridization should make it challenging to identify a sequential history of volatile loss from the LMO, but it is testable through two of the most studied isotopic systems in lunar samples, Zn (compatible) and Cl (incompatible).

We have already noted that mare basalts of different geochemical groups have indistinguishable δ^{66}Zn signatures (Moynier et al. 2006; Herzog et al. 2009; Kato et al. 2015). Therefore, taken at face value, the near constant δ^{66}Zn values would indicate that either Zn was partially lost from the Moon before the onset of LMO crystallization or that ^{64}Zn was inefficiently stripped from a primitive lunar atmosphere so that just enough ^{64}Zn escape occurred to produce fractionated values compared to Earth, but only enough so that the majority of ^{64}Zn was mixed back into the LMO surface melts to produce homogeneous δ^{66}Zn values of the mantle cumulates. Day and Moynier (2014) pointed out that to explain the differences in the volatile abundances of pyroclastic glass beads and mare basalts, a volatile-rich reservoir could be preserved within the deep lunar interior that has so far only been tapped by the pyroclastic glasses. Analyses of melt inclusions from 74220 showed that this pyroclastic deposit is not enriched in most volatiles such as F, Cl, S, Cu, Zn, Pb, Rb, Cs, and Ga compared to mare basalts (Chen et al. 2015; Ni et al. 2019). The higher H_2O/Ce for 74220 melt inclusions compared to mare basalts, however, is still consistent with a deep reservoir enriched in H_2O. Therefore, it is possible that such a reservoir is relatively unfractionated with respect to volatiles as it would have been locked away deep enough not to interact with surface convecting LMO melts. Unfortunately, this cannot be tested as no samples have been returned from the Moon that represent pure samples of the mantle (i.e., mantle xenoliths or peridotites) and Zn isotopes have not yet been measured on trapped lunar melt inclusions. As will be discussed below, deconvolving the isotopic composition of the melt from which the pyroclastic glasses originated is challenging for such samples due to localized volatile loss during eruption.

If the pristine FAN (15415) is a relic of the flotation crust of the LMO, it would have recorded the Zn isotopic composition of the late stage LMO melt at the onset of plagioclase crystallization (i.e., >60–80% solid). The fractionated values recorded by the FAN are then reconcilable with evaporation during the later stages of LMO solidification (Kato et al. 2015). This hypothesis agrees well with the observation that the lunar mantle is characterized by a homogeneous and lighter δ^{66}Zn value than the crust (if represented by 15415). The Mg-suite samples allow us to place further constraints on this hypothesis because their parent melts were most likely formed by either (1) mixing of primitive mantle cumulates with *ur*KREEP during mantle overturn, or (2) primitive Mg-rich melts that assimilated KREEP-rich crustal material at the base of the crust (Snyder et al. 1995; Shearer et al. 2015). Either way, these samples were not formed from plagioclase floatation during the presence of an LMO, and from what we know from the mare basalts (δ^{66}Zn basalts < δ^{66}Zn highlands), indicates that *ur*KREEP must also be characterized by a high δ^{66}Zn signature. The fact that late-stage LMO products such as pristine FAN and the oldest secondary crustal rocks such as the Mg-suite samples all share isotopically

fractionated Zn suggests that degassing of Zn was a prevalent process throughout the differentiation of the Moon via a magma ocean (Dhaliwal et al. 2018).

Chlorine, like Zn, is a candidate for being lost from the LMO by degassing. Unlike Zn, however, Cl is an incompatible element and so would have been preferentially partitioned into the remaining LMO liquid as crystallization proceeded and would have been most concentrated in *ur*KREEP (Warren and Wasson 1979). During the overturn of LMO cumulates, it is postulated that *ur*KREEP was heterogeneously mixed into the first-formed cumulates, as was residual ilmenite to create the high-Ti basalt sources. As has already been noted, most lunar samples contain Cl that is fractionated from terrestrial basalt values, and there is a strong correlation between basalt composition and Cl isotopes recorded by apatite (Boyce et al. 2015; Barnes et al. 2016b). In fact, the bulk-rock incompatible trace element abundances of low-Ti basalts, including KREEP basalts that are also low in ilmenite content, positively correlate with δ^{37}Cl of apatite (Boyce et al. 2015; Barnes et al. 2016b; Boyce et al. 2018). This correlation indicates that *ur*KREEP was likely enriched in volatiles and may have had a higher δ^{37}Cl value than Cl trapped, presumably as instantaneous trapped liquid, in the first-formed mantle cumulates (McCubbin et al. 2015b; Barnes et al. 2016b). The higher δ^{37}Cl of *ur*KREEP is consistent with degassing of metal chlorides from a melt of high Cl/H_2O ratio (Sharp et al. 2010; Boyce et al. 2015; Barnes et al. 2016b). Such a ratio is consistent with the Cl abundances of KREEP-rich glasses as well as the apatite compositions within the KREEP-rich highlands alkali-suite and magnesian-suite rocks (McCubbin et al. 2011; McCubbin et al. 2015b; Greenwood et al. 2017). Degassing of Cl directly from the LMO (Boyce et al. 2015) suffers similar problems to Zn, in that efficient loss of ^{35}Cl-rich vapors would be restricted to the uppermost portions of the LMO and isotopic fractionation of Cl would be hampered by the presence of an atmosphere and by a growing crust acting as a lid on the LMO that results in degassing to occur at elevated pressure (Barnes et al. 2016b). An alternative scenario to continued LMO degassing is the degassing of late stage LMO melts (rich in Cl and other incompatible elements) after significant crystallization of the lunar crust. Such a process could be linked to impact events weakening the crust to expose *ur*KREEP to hard vacuum long after the dissipation of the atmosphere or weakening of the crust enough to form conduits through which ^{35}Cl-rich vapors could escape (Barnes et al. 2016b). It should be noted that it is possible that the mantle Cl isotopic composition is not fractionated compared to Earth since KREEP-poor basaltic meteorite MIL 05035 has the lowest lunar δ^{37}Cl value recorded, and it is identical to nebular values (Boyce et al. 2015; Sharp et al. 2016).

The heavier K isotopic compositions of KREEPy non-mare materials compared to mare basalts also implicates a link between fractionation of K isotopes and *ur*KREEP petrogenesis (Tian et al. 2020). Loss of a ^{39}K-rich vapor, as has been discussed for Cl, during or subsequent to the formation of the *ur*KREEP reservoir could have provided a fractionation pathway leading to a reservoir enriched in ^{41}K relative to ^{39}K (Tian et al. 2020).

Interestingly, the impact degassing model for *ur*KREEP may also explain the highly fractionated Pb isotope compositions proposed for *ur*KREEP (^{238}U/^{204}Pb >2000, Snape et al. 2016) compared to mare basalt sources (^{238}U/^{204}Pb ~100–650, Tatsumoto 1970; Tera and Wasserburg 1972; Tatsumoto et al. 1987; Gaffney et al. 2007; Nemchin et al. 2011; Snape et al. 2016), and the terrestrial mantle (^{238}U/^{204}Pb ~8–10, Zartman and Doe 1981; Kramers and Tolstikhin 1997).

6.3 Localized degassing and redistribution of volatile elements at the lunar surface

The surfaces of green and orange pyroclastic glasses are highly enriched in volatiles compared to their interiors (e.g., Wänke et al. 1973; Meyer et al. 1975; Wasson et al. 1976). Herzog et al. (2009) reported on the increase in Zn and Cu concentrations with decreasing glass bead size, which is consistent with volatile enrichment on bead surfaces from a vapor. Additionally, correlated volatile abundance profiles for glass beads (H, Cl, F, S, C) indicate that highly volatile elements were lost during basalt eruptions on the Moon (e.g., Saal et al. 2008; Wetzel et al. 2015). Notably, orange pyroclastic glasses are more depleted in ^{66}Zn than most mare basalts (δ^{66}Zn value of –3.5 ± 0.3 ‰ 2SD, n=6; Moynier et al. 2006; Herzog et al. 2009), as are green glasses (δ^{66}Zn value of –0.89 ‰; Kato et al. 2015), and basalts 10017 (δ^{66}Zn value of –5.4 ± 0.1 ‰, 2SD, n=3; Herzog et al. 2009) and 12018 (δ^{66}Zn value of –3.1 ‰; Paniello et al. 2012). In addition to Zn, Cu in orange glasses is also isotopically light (δ^{65}Cu value of –0.71 ± 0.71 ‰, 2SD n = 4; Herzog et al. 2009) and the green glasses record a negative δ^{71}Ga isotopic value of –0.35 ± 0.05 ‰ (Kato and Moynier 2017b). Such light isotopic compositions, lighter than even terrestrial basalts, have been interpreted as contamination of the sample by vapor condensates derived from degassing events (i.e., the light component that separated from the melt during degassing).

High-Al basalt 14053 exhibits more negative δ^{66}Zn (Kato et al. 2015) and δ^{71}Ga (Kato and Moynier 2017b) than the averages of the high- and low-Ti basalts and BSE, indicating that Zn and Ga may record the reduction history of this rock already proposed from textural, chemical, and mineralogical observations (Taylor et al. 2004). The preservation of a component that is isotopically enriched in light isotopes (i.e., condensed vapor) is also apparent in brecciated highlands samples. In such samples, isotopic compositions of K (Humayun and Clayton 1995a), B (Zhai et al. 1996), and Ga (Kato and Moynier 2017b) vary drastically from mare-basalt like compositions to highly negative values. Sample 66095, also referred to as "Rusty Rock", is a volatile rich lunar sample that contains high Zn concentrations and extremely fractionated Zn isotopes, with a δ^{66}Zn value as low as –13.7 ± 0.05 ‰ (Day et al. 2017a). Additionally, several Apollo 16 cataclastic anorthosites and noritic anorthosites yielded δ^{66}Zn values ranging from –11.4 to 0.0 ‰ (Kato et al. 2015). Visible alteration of lunar plutonic rocks adds credence to the idea of re-mobilization of volatile elements in the lunar crust, for example clasts of Mg-suite and ferroan anorthosite display sulfide replacement textures with δ^{34}S values of sulfides ranging from –3.4 to –1 ‰ (Shearer et al. 2012). Therefore, attention to petrology and mineralogy of samples, particularly from the lunar highlands, is crucial to interpreting volatile abundances and isotopic data.

6.4 Fractionation of volatiles during mare basalt formation

Lunar basalts and pyroclastic glasses have similar δ^{7}Li isotopic compositions (+3.1 to +6.6 ‰, Magna et al. 2006; Seitz et al. 2006; Day et al. 2016) to terrestrial basalts, eucrites, and shergottites (Magna et al. 2006; Seitz et al. 2006; Tomascak et al. 2008; Pogge von Strandmann et al. 2011; Magna et al. 2014; Magna et al. 2015; Marschall et al. 2017) but are slightly heavier than chondritic meteorites and their components (+2.1 ± 1.3‰ 2σ, Magna et al. 2006; Seitz et al. 2007; Pogge von Strandmann et al. 2011; Seitz et al. 2012; Day et al. 2016). Within the lunar basalts, the δ^{7}Li values of the high-Ti basalts are significantly heavier than those of the low-Ti basalts (Magna et al. 2006; Seitz et al. 2006; Day et al. 2016). Lithium abundances have been observed to positively correlate with δ^{7}Li values (Magna et al. 2006; Seitz et al. 2006; Day et al. 2016). Additionally, O (^{18}O/^{16}O) and Fe (^{56}Fe/^{54}Fe) stable isotopic systematics of lunar basalts

indicate that increases in $^{7}Li/^{6}Li$ are correlated with increases in $^{56}Fe/^{54}Fe$ and depletions in $^{18}O/^{16}O$ for low-Ti basalts, with the reverse being observed for high-Ti mare basalts (Day et al. 2016). Overall, the fractionated Li isotopic compositions of the mare basalts together with the range in values between compositionally distinct basalts (low- and high-Ti) strongly suggest heterogeneity in their source regions. This implicates large-scale, high-temperature igneous differentiation in the formation of the basaltic mantle source regions. Specifically, progressive crystallization of the Moon via a magma ocean possibly led to the enrichment of Li and equilibrium fractionation of $^{7}Li/^{6}Li$ in residual magma ocean cumulates (Fe-Ti oxides and *ur*KREEP) compared to early formed olivine and pyroxene cumulates (Magna et al. 2006; Day et al. 2016). The positive correlation of Li abundance with $\delta^{7}Li$ values shows that magmatic degassing is not the mechanism causing the isotopic fractionation, as Li abundance would decrease with increasing $\delta^{7}Li$ values if that were the case. There is evidence that ^{7}Li is preferentially retained in the surrounding melt, and over large-scale planetary differentiation, this has a measurable effect on $\delta^{7}Li$ values. The fact that the terrestrial mantle, Mars, the Moon, and the eucrite-parent body show similarity in $\delta^{7}Li$ values of ~+4‰ strongly indicates Li isotope fractionation during planet formation/differentiation was a common phenomenon, perhaps more heightened on the Moon due to the global or near-global nature of the LMO.

6.5 Enigmatic highly volatile elements

Mortimer et al. (2015) and Füri et al. (2015) showed that lunar basalts were characterized by $\delta^{15}N$ values of between −46 and +27 ‰, values that are in excellent agreement with the range of $\delta^{15}N$ values (~0 to +20 ‰) previously proposed for lunar N (McCubbin et al. 2015b and references therein). Füri et al. (2015) argued that the $\delta^{15}N$ values of basalts 14053 and 15555 were representative of the Moon because they recorded both the lowest $\delta^{15}N$ values and also lacked noble gases of solar origin. Since only minimal fractionation of N isotopes occurs during magmatic degassing (Cartigny and Marty 2013), the range of values reported for lunar N provides evidence for heterogeneity of the isotopic composition of N in the mantle sources for the mare basalts (Füri et al. 2015; Mortimer et al. 2015). This N heterogeneity within the lunar mantle may provide a valuable geochemical signature for large scale lunar evolutionary processes. When compared to other sources of N, indigenous lunar nitrogen matches the range of isotopic compositions recorded by Earth's primordial mantle ($\delta^{15}N \leq -40$ to −5 ‰; e.g., Javoy et al. 1986; Mohapatra et al. 2009; Palot et al. 2012; Cartigny and Marty 2013), enstatite chondrites ($\delta^{15}N = -30 \pm 10$ ‰; Kung and Clayton 1978), and carbonaceous chondrites ($\delta^{15}N$ mean = +20 ± 20 ‰; Kerridge 1985; Marty 2012). It has been suggested that the range of N isotopic compositions seen in mare basalts may be the result of inefficient mixing of both Earth and impactor material after the giant impact (Füri et al. 2015).

Regarding the isotopic composition of H in lunar H_2O, H isotopes have been measured in apatite in numerous lunar lithologies, pyroclastic glass beads, and melt inclusions, spanning from –750 to >+1000 ‰ (Fig. 4, Table S11). Generally, mare basalts of all geochemical types span the range from –150 to >+1000 ‰ (Greenwood et al. 2011; Barnes et al. 2013; Tartèse et al. 2013; Tartèse et al. 2014a; Tartèse et al. 2014b; Boyce et al. 2015; Treiman et al. 2016). In comparison, terrestrial mantle values are considered to lie between –90 and –30 ‰ (e.g., Dixon et al. 2017; McCubbin and Barnes 2019). It is worth noting that the crystallization of nominally anhydrous minerals has a limited fractionation (on the order of a few tens of ‰) effect on H and D isotopes (e.g., Bindeman et al. 2012). Mare basalts and picritic glasses that display δD values >0‰ have

generally been interpreted as resulting from local degassing of H-bearing species from basaltic melts during eruption at the lunar surface (Saal et al. 2013; Tartèse and Anand 2013; Tartèse et al. 2013; Füri et al. 2014; Tartèse et al. 2014b). Under the relatively reducing conditions of the Moon (fO_2 ~IW–1, Herd 2008; Wadhwa 2008) it has been proposed that H_2 was the main H-bearing vapor species lost during magmatic degassing, along with ~10 mol% each of H_2S, HF, and HCl (Ustunisik et al. 2011; Sharp et al. 2013a; Tartèse and Anand 2013; Tartèse et al. 2013; Ustunisik et al. 2015; Newcombe et al. 2017). Assuming fractionation factors of Richet et al. (1977) loss of H_2, H_2S, or HCl as major species would increase D/H of remaining melt while loss of HF would decrease D/H of remaining melt (Tartèse et al. 2013). For a few lunar basalts, petrographic context has helped to identify this process in action. In KREEP basalts, early formed apatite (identified on the basis of occurring with earlier crystallizing phases like Mg-rich pyroxene) contained higher OH^- contents and δD values close to unfractionated values, whereas apatite occurring in late-stage mesostasis regions contained lower OH^- contents and more fractionated δD values (Tartèse et al. 2014b). These trends were shown to be incompatible with mixing of a very fractionated lunar D/H ratio and solar wind (Tartèse et al. 2014b). The results from the KREEP basalts agree well with the lightest, potentially least degassed D/H value of melt inclusions in pyroclastic glasses (Saal et al. 2013). Although comparable to the results of KREEP basalts like 15386, it is worth pointing out that the 74220 melt inclusion value is >200 ‰ higher than Earth's mantle (e.g., Dixon et al. 2017; McCubbin and Barnes 2019). If the lowest D/H ratios of the KREEP basalts and 74220 melt inclusions represent un-degassed magmatic values (ranging from ca. –280 to +190 ‰, Saal et al. 2013; Tartèse et al. 2014b), then they may prove to be our best estimate for understanding the D/H ratio of the lunar interior.

Like the mare basalts, plutonic rocks from the lunar highlands span the entire range of D/H ratios from –750 to +900 ‰ (Greenwood et al. 2011; Barnes et al. 2014; Robinson et al. 2016). Several KREEP-rich Mg- and alkali-suite rocks contain apatite with relatively high H_2O contents and with minimally fractionated D/H ratios that are similar to terrestrial values, and these were interpreted as being indicative of the D/H ratio of the primitive Moon (Barnes et al. 2014). These estimates agreed well with the least fractionated results from KREEP basalts (Tartèse et al. 2014b). Additionally, very low D/H values from apatite in an Apollo 15 felsite clast have the most depleted D/H ratios of lunar rocks and were also interpreted as indigenous values, which could imply an extremely heterogeneous lunar interior with regards to H isotopes (Robinson et al. 2016).

As mentioned earlier, the source regions for the orange glasses indicate terrestrial, depleted MORB-like abundances of H_2O (e.g., Hauri et al. 2011; Chen et al. 2015). Therefore, it is possible that pyroclastic glasses derived from depths of >250 km (Grove and Krawczynski 2009) in the lunar interior represent a deep reservoir enriched in H_2O that represents a very small fraction of BSM (Day and Moynier 2014). From work on pyroclastic glass beads and KREEP basalts, several groups have converged on the idea that the apparent enrichment of highly volatile elements in the lunar interior, in light of the global volatile depletion in moderately volatile elements (like Zn, K,), coupled with the similarity in N and H isotopes between terrestrial and lunar interiors indicate that these highly volatile species may have been delivered to the lunar mantle by impacting bodies (e.g., Saal et al. 2013; Tartèse and Anand 2013; Füri et al. 2014). Notably, this mechanism for volatile delivery may also agree with estimated chondritic addition to the Moon on the basis of highly siderophile elements (Day et al. 2007; Day and Walker 2015). Any post-core formation accretion of volatiles is likely confined to after accretion of the Moon but before mantle overturn i.e., before the formation of a significantly thick conductive lid. Overall, The isotopic similarity in H and N between the Earth, the Moon, and H_2O-rich

carbonaceous chondrites has been used as evidence to suggest that carbonaceous chondrites delivered volatiles to the lunar mantle (Saal et al. 2013; Tartèse and Anand 2013; Tartèse et al. 2013; Füri et al. 2014; Tartèse et al. 2014a; Barnes et al. 2016a).

For several lunar basalts, it has been proposed that hydrogen may have been exchanged with the lunar regolith (dominated by solar wind and cosmogenically produced H and D), resulting in a net decrease in the D/H ratio of lunar apatite in samples such as mare basalt 12040 or 14053 (e.g., Treiman et al. 2016). Clearly, further investigation into hydrogen diffusion is required to fully interpret H isotope data from lunar samples, especially in light of recent experimental work on apatite (Higashi et al. 2017). This might be particularly relevant to accurately interpreting the volatile data from plutonic samples. In order to reconcile data from isotopic systems like the more refractory Zn and S from the more volatile H, the possibility must be considered that volatile data from plutonic rocks from the lunar highlands do not represent magmatic lunar values. Rather they may represent the re-equilibration of H in the crust in response to mobilization of volatiles during billions of years of impact gardening and space weathering (Cohen et al. 2021, this volume; Denevi et al. 2021, this volume; Osinski et al. 2021, this volume; Plescia et al. 2021, this volume).

7. ENABLING THE RENAISSANCE OF LUNAR VOLATILES

The Apollo 11 samples were brought to Earth on July 24, 1969 at 12:50 EDT, four days after the first successful human landing on the Moon. This round-trip journey marked a transformative milestone in human history and as the first sample return mission, provided the initial fuel to drive the burgeoning field of planetary sample science. Over the past 50+ years, there have been over 3,000 different studies of Apollo samples, which have enabled numerous discoveries about the Moon, the Earth-Moon system, and the Solar system in general (Zeigler et al. 2019). Notably, the discovery of endogenous lunar H_2O is among the most important scientific discoveries made from the lunar samples, but it did not occur until nearly 40 years after the first lunar samples were brought to Earth (Saal et al. 2008). Furthermore, the initial discovery of endogenous lunar H_2O marked the start of a resurgence of lunar sample studies, particularly focused on lunar volatiles. We refer to this as the renaissance of lunar volatiles, and the factors that enabled this renaissance represent an important lesson learned with respect to sample return missions in general.

One of the major factors for enabling future scientific discoveries from returned samples is in having stringent protocols in the handling, storage, and processing of samples. These protocols are designed to ensure that portions of the samples are kept pristine or as close to an "as returned" state as possible in perpetuity (McCubbin et al. 2019). The Astromaterials Acquisition and Curation Office at NASA Johnson Space Center is tasked with this charge, and NASA has continually supported the long-term curation of Apollo samples and all other NASA-owned astromaterials collections (Fig. 7), as well as portions of samples collected by other countries (e.g., Luna and Hayabusa samples), since the inception of Apollo sample return (Allen et al. 2011). The investments in maintaining the integrity of astromaterials samples continue to enable cutting edge scientific discoveries from these samples, decades after the lifetime of the sample return missions themselves (e.g., the detection of ppm levels of water in Apollo samples 40 years after their return).

Another important factor that enabled the discovery of endogenous lunar H_2O 39 years after Apollo sample return is in technological advancements of analytical instrumentation.

Numerous studies attempted to quantify the abundances of H_2O in lunar samples when they were initially returned, but the H_2O abundances were at or below the detection limit of the analytical instrumentation that was available in the 1970's. These early studies led to the perception that the Moon was "bone dry", and that perception became entrenched in the lunar science community. Advancements in secondary ion mass spectrometry in the 1990s and early 2000s enabled the quantitative detection of H_2O in geological materials down to the 1 ppm level. This technological advancement facilitated above-detection measurements of endogenous H_2O in lunar samples for the first time. Consequently, one of the benefits of sample return is that it facilitates answering scientific questions with the technology of tomorrow provided the samples are maintained in such a way that allows the questions to be answered.

In summary, investments in sample return missions enable transformative science to occur at the time of the primary mission, and investments in the proper curation of those materials enables transformative science to continue in perpetuity as technology advances and/or new scientific questions arise.

8. LOOKING FORWARD

Substantial progress has been made in understanding the abundances and isotopic compositions of volatile elements in the Moon within the last decade, and this progress has provided invaluable constraints on our understanding of the Moon and its thermochemical evolution. However, there are still numerous gaps in our understanding that require additional efforts before we can reach a point of consensus of volatile-element systematics in the Moon. We have highlighted a number of the avenues of future research requiring the most obvious attention.

First and foremost, additional volatile data from lunar samples are needed that cover the broad range of available lunar lithologies that have been identified. The petrology and petrogenetic histories of lunar rocks when coupled with their geochemistry are a powerful tool for assessing the distribution of volatiles in the Moon and accounting for distinct geochemical reservoirs. Furthermore, bulk analysis of whole rock samples has provided very important constraints on lunar volatiles, but going forward, it will be important to integrate high-precision bulk analyses with low-precision *in situ* analyses to identify and understand intrasample heterogeneity and geological processes. For example, textural context for lunar apatite has been important for distinguishing degassing trends from fractional crystallization trends, which have similar evolutionary trends but with paths that evolve in opposite directions with respect to F^-, Cl^-, S^{2-}, and OH^- abundances (Boyce et al. 2014; Tartèse et al. 2014b; McCubbin et al. 2016). Additionally, determination of pre-eruptive abundances and stable isotopic compositions of volatile elements (e.g., Zn, Cu, Pb, Rb, etc.) for the pyroclastic glasses are heavily affected by surface-correlated volatiles, which complicates comparisons of their source region to that of the mare basalts. A growing dataset of *in-situ* analyses would enable us to better compare the source regions for pyroclastic deposits and mare basalts. Moreover, investigations of condensate material on the lunar surface (e.g., 66095) and on the surfaces of pyroclastic glass beads should be facilitated using modern analytical techniques to complement all of the important work that occurred in the first two decades after the samples were delivered to Earth. Additional studies are also needed about the effect of cosmic ray spallation on glasses and different minerals with the aim of developing a more systematic way to correct for its effects on D/H ratios. A wealth of information on lunar volatiles have been gleaned from olivine-hosted melt inclusions, but only a limited number of samples have been investigated to date due to the limited availability of

partially glassy and glassy melt inclusions in lunar samples and the difficulties in homogenization experiments. More data on volatile element abundances and isotopic compositions for mineral-hosted melt inclusions are needed, from a broader suite of samples. Furthermore, additional analyses of nominally anhydrous minerals from a broader suite of samples could also provide important insights into endogenous lunar volatiles.

In addition to more extensive analyses of existing lunar samples, additional samples from the Moon from previously unexplored regions of the lunar surface will greatly improve the depth of our understanding of lunar volatiles and help to place existing data into a broader context than is currently possible. Despite the fruitful return of samples by the Apollo missions, the lunar samples we have represent only a relatively small portion of the lunar surface, mostly within the Procellarum KREEP Terrane (PKT). Luna samples are also from the nearside, and lunar meteorites have limited geologic context. Remote sensing observations are globally extensive on the Moon, and they are likely going to drive future discussions of landing site selection and sampling opportunities for human and robotic explorers. Therefore, greater efforts are needed to combine remote sensing observations of volatiles with volatile data from lunar samples. Not only will these combined efforts provide unique constraints on endogenous lunar volatiles, but continued collaboration between the sample science and remote sensing communities will only benefit our ambitions of understanding the geologic history of the Moon and sustaining its human and robotic exploration. Looking towards the future, the combination of sample science and remote sensing will facilitate lunar sample return missions that will be extremely valuable for resolving outstanding questions about the nature of endogenous lunar volatiles. For example, orbital data have been used to identify many locations of interest, from evolved silicic constructs, through pyroclastic deposits and mare basalts that are compositionally different from those in the existing collection, to lower crust and potentially lunar mantle exposures (Elardo et al. 2021, this volume; Shearer et al. 2021, this volume). Although *in-situ* analyses could resolve some specific questions, the Apollo experience has shown that there is no substitute for having samples in hand on Earth that can be examined with existing technologies and curated for those that will develop in the future.

In order to better interpret sample data on endogenous lunar volatiles, additional experimental work is needed to place quantitative constraints on volatile element (from moderately to highly volatile) behavior under physicochemical conditions that are relevant to the Moon, including pressure, temperature, oxygen fugacity, melt composition, and mineral composition. These experiments will help to establish the differences in elemental behavior and mineral-melt partitioning between terrestrial and lunar systems. Specifically, additional experiments to help constrain the partitioning of volatiles between various phases (e.g., apatite-melt, NAM-melt, melt-melt, melt-vapor) under lunar conditions should be completed. Additionally, theoretical or experimental studies of the behavior of moderately and highly volatile element stable isotopes (e.g. Cu, Zn, Li, B, Pb, Ga, S, H, Cl, etc.) during various lunar processes (e.g., giant impact, LMO evaporation, volcanic eruption) are needed to understand to what extent these isotope systems are fractionated relative to the silicate Earth and at what stage of lunar evolution the isotopic systems were modified from their primordial values. Finally, additional efforts are needed to understand the speciation of volatile elements in silicate melts and reduced fluids that are relevant to the Moon. These data are key to place better constraints on the physicochemical properties of lunar melts, fluids, and vapors, and they will provide further insights into volatile element transport processes and mechanisms in the mantle, crust, and at the lunar surface.

The origin and evolution of lunar volatiles and their resulting geochemical reservoirs remains one of the primary open questions in the field of endogenous lunar volatiles, and this question will require both additional analyses as well as additional experimental data as outlined in the preceding text. Several examples of specific open questions include: (1) What do volatile abundances and isotope ratios record with respect to the formation and history of KREEP and the PKT? (2) Why are eruption style and depth of origin correlated for mare basalts and pyroclastic glasses? Does this suggest a more volatile-rich deep interior? (3) What role did LMO crystallization and subsequent cumulate overturn play in the transport, degassing, and present-day distribution of volatiles and their isotopically distinct reservoirs in the lunar interior? Volatile element heterogeneities within the lunar mantle have been identified and to a certain extent quantified, but how these reservoirs formed and subsequently interacted are poorly understood. Additional modeling efforts to synthesize data from numerous lunar lithologies into the context of lunar formation and evolution models can help to better constrain the timing of volatile loss and gain throughout the steps of this process. Additionally, constraining the behavior of volatile species during specific stages of lunar thermochemical evolution, such as the proto-lunar disk, LMO differentiation, and post-differentiation eruption through the lunar crust, will help to explain and better quantify the role of volatiles in the formation and evolution of other planetary bodies.

9. ACKNOWLEDGEMENTS

This work has benefited greatly from the insightful reviews by James Greenwood, and two anonymous reviewers as well as the editorial handling by Clive Neal and the NVM-2 Steering Committee. We dedicate this chapter to the memory of Erik Hauri who, with Alberto Saal, pioneered the renaissance of endogenous lunar volatiles. Scott Eckley is thanked for computing the volume of vesicles in sample 15556 from the XCT data. FMM, JWB, and KEVK were supported by NASA's Planetary Science Research Program during this work. JJB was supported by NASA's postdoctoral program and The University of Arizona. JMDD acknowledges support from NASA Emerging Worlds grant 80NSSC19K0932 awarded to JMDD. RT acknowledges the UK Science and Technology Facilities Council for financial support (grant #ST/P005225/1). TM contributed through the Strategic Research Plan of the Czech Geological Survey (DKRVO/ČGS 2018-2022). SME acknowledges support from NASA Solar System Workings grant 80NSSC19K0752 awarded to SME.

10. REFERENCES

Albarede F (2004) The stable isotope geochemistry of copper and zinc. Rev Mineral Geochem 55:409-427

Albarede F (2009) Volatile accretion history of the terrestrial planets and dynamic implications. Nature 461:1227-1233, doi:10.1038/nature08477

Albarede F, Albalat E, Lee CTA (2015) An intrinsic volatility scale relevant to the Earth and Moon and the status of water in the Moon. Meteorit Planet Sci 50:568-577, doi:10.1111/maps.12331

Alexander CMOD, Bowden R, Fogel ML, Howard KT, Herd CDK, Nittler LR (2012) The provenances of asteroids, and their contributions to the volatile inventories of the terrestrial planets. Science 337:721-723, doi:10.1126/science.1223474

Allen C, Allton J, Lofgren G, Righter K, Zolensky M (2011) Curating NASA's extraterrestrial samples: Past, present, and future. Chem Erde 71:1-20, doi:10.1016/j.chemer.2010.12.003
Alletti M, Baker DR, Freda C (2007) Halogen diffusion in a basaltic melt. Geochim Cosmochim Acta 71:3570-3580, doi:10.1016/j.gca.2007.04.018
Anderson AT (1974) Evidence for a picritic, volatile-rich magma beneath Mt. Shasta, California. J Petrol 15:243-267, doi:10.1093/petrology/15.2.243
Andrews-Hanna JC, Weber RC, Garrick-Bethell I, Evans AJ, Kiefer WS, Grimm RE, Keane JT, Ishihara Y, Kamata S, Matsuyama I (2021) The Structure and Evolution of the Lunar Interior. Rev Mineral Geochem XX:xxx-xxx
Bacon CR (1989) Crystallization of accessory phases in magmas by local saturation adjacent to phenocrysts. Geochim Cosmochim Acta 53:1055-1066
Baker DR (2008) The fidelity of melt inclusions as records of melt composition. Contrib Mineral Petrol 156:377-395, doi:10.1007/s00410-008-0291-3
Bandfield JL, Poston MJ, Klima RL, Edwards CS (2018) Widespread distribution of OH/H_2O on the lunar surface inferred from spectral data. Nat Geosci 11:173-177, doi:10.1038/s41561-018-0065-0
Barnes JJ, Franchi IA, Anand M, Tartèse R, Starkey NA, Koike M, Sano Y, Russell SS (2013) Accurate and precise measurements of the D/H ratio and hydroxyl content in lunar apatites using NanoSIMS. Chem Geol 337-338:48-55
Barnes JJ, Tartèse R, Anand M, McCubbin FM, Franchi IA, Starkey NA, Russell SS (2014) The origin of water in the primitive Moon as revealed by the lunar highlands samples. Earth Planet Sci Lett 390:244-252, doi:10.1016/j.epsl.2014.01.015
Barnes JJ, Kring DA, Tartèse R, Franchi IA, Anand M, Russell SS (2016a) An asteroidal origin for water in the Moon. Nat Commun 7, doi:10.1038/ncomms11684
Barnes JJ, Tartèse R, Anand M, McCubbin FM, Neal CR, Franchi IA (2016b) Early degassing of lunar *ur*KREEP by crust-breaching impact(s). Earth Planet Sci Lett 447:84-94, doi:http://dx.doi.org/10.1016/j.epsl.2016.04.036
Barnes JJ, Franchi IA, McCubbin FM, Anand M (2019) Multiple volatile reservoirs on the Moon revealed by the isotopic composition of chlorine in lunar basalts. Geochim Cosmochim Acta 266:144-162
Beaudoin G, Taylor BE, Rumble D, Thiemens M (1994) Variations in the sulfur isotope composition of troilite from the Canyon Diablo iron meteorite. Geochim Cosmochim Acta 58:4253-4255, doi:10.1016/0016-7037(94)90277-1
Bell AS, Shearer C, deMoor JM, Provencio P (2015) Using the sulfide replacement petrology in lunar breccia 67915 to construct a thermodynamic model of S-bearing fluid in the lunar crust. Geochim Cosmochim Acta 171:50-60, doi:10.1016/j.gca.2015.08.002
Bell DR, Rossman GR (1992) Water in Earth's mantle: The role of nominally anhydrous minerals. Science 255:1391-1397, doi:10.1126/science.255.5050.1391
Bhattacharya S, Saran S, Dagar A, Chauhan P, Chauhan M, Ajai, Kumar ASK (2013) Endogenic water on the Moon associated with non-mare silicic volcanism: implications for hydrated lunar interior. Curr Sci 105:685-691
Bigeleisen J, Mayer MG (1947) Calculation of equilibrium constants for isotopic exchange reactions. J Chem Phys 15:261-267, doi:10.1063/1.1746492
Bindeman IN, Kamenetsky V, Palandri J, Vennemann T (2012) Hydrogen and oxygen isotope behaviors during variable degrees of upper mantle melting: Example from the basaltic

glasses from Macquarie Island. Chem Geol 310:126-136, doi:10.1016/j.chemgeo.2012.03.031
Bonifacie M, Jendrzejewski N, Agrinier P, Humler E, Coleman M, Javoy M (2008) The chlorine isotope composition of Earth's mantle. Science 319:1518-1520, doi:10.1126/science.1150988
Borg LE, Gaffney AM, Shearer CK (2015) A review of lunar chronology revealing a preponderance of 4.34-4.37 Ga ages. Meteorit Planet Sci 50:715-732, doi:10.1111/maps.12373
Borg LE, Connelly JN, Cassata WS, Gaffney AM, Bizzarro M (2017) Chronologic implications for slow cooling of troctolite 76535 and temporal relationships between the Mg-suite and the ferroan anorthosite suite. Geochim Cosmochim Acta 201:377-391, doi:10.1016/j.gca.2016.11.021
Boyce JW, Liu Y, Rossman GR, Guan Y, Eiler JM, Stolper EM, Taylor LA (2010) Lunar apatite with terrestrial volatile abundances. Nature 466:466-469
Boyce JW, Tomlinson SM, McCubbin FM, Greenwood JP, Treiman AH (2014) The lunar apatite paradox. Science 344:400-402, doi:10.1126/science.1250398
Boyce JW, Treiman AH, Guan Y, Ma C, Eiler JM, Gross J, Greenwood JP, Stolper EM (2015) The chlorine isotope fingerprint of the lunar magma ocean. Sci Adv 1, doi:10.1126/sciadv.1500380
Boyce JW, Kanee SA, McCubbin FM, Barnes JJ, Bricker H, Treiman AH (2018) Chlorine isotopes in the low-Ti basalts, and the early loss of volatiles from the Earth-Moon system. Earth Planet Sci Lett 500:205-214
Boynton WV, Taylor GJ, Evans LG, Reedy RC, Starr R, Janes DM, Kerry KE, Drake DM, Kim KJ, Williams RMS, Crombie MK, Dohm JM, Baker V, Metzger AE, Karunatillake S, Keller JM, Newsom HE, Arnold JR, Bruckner J, Englert PAJ, Gasnault O, Sprague AL, Mitrofanov I, Squyres SW, Trombka JI, d'Uston L, Wänke H, Hamara DK (2007) Concentration of H, Si, Cl, K, Fe, and Th in the low- and mid-latitude regions of Mars. J Geophys Res: Planets 112, doi:E12s99 10.1029/2007je002887
Brounce M, Boyce J, McCubbin FM, Humphreys J, Reppart J, Stolper E, Eiler J (2019) The oxidation state of sulfur in lunar apatite. Am Mineral 104:307-312, doi:10.2138/am-2019-6804
Bucholz CE, Gaetani GA, Behn MD, Shimizu N (2013) Post-entrapment modification of volatiles and oxygen fugacity in olivine-hosted melt inclusions. Earth Planet Sci Lett 374:145-155, doi:10.1016/j.epsl.2013.05.033
Butler P, Meyer C (1976) Sulfur prevails in coatings on glass droplets: Apollo 15 green and brown glasses and Apollo 17 orange and black (devitrified) glasses. Proc 7th Lun Sci Conf 7:1561-1581
Canup RM, Asphaug E (2001) Origin of the Moon in a giant impact near the end of the Earth's formation. Nature 412:708-712, doi:10.1038/35089010
Canup RM, Righter K, Dauphas N, Pahlevan K, Ćuk M, Lock SJ, Stewart ST, Salmon J, Rufu R, Nakajima M, Magna T (2021) Origin of the Moon and Earth system. Rev Mineral Geochem XX:xxx-xxx
Cartigny P, Marty B (2013) Nitrogen isotopes and mantle geodynamics: The emergence of life and the atmosphere-crust-mantle connection. Elements 9:359-366, doi:10.2113/gselements.9.5.359

Chang S, Lawless J, Romiez M, Kaplan IR, Petrowski C, Sakai H, Smith JW (1974) Carbon, nitrogen and sulfur in lunar fines 15012 and 15013: Abundances, distributions and isotopic compositions. Geochim Cosmochim Acta 38:853-872, doi:https://doi.org/10.1016/0016-7037(74)90060-X

Charlier B, Grove TL, Namur O, Holtz F (2018) Crystallization of the lunar magma ocean and the primordial mantle-crust differentiation of the Moon. Geochim Cosmochim Acta 234:50-69, doi:https://doi.org/10.1016/j.gca.2018.05.006

Chen H, Savage PS, Teng FZ, Helz RT, Moynier F (2013) Zinc isotope fractionation during magmatic differentiation and the isotopic composition of the bulk Earth. Earth Planet Sci Lett 369:34-42, doi:10.1016/j.epsl.2013.02.037

Chen Y, Zhang YX (2008) Olivine dissolution in basaltic melt. Geochim Cosmochim Acta 72:4756-4777, doi:10.1016/j.gca.2008.07.014

Chen Y, Provost A, Schiano P, Cluzel N (2011) The rate of water loss from olivine-hosted melt inclusions. Contrib. Mineral Petrol 162:625-636, doi:10.1007/s00410-011-0616-5

Chen Y, Zhang YX, Liu Y, Guan YB, Eiler J, Stolper EM (2015) Water, fluorine, and sulfur concentrations in the lunar mantle. Earth Planet Sci Lett 427:37-46, doi:10.1016/j.epsl.2015.06.046

Chou C-L, Boynton WV, Sundberg LL, Wasson JT (1975) Volatiles on the surface of Apollo 15 green glass and trace-element distributions among Apollo 15 soils. Proc 6th Lun Sci Conf 6:1701-1727

Clark RN (2009) Detection of adsorbed water and hydroxyl on the Moon. Science 326:562-564, doi:10.1126/science.1178105

Clark RN, Pieters CM, Green RO, Boardman JW, Petro NE (2011) Thermal removal from near-infrared imaging spectroscopy data of the Moon. J Geophys Res: Planets 116, doi:10.1029/2010je003751

Cohen BA, van der Bogert CH, Bottke WF, Curran NM, Fassett CI, Hiesinger H, Joy KH, Mazrouei S, Nemchin A, Neumann GA, Norman MV, Zellner NEB (2021) Impact History of the Moon. Rev Mineral Geochem XX:xxx-xxx

Colson RO (1992) Mineralization on the Moon - Theoretical considerations of Apollo 16 rusty rocks, sulfide replacement in 67016, and surface-correlated volatiles on lunar volcanic glass. Proc 23rd Lun Planet Sci Conf 22:427-436

Coplen TB, Hopple JA, Böhlke JK, Peiser HS, Rieder SE, Krouse HR, Rosman KJR, Ding T, Vocke RD, Révész KM, Lamberty A, Taylor P, De Bièvre P (2002) Compilation of minimum and maximum isotope ratios of selected elements in naturally occurring terrestrial materials and reagents. *In* Book Compilation of Minimum and Maximum Isotope Ratios of Selected Elements in Naturally Occurring Terrestrial Materials and Reagents. Vol U.S. Geological Survey Water-Resources Investigations Report, Reston, Virginia

Crawford I, Anand M, Barber S, Cowley A, Crites S, Fa W, Flahaut J, Gaddis LR, Greenhagen BT, Haruyama J, Hurley DM, McLeod CL, Morse A, Neal CR, Sargeant H, Sefton-Nash E, Tartèse R (2021) Lunar resources. Rev Mineral Geochem XX:xxx-xxx

Danyushevsky LV, Della-Pasqua FN, Sokolov S (2000) Re-equilibration of melt inclusions trapped by magnesian olivine phenocrysts from subduction-related magmas: petrological implications. Contrib Mineral Petrol 138:68-83, doi:10.1007/pl00007664

Danyushevsky LV, McNeill AW, Sobolev AV (2002) Experimental and petrological studies of melt inclusions in phenocrysts from mantle-derived magmas: an overview of techniques,

advantages and complications. Chem Geol 183:5-24, doi:10.1016/s0009-2541(01)00369-2
Day JMD, Moynier F (2014) Evaporative fractionation of volatile stable isotopes and their bearing on the origin of the Moon. Philos Trans R Soc London, Ser A 372, doi:10.1098/rsta.2013.0259
Day JMD, Walker RJ (2015) Highly siderophile element depletion in the Moon. Earth Planet Sci Lett 423:114-124, doi:10.1016/j.epsl.2015.05.001
Day JMD, Pearson DG, Taylor LA (2007) Highly siderophile element constraints on accretion and differentiation of the Earth-Moon system. Science 315:217-219, doi:10.1126/science.1133355
Day JMD, Qiu L, Ash RD, McDonough WF, Teng FZ, Rudnick RL, Taylor LA (2016) Evidence for high-temperature fractionation of lithium isotopes during differentiation of the Moon. Meteorit Planet Sci 51:1046-1062, doi:10.1111/maps.12643
Day JMD, Moynier F, Shearer CK (2017a) Late-stage magmatic outgassing from a volatile-depleted Moon. Proc Natl Acad Sci USA 114:9547-9551, doi:10.1073/pnas.1708236114
Day JMD, Moynier F, Meshik AP, Pradivtseva OV, Petit DR (2017b) Evaporative fractionation of zinc during the first nuclear detonation. Sci Adv 3, doi:10.1126/sciadv.1602668
Day JMD, Sossi PA, Shearer CK, Moynier F (2019) Volatile distributions in and on the Moon revealed by Cu and Fe isotopes in the 'Rusty Rock' 66095. Geochim Cosmochim Acta 266:131-143, doi:https://doi.org/10.1016/j.gca.2019.02.036
Day JMD, van Kooten EMME, Hofmann BA, Moynier F (2020a) Mare basalt meteorites, magnesian-suite rocks and KREEP reveal loss of zinc during and after lunar formation. Earth Planet Sci Lett 531:115998, doi:https://doi.org/10.1016/j.epsl.2019.115998
Day JMD, Moynier F, Sossi PA, Wang K, Meshik AP, Pravdivtseva OV, Pettit DR (2020b) Moderately volatile element behaviour at high temperature determined from nuclear detonation. Geochem Perspect Lett 13:54-60, doi:http://dx.doi.org/10.7185/geochemlet.2014
De Wit JC, Van der Straaten CM, Mook WG (1980) Determination of the absolute isotopic ratio of V-SMOW and SLAP. Geostand.Geoanal Res 4:33-36
Delano JW (1986) Pristine lunar glasses: Criteria, data, and implications. J Geophys Res 91:D201-D213
Denevi BW, Noble SK, Blewett DT, Christoffersen R, Garrick-Bethel I, Gillis-Davis JJ, Glotch TD, Greenhagen BT, Hendrix AR, Hurley DM, Keller LP, Kramer GY, Thompson MS, Trang D (2021) Space Weathering and Exosphere-Surface Interactions. Rev Mineral Geochem XX:xxx-xxx
Dhaliwal JK, Day JMD, Moynier F (2018) Volatile element loss during planetary magma ocean phases. Icarus 300:249-260, doi:10.1016/j.icarus.2017.09.002
Dixon JE, Clague DA, Stolper EM (1991) Degassing history of water, sulfur, and carbon in submarine lavas from Kilauea Volcano, HawaiiI. J Geol 99:371-394
Dixon JE, Bindeman IN, Kingsley RH, Simons KK, Le Roux PJ, Hajewski TR, Swart P, Langmuir CH, Ryan JG, Walowski KJ, Wada I, Wallace PJ (2017) Light stable isotopic compositions of enriched mantle sources: Resolving the dehydration paradox. Geochem Geophys Geosyst 18:3801-3839, doi:10.1002/2016gc006743
Dohmen R, Becker H-W, Chakraborty S (2007) Fe-Mg diffusion in olivine I: Experimental determination between 700 and 1,200 °C as a function of composition, crystal orientation and oxygen fugacity. Phys Chem Miner 34:389-407, doi:10.1007/s00269-007-0157-7

Elardo SM, Draper DS, Shearer CK (2011) Lunar magma ocean crystallization revisited: Bulk composition, early cumulate mineralogy, and the source regions of the highlands Mg-suite. Geochim Cosmochim Acta 75:3024-3045, doi:10.1016/j.gca.2011.02.033

Elardo SM, McCubbin FM, Shearer CK (2012) Chromite symplectites in Mg-suite troctolite 76535 as evidence for infiltration metasomatism of a lunar layered intrusion. Geochim Cosmochim Acta 87:154-177, doi:10.1016/j.gca.2012.03.030

Elardo SM, Pieters CM, Dhingra D, Donaldson Hanna KL, Glotch TD, Greenhagen BT, Gross J, Head JW, Jolliff BL, Klima RL, Magna T, McCubbin FM, Ohtake M (2021) The evolution of the lunar crust. Rev Mineral Geochem XX:xxx-xxx

Elkins-Tanton LT, Van Orman JA, Hager BH, Grove TL (2002) Re-examination of the lunar magma ocean cumulate overturn hypothesis: melting or mixing is required. Earth Planet Sci Lett 196:239-249

Elkins-Tanton LT, Chatterjee N, Grove TL (2003) Experimental and petrological constraints on lunar differentiation from the Apollo 15 green picritic glasses. Meteorit Planet Sci 38:515-527, doi:10.1111/j.1945-5100.2003.tb00024.x

Evans LG, Peplowski PN, McCubbin FM, McCoy TJ, Nittler LR, Zolotov MY, Ebel DS, Lawrence DJ, Starr RD, Weider SZ, Solomon SC (2015) Chlorine on the surface of Mercury: MESSENGER gamma-ray measurements and implications for the planet's formation and evolution. Icarus 257:417-427, doi:10.1016/j.icarus.2015.04.039

Farquhar J, Wing BA, McKeegan KD, Harris JW, Cartigny P, Thiemens MH (2002) Mass-independent sulfur of inclusions in diamond and sulfur recycling on early earth. Science 298:2369-2372, doi:10.1126/science.1078617

Feldman WC, Maurice S, Binder AB, Barraclough BL, Elphic RC, Lawrence DJ (1998) Fluxes of fast and epithermal neutrons from lunar prospector: Evidence for water ice at the lunar poles. Science 281:1496-1500, doi:10.1126/science.281.5382.1496

Filiberto J, Gross J, McCubbin FM (2016) Constraints on the water, chlorine, and fluorine content of the Martian mantle. Meteorit Planet Sci 51:2023-2035

Flesch GD, Anderson AR, Svec HJ (1973) A secondary isotopic standard for $^{6}Li/^{7}Li$ determinations. Int J Mass Spectrom Ion Phys 12:265-272, doi:https://doi.org/10.1016/0020-7381(73)80043-9

Freda C, Baker DR, Scarlato P (2005) Sulfur diffusion in basaltic melts. Geochim Cosmochim Acta 69:5061-5069, doi:10.1016/j.gca.2005.02.002

Füri E, Deloule E, Gurenko A, Marty B (2014) New evidence for chondritic lunar water from combined D/H and noble gas analyses of single Apollo 17 volcanic glasses. Icarus 229:109-120, doi:10.1016/j.icarus.2013.10.029

Füri E, Barry PH, Taylor LA, Marty B (2015) Indigenous nitrogen in the Moon: Constraints from coupled nitrogen-noble gas analyses of mare basalts. Earth Planet Sci Lett 431:195-205, doi:10.1016/j.epsl.2015.09.022

Füri E, Deloule E, Trappitsch R (2017) The production rate of cosmogenic deuterium at the Moon's surface. Earth Planet Sci Lett 474:76-82, doi:10.1016/j.epsl.2017.05.042

Gaddis LR, Joy KH, Carpenter J, Crawford IA, Elphic RC, Halekas J, Lawrence S, Xiao L (2021) Recent Exploration of the Moon: Science from Lunar Missions Since 2006. Rev Mineral Geochem XX:xxx-xxx

Gaetani GA, Watson EB (2000) Open system behavior of olivine-hosted melt inclusions. Earth Planet Sci Lett 183:27-41, doi:10.1016/s0012-821x(00)00260-0

Gaetani GA, Watson EB (2002) Modeling the major-element evolution of olivine-hosted melt inclusions. Chem Geol 183:25-41

Gaetani GA, O'Leary JA, Shimizu N, Bucholz CE, Newville M (2012) Rapid reequilibration of H_2O and oxygen fugacity in olivine-hosted melt inclusions. Geology 40:915-918, doi:10.1130/G32992.1

Gaffney AM, Borg LE, Asmerom Y (2007) The origin of geochemical diversity of lunar mantle sources inferred from the combined U-Pb, Rb-Sr, and Sm-Nd isotope systematics of mare basalt 10017. Geochim Cosmochim Acta 71:3656-3671, doi:10.1016/j.gca.2007.05.005

Gaffney AM, Gross J, Borg LE, Donaldson Hanna KL, Draper DS, Dygert N, Elkins-Tanton LT, Prissel KB, Prissel TC, Steenstra ES, Warren PH, Westrenen W (2021) Magmatic evolution 1. Rev Mineral Geochem XX:xxx-xxx

Gillis JJ, Jolliff BL, Korotev RL (2004) Lunar surface geochemistry: Global concentrations of Th, K, and FeO as derived from lunar prospector and Clementine data. Geochim Cosmochim Acta 68:3791-3805, doi:10.1016/j.gca.2004.03.024

Goldschmidt VM (1937) The principles of distribution of chemical elements in minerals and rocks. The seventh Hugo Muller Lecture, delivered before the Chemical Society on March 17th, 1937. J Chem Soc 655-673, doi:10.1039/jr9370000655

Gooding JL, Muenow DW (1976) Activated release of alkalis during vesiculation of molten basalts under high vacuum: Implications for lunar volcanism. Geochim Cosmochim Acta 40:675-686, doi:10.1016/0016-7037(76)90113-7

Goswami JN, Annadurai M (2009) Chandrayaan-1: India's first planetary science mission to the moon. Curr Sci 96:486-491

Green RO, Pieters C, Mouroulis P, Eastwood M, Boardman J, Glavich T, Isaacson P, Annadurai M, Besse S, Barr D, Buratti B, Cate D, Chatterjee A, Clark R, Cheek L, Combe J, Dhingra D, Essandoh V, Geier S, Goswami JN, Green R, Haemmerle V, Head J, Hovland L, Hyman S, Klima R, Koch T, Kramer G, Kumar ASK, Lee K, Lundeen S, Malaret E, McCord T, McLaughlin S, Mustard J, Nettles J, Petro N, Plourde K, Racho C, Rodriquez J, Runyon C, Sellar G, Smith C, Sobel H, Staid M, Sunshine J, Taylor L, Thaisen K, Tompkins S, Tseng H, Vane G, Varanasi P, White M, Wilson D (2011) The Moon Mineralogy Mapper (M^3) imaging spectrometer for lunar science: Instrument description, calibration, on-orbit measurements, science data calibration and on-orbit validation. J Geophys Res: Planets 116, doi:10.1029/2011je003797

Greenwood JP, Itoh S, Sakamoto N, Warren P, Taylor L, Yurimoto H (2011) Hydrogen isotope ratios in lunar rocks indicate delivery of cometary water to the Moon. Nat Geosci 4:79-82

Greenwood JP, Sakamoto N, Itoh S, Warren PH, Singer JA, Yanai K, Yurimoto H (2017) The lunar magma ocean volatile signature recorded in chlorine-rich glasses in KREEP basalts 15382 and 15386. Geochem J 51:105-114, doi:10.2343/geochemj.2.0453

Griffin WL, Heier KS, Amli R (1972) Whitlockite and apatite from lunar rock 14310 and from Odegarden, Norway. Earth Planet Sci Lett 15:53-58

Grove TL, Krawczynski MJ (2009) Lunar mare volcanism: Where did the magmas come from? Elements 5:29-34, doi:10.2113/gselements.5.1.29

Gussone N, Schmitt A-D, Heuser A, Wombacher F, Dietzel M, Tipper E, Schiller M (2016) Calcium stable isotope geochemistry Springer-Verlag Berlin Heidelberg, Germany

Hamada M, Ushioda M, Fujii T, Takahashi E (2013) Hydrogen concentration in plagioclase as a hygrometer of arc basaltic melts: Approaches from melt inclusion analyses and hydrous melting experiments. Earth Planet Sci Lett 365:253-262, doi:10.1016/j.epsl.2013.01.026

Harrison TM, Watson EB (1984) The behavior of apatite during crustal anatexis: Equilibrium and kinetic considerations. Geochim Cosmochim Acta 48:1467-1477

Hartmann WK, Davis DR (1975) Satellite-sized planetesimals and lunar origin. Icarus 24:504-515, doi:10.1016/0019-1035(75)90070-6

Hauri E, Wang JH, Dixon JE, King PL, Mandeville C, Newman S (2002) SIMS analysis of volatiles in silicate glasses 1. Calibration, matrix effects and comparisons with FTIR. Chem Geol 183:99-114

Hauri EH, Gaetani GA, Green TH (2006) Partitioning of water during melting of the Earth's upper mantle at H_2O-undersaturated conditions. Earth Planet Sci Lett 248:715-734, doi:10.1016/j.epsl.2006.06.014

Hauri EH, Weinreich T, Saal AE, Rutherford MC, Van Orman JA (2011) High pre-eruptive water contents preserved in lunar melt inclusions. Science 333:213-215, doi:10.1126/science.1204626

Hauri EH, Saal AE, Rutherford MJ, Van Orman JA (2015) Water in the Moon's interior: Truth and consequences. Earth Planet Sci Lett 409:252-264, doi:10.1016/j.epsl.2014.10.053

Head III JW, Wilson L, Hiesinger H, van der Bogert CH, Chen Y, Dickson JL, Gaddis LR, Haruyama J, Jozwiak L, Li C, Liu J, Morota T, Needham D, Ostrach LR, Pieters CM, Prissel TC, Qian Y, Iao L, Rutherford M, Scott DR, Whitten JL, Xiao L, Zhang F, Ziyuan O (2021) Lunar Volcanism: Volcanic Features and Processes. Rev Mineral Geochem XX:xxx-xxx

Heiken G, McKay DS (1977) A model for eruption behavior of a volcanic vent in eastern Mare Serenitatis. Proc. 8th Lun. Sci. Conf. 8:3243-3255

Heiken G, Vaniman D, French BM (1991) Lunar sourcebook: A user's guide to the Moon Cambridge University Press, Cambridge

Herd CDK (2008) Basalts as probes of planetary interior redox state. Rev Mineral Geochem 68:527-553, doi:10.2138/rmg.2008.68.19

Herzog GF, Moynier F, Albarede F, Berezhnoy AA (2009) Isotopic and elemental abundances of copper and zinc in lunar samples, Zagami, Pele's hairs, and a terrestrial basalt. Geochim Cosmochim Acta 73:5884-5904, doi:10.1016/j.gca.2009.05.067

Higashi Y, Itoh S, Hashiguchi M, Sakata S, Hirata T, Watanabe K, Sakaguchi I (2017) Hydrogen diffusion in the apatite-water system: Fluorapatite parallel to the *c*-axis. Geochem J 51:115-122, doi:10.2343/geochemj.2.0460

Hirschmann MM, Withers AC, Ardia P, Foley NT (2012) Solubility of molecular hydrogen in silicate melts and consequences for volatile evolution of terrestrial planets. Earth Planet Sci Lett 345:38-48, doi:10.1016/j.epsl.2012.06.031

Hofmann AW, White WM (1983) Ba, Rb and Cs in the Earth's mantle. Z Naturforsch, A: Phys. Sci. 38:256-266

Hofmann AW (1988) Chemical differentiation of the Earth: The relationship between mantle, continental crust, and oceanic crust. Earth Planet Sci Lett 90:297-314, doi:10.1016/0012-821x(88)90132-x

Hui H, Peslier AH, Zhang Y, Neal CR (2013) Water in lunar anorthosites and evidence for a wet early Moon. Nat Geosci 6:177-180

Hui HJ, Peslier AH, Rudnick RL, Simonetti A, Neal CR (2015) Plume-cratonic lithosphere interaction recorded by water and other trace elements in peridotite xenoliths from the Labait volcano, Tanzania. Geochem Geophys Geosyst 16:1687-1710, doi:10.1002/2015gc005779

Hui H, Guan Y, Chen Y, Peslier AH, Zhang Y, Liu Y, Flemming RL, Rossman GR, Eiler JM, Neal CR, Osinski GR (2017) A heterogeneous lunar interior for hydrogen isotopes as revealed by the lunar highlands samples. Earth Planet Sci Lett 473:14-23, doi:10.1016/j.epsl.2017.05.029

Humayun M, Clayton RN (1995a) Potassium isotope cosmochemistry: Genetic implications of volatile element depletion. Geochim Cosmochim Acta 59:2131-2148

Humayun M, Clayton RN (1995b) Precise determination of the isotopic composition of potassium: Application to terrestrial rocks and lunar soils. Geochim Cosmochim Acta 59:2115-2130, doi:10.1016/0016-7037(95)00131-x

Hurley DM, Siegler MA, Cahill JTS, Colaprete A, Costello E, Deutsch AN, Elphic RC, Fa W, Grava C, Hayne PO, Heldmann J, Hendrix AR, Jordan AP, Killen RM, Klima RL, Kramer G, Li S, Liu Y, Lucey PG, Mazarico E, Pendleton Y, Poston M, Prem P, Retherford KD, Schaible M (2021) Surface volatiles on the Moon. Rev Mineral Geochem XX:xxx-xxx

Javoy M, Pineau F, Delorme H (1986) Carbon and nitrogen isotopes in the mantle. Chem Geol 57:41-62, doi:10.1016/0009-2541(86)90093-8

Jenner FE, O'Neill HS (2012) Analysis of 60 elements in 616 ocean floor basaltic glasses. Geochem Geophys Geosyst 13, doi:10.1029/2011gc004009

Jochum KP, Hofmann AW, Ito E, Seufert HM, White WM (1983) K, U, and Th in mid-ocean ridge basalt glasses and heat-production, K/U, and K/Rb in the mantle. Nature 306:431-436, doi:10.1038/306431a0

Johnson EA (2006) Water in nominally anhydrous crustal minerals: Speciation, concentration, and geologic significance. Rev Mineral Geochem 62:117-154, doi:10.2138/rmg.2006.62.6

Johnson EA, Rossman GR (2013) The diffusion behavior of hydrogen in plagioclase feldspar at 800-1000 °C: Implications for re-equilibration of hydroxyl in volcanic phenocrysts. Am Mineral 98:1779-1787, doi:10.2138/am.2013.4521

Jolliff BL (2006) Preface. Rev Mineral Geochem 60:V-XV, doi:10.2138/rmg.2006.60.0

Jolliff BL, Wiseman SA, Lawrence SJ, Tran TN, Robinson MS, Sato H, Hawke BR, Scholten F, Oberst J, Hiesinger H, van der Bogert CH, Greenhagen BT, Glotch TD, Paige DA (2011) Non-mare silicic volcanism on the lunar farside at Compton-Belkovich. Nat Geosci 4:566-571, doi:10.1038/ngeo1212

Joy KH, Gross J, Korotev RL, Zeigler RA, McCubbin FM, Snape JF, Curran NM, Pernet-Fisher J, Arai T (2021) Lunar meteorites. Rev Mineral Geochem XX:xxx-xxx

Kato C, Moynier F (2017a) Gallium isotopic evidence for the fate of moderately volatile elements in planetary bodies and refractory inclusions. Earth Planet Sci Lett 479:330-339, doi:10.1016/j.epsl.2017.09.028

Kato C, Moynier F (2017b) Gallium isotopic evidence for extensive volatile loss from the Moon during its formation. Sci Adv 3, doi:10.1126/sciadv.1700571

Kato C, Moynier F, Valdes MC, Dhaliwal JK, Day JMD (2015) Extensive volatile loss during formation and differentiation of the Moon. Nat Commun 6, doi:10.1038/ncomms8617

Kato C, Moynier F, Foriel J, Teng FZ, Puchtel IS (2017) The gallium isotopic composition of the bulk silicate Earth. Chem Geol 448:164-172, doi:10.1016/j.chemgeo.2016.11.020

Kaufmann R, Long A, Bentley H, Davis S (1984) Natural chlorine isotope variations. Nature 309:338-340, doi:10.1038/309338a0

Kerridge JF (1985) Carbon, hydrogen, and nitrogen in carbonaceous chondrites: Abundances and isotopic compositions in bulk samples. Geochim Cosmochim Acta 49:1707-1714, doi:10.1016/0016-7037(85)90141-3

Klemme S, Gunther D, Hametner K, Prowatke S, Zack T (2006) The partitioning of trace elements between ilmenite, ulvöspinel, armalcolite, and silicate melts with implications for the early differentiation of the Moon. Chem Geol 234:251-263, doi:10.1016/j.chemgeo.2006.05.005

Klima R, Cahill J, Hagerty J, Lawrence D (2013) Remote detection of magmatic water in Bullialdus Crater on the Moon. Nat Geosci 6:737-741, doi:10.1038/ngeo1909

Klima RL, Petro NE (2017) Remotely distinguishing and mapping endogenic water on the Moon. Philos. Trans R Soc London, Ser A 375, doi:10.1098/rsta.2015.0391

Koga KT, Rose-Koga EF (2018) Fluorine in the Earth and the Solar System, where does it come from and can it be found? C R Chim 21:749-756, doi:https://doi.org/10.1016/j.crci.2018.02.002

Kohlstedt DL, Mackwell SJ (1998) Diffusion of hydrogen and intrinsic point defects in olivine. Z Phys Chem 207:147-162, doi:10.1524/zpch.1998.207.Part_1_2.147

Kramers JD, Tolstikhin IN (1997) Two terrestrial lead isotope paradoxes, forward transport modelling, core formation and the history of the continental crust. Chem Geol 139:75-110, doi:10.1016/s0009-2541(97)00027-2

Krawczynski MJ, Grove TL (2012) Experimental investigation of the influence of oxygen fugacity on the source depths for high titanium lunar ultramafic magmas. Geochim Cosmochim Acta 79:1-19, doi:10.1016/j.gca.2011.10.043

Kung CC, Clayton RN (1978) Nitrogen abundances and isotopic compositions in stony meteorites. Earth Planet Sci Lett 38:421-435, doi:10.1016/0012-821x(78)90117-6

Kushiro I, Nakamura Y, Haramura H, Akimoto SI (1970) Crystallization of some lunar mafic magmas and generation of rhyolitic liquid. Science 167:610-612, doi:10.1126/science.167.3918.610

Labidi J, Cartigny P, Moreira M (2013) Non-chondritic sulphur isotope composition of the terrestrial mantle. Nature 501:208-211, doi:10.1038/nature12490

Labidi J, Shahar A, Le Losq C, Hillgren VJ, Mysen BO, Farquhar J (2016) Experimentally determined sulfur isotope fractionation between metal and silicate and implications for planetary differentiation. Geochim Cosmochim Acta 175:181-194, doi:10.1016/j.gca.2015.12.001

Lawrence DJ, Puetter RC, Elphic RC, Feldman WC, Hagerty JJ, Prettyman TH, Spudis PD (2007) Global spatial deconvolution of Lunar Prospector Th abundances. Geophys Res Lett 34, doi:10.1029/2006gl028530

Le Roux V, Lee CTA, Turner SJ (2010) Zn/Fe systematics in mafic and ultramafic systems: Implications for detecting major element heterogeneities in the Earth's mantle. Geochim Cosmochim Acta 74:2779-2796, doi:10.1016/j.gca.2010.02.004

Le Voyer M, Asimow PD, Mosenfelder JL, Guan Y, Wallace PJ, Schiano P, Stolper EM, Eiler JM (2014) Zonation of H_2O and F concentrations around melt inclusions in olivines. J Petrol 55:685-707, doi:10.1093/petrology/egu003

Li S, Milliken RE (2016) An empirical thermal correction model for Moon Mineralogy Mapper data constrained by laboratory spectra and Diviner temperatures. J Geophys Res: Planets 121:2081-2107, doi:10.1002/2016je005035

Li S, Milliken RE (2017) Water on the surface of the Moon as seen by the Moon Mineralogy Mapper: Distribution, abundance, and origins. Sci Adv 3, doi:10.1126/sciadv.1701471

Li WQ, Beard BL, Li SL (2016) Precise measurement of stable potassium isotope ratios using a single focusing collision cell multi-collector ICP-MS. J Anal At Spectrom 31:1023-1029, doi:10.1039/c5ja00487j

Li Y, Dasgupta R, Tsuno K (2015) The effects of sulfur, silicon, water, and oxygen fugacity on carbon solubility and partitioning in Fe-rich alloy and silicate melt systems at 3 GPa and 1600 °C: Implications for core-mantle differentiation and degassing of magma oceans and reduced planetary mantles. Earth Planet Sci Lett 415:54-66, doi:10.1016/j.epsl.2015.01.017

Li Y, Dasgupta R, Tsuno K (2017) Carbon contents in reduced basalts at graphite saturation: Implications for the degassing of Mars, Mercury, and the Moon. J Geophys Res: Planets 122, doi:10.1002/2017JE005289

Lin YH, Hui HJ, Li Y, Xu Y, van Westrenan W (2019) A lunar hygrometer based on plagioclase-melt partitioning of water. Geochem Perspect Lett 10:14-19, doi: 10.7185/geochemlet.1908

Lindsley DH (1969) Melting relations of plagioclase at high pressures. *In*: Origin of Anorthosite and Related Rocks. Isachsen YA, (ed) State Education Department, Univ. of the State of New York, Albany, New York, p 39-46

Liu Y, Chen Y, Guan YB, Ma C, Rossman GR, Eiler JM, Zhang YX (2018) Impact-melt hygrometer for Mars: The case of shergottite Elephant Moraine (EETA) 79001. Earth Planet Sci Lett 490:206-215, doi:10.1016/j.epsl.2018.03.019

Lock SJ, Stewart ST, Petaev MI, Leinhardt Z, Mace MT, Jacobsen SB, Cuk M (2018) The origin of the Moon within a terrestrial synestia. J Geophys Res: Planets 123:910-951, doi:10.1002/2017je005333

Lodders K (2003) Solar system abundances and condensation temperatures of the elements. Astrophys J 591:1220-1247, doi:10.1086/375492

Magna T, Wiechert U, Halliday AN (2006) New constraints on the lithium isotope compositions of the Moon and terrestrial planets. Earth Planet Sci Lett 243:336-353, doi:10.1016/j.epsl.2006.01.005

Magna T, Simcikova M, Moynier F (2014) Lithium systematics in howardite-eucrite-diogenite meteorites: Implications for crust-mantle evolution of planetary embryos. Geochim Cosmochim Acta 125:131-145, doi:10.1016/j.gca.2013.10.015

Magna T, Day JMD, Mezger K, Fehr MA, Dohmen R, Aoudjehane HC, Agee CB (2015) Lithium isotope constraints on crust-mantle interactions and surface processes on Mars. Geochim Cosmochim Acta 162:46-65, doi:10.1016/j.gca.2015.04.029

Mahan B, Siebert J, Pringle EA, Moynier F (2017) Elemental partitioning and isotopic fractionation of Zn between metal and silicate and geochemical estimation of the S content of the Earth's core. Geochim Cosmochim Acta 196:252-270, doi:10.1016/j.gca.2016.09.013

Marechal C, Albarede F (2002) Ion-exchange fractionation of copper and zinc isotopes. Geochim Cosmochim Acta 66:1499-1509, doi:10.1016/s0016-7037(01)00815-8

Marechal CN, Telouk P, Albarede F (1999) Precise analysis of copper and zinc isotopic compositions by plasma-source mass spectrometry. Chem Geol 156:251-273, doi:10.1016/s0009-2541(98)00191-0

Marschall HR, Wanless VD, Shimizu N, von Strandmann P, Elliott T, Monteleone BD (2017) The boron and lithium isotopic composition of mid-ocean ridge basalts and the mantle. Geochim Cosmochim Acta 207:102-138, doi:10.1016/j.gca.2017.03.028

Marty B (2012) The origins and concentrations of water, carbon, nitrogen and noble gases on Earth. Earth Planet Sci Lett 313:56-66, doi:10.1016/j.epsl.2011.10.040

McCallum IS, Obrien HE (1996) Stratigraphy of the lunar highland crust: Depths of burial of lunar samples from cooling-rate studies. Am Mineral 81:1166-1175

McCord TB, Taylor LA, Combe JP, Kramer G, Pieters CM, Sunshine JM, Clark RN (2011) Sources and physical processes responsible for OH/H_2O in the lunar soil as revealed by the Moon Mineralogy Mapper (M^3). J Geophys Res: Planets 116, doi:10.1029/2010je003711

McCubbin FM, Jones RH (2015) Extraterrestrial apatite: Planetary geochemistry to astrobiology. Elements 11:183-188, doi:10.2113/gselements.11.3.183

McCubbin FM, Ustunisik G (2018) Experimental investigation of F and Cl partitioning between apatite and Fe-rich basaltic melt at 0 GPa and 950-1050 ºC: Evidence for steric controls on apatite-melt exchange equilibria in OH-poor apatite. Am Mineral 103:1455-1467

McCubbin FM, Barnes JJ (2019) Origin and abundances of H_2O in the terrestrial planets, Moon, and asteroids. Earth Planet Sci. Lett 526:115771

McCubbin FM, Barnes JJ (2020) The chlorine-isotopic compoisiton of lunar KREEP from magnesian-suite troctolite 76535. Am Mineral 105:1270-1274

McCubbin FM, Steele A, Hauri EH, Nekvasil H, Yamashita S, Hemley RJ (2010a) Nominally hydrous magmatism on the Moon. Proc Natl Acad Sci USA 27:11223-11228, doi:10.1073/pnas.1006677107

McCubbin FM, Steele A, Nekvasil H, Schnieders A, Rose T, Fries M, Carpenter PK, Jolliff BL (2010b) Detection of structurally bound hydroxyl in fluorapatite from Apollo mare basalt 15058,128 using TOF-SIMS. Am Mineral 95:1141-1150, doi:10.2138/am.2010.3448

McCubbin FM, Jolliff BL, Nekvasil H, Carpenter PK, Zeigler RA, Steele A, Elardo SM, Lindsley DH (2011) Fluorine and chlorine abundances in lunar apatite: Implications for heterogeneous distributions of magmatic volatiles in the lunar interior. Geochim Cosmochim Acta 75:5073-5093

McCubbin FM, Riner MA, Vander Kaaden KE, Burkemper LK (2012) Is Mercury a volatile-rich planet? Geophys Res Lett 39, doi:L0920210.1029/2012gl051711

McCubbin FM, Vander Kaaden KE, Tartèse R, Boyce JW, Mikhail S, Whitson ES, Bell AS, Anand M, Franchi IA, Wang JH, Hauri EH (2015a) Experimental investigation of F, Cl, and OH partitioning between apatite and Fe-rich basaltic melt at 1.0-1.2 GPa and 950-1000 ºC. Am Mineral 100:1790-1802, doi:10.2138/am-2015-5233

McCubbin FM, Vander Kaaden KE, Tartèse R, Klima RL, Liu Y, Mortimer J, Barnes JJ, Shearer CK, Treiman AH, Lawrence DJ, Elardo SM, Hurley DM, Boyce JW, Anand M (2015b) Magmatic volatiles (H, C, N, F, S, Cl) in the lunar mantle, crust, and regolith: Abundances, distributions, processes, and reservoirs. Am Mineral 100:1668-1707, doi:10.2138/am-2015-4934CCBYNCND

McCubbin FM, Boyce JW, Srinivasan P, Santos AR, Elardo SM, Filiberto J, Steele A, Shearer CK (2016) Heterogeneous distribution of H_2O in the martian interior: Implications for the abundance of H_2O in depleted and enriched mantle sources. Meteorit Planet Sci 51:2036-2060

McCubbin FM, Herd CDK, Yada T, Hutzler A, Allton JH, Calaway MJ, Corrigan CM, Fries MD, Harrington AD, McCoy TJ, Mitchell JL, Regberg AB, Righter K, Snead CJ, Tait KT, Zolensky M, Zeigler RA (2019) Advanced curation of astromaterials for planetary science. Space Sci Rev 215, doi:10.1007/s11214-019-0615-9

McDonough WF (2003) Compositional model for the Earth's core. *In*: Treatise on Geochemistry Volume 2: The Mantle and Core. Holland HD, Turekian KK, (eds). Elsevier, p 547-568

McDonough WF, Sun SS (1995) The composition of the Earth. Chem Geol 120:223-253, doi:10.1016/0009-2541(94)00140-4

McDonough WF, Sun SS, Ringwood AE, Jagoutz E, Hofmann AW (1992) Potassium, rubidium, and cesium in the Earth and Moon and the evolution of the mantle of the Earth. Geochim Cosmochim Acta 56:1001–1012

Merlivat L, Lelu M, Nief G, Roth E (1976) Spallation deuterium in rock 70215. Proc 7th Lun Sci Conf 7:649-658

Metrich N, Wallace PJ (2008) Volatile abundances in basaltic magmas and their degassing paths tracked by melt inclusions. Rev Mineral Geochem 69:363-402

Meyer C, McKay DS, Anderson DH, Butler P (1975) The source of sublimates on the Apollo 15 green and Apollo 17 orange glass samples. Proc 6th Lun Sci Conf 6:1673-1679

Milliken RE, Li S (2017) Remote detection of widespread indigenous water in lunar pyroclastic deposits. Nat Geosci 10:561-565, doi:10.1038/ngeo2993

Millot R, Guerrot C, Vigier N (2004) Accurate and high-precision measurement of lithium isotopes in two reference materials by MC-ICP-MS. Geostand Geoanal Res 28:153-159, doi:10.1111/j.1751-908X.2004.tb01052.x

Mills RD, Simon JI, Alexander CMOD, Wang J, Hauri EH (2017) Water in alkali feldspar: The effect of rhyolite generation on the lunar hydrogen budget. Geochem Perspect Lett 3:115-123, doi:http://dx.doi.org/10.7185/geochemlet.1712

Mohapatra RK, Harrison D, Ott U, Gilmour JD, Trieloff M (2009) Noble gas and nitrogen isotopic components in oceanic island basalts. Chem Geol 266:29-37, doi:10.1016/j.chemgeo.2009.03.022

Mortimer J, Verchovsky AB, Anand M, Gilmour I, Pillinger CT (2015) Simultaneous analysis of abundance and isotopic composition of nitrogen, carbon, and noble gases in lunar basalts: Insights into interior and surface processes on the Moon. Icarus 255:3-17, doi:10.1016/j.icarus.2014.10.006

Mortimer J, Verchovsky AB, Anand M (2016) Predominantly non-solar origin of nitrogen in lunar soils. Geochim Cosmochim Acta 193:36-53, doi:10.1016/j.gca.2016.08.006

Mosenfelder JL, Deligne NI, Asimow PD, Rossman GR (2006) Hydrogen incorporation in olivine from 2-12 GPa. Am Mineral 91:285-294, doi:10.2138/am.2006.1943

Mosenfelder JL, Rossman GR, Johnson EA (2015) Hydrous species in feldspars: A reassessment based on FTIR and SIMS. Am Mineral 100:1209-1221, doi:10.2138/am-2015-5034

Moynier F, Albarede F, Herzog GF (2006) Isotopic composition of zinc, copper, and iron in lunar samples. Geochim Cosmochim Acta 70:6103-6117, doi:10.1016/j.gca.2006.02.030

Moynier F, Paniello RC, Gounelle M, Albarede F, Beck P, Podosek F, Zanda B (2011) Nature of volatile depletion and genetic relationships in enstatite chondrites and aubrites inferred from Zn isotopes. Geochim Cosmochim Acta 75:297-307, doi:10.1016/j.gca.2010.09.022

Nekvasil H, Lindsley DH, DiFrancesco N, Catalano T, Coraor AE, Charlier B (2015) Uncommon behavior of plagioclase and the ancient lunar crust. Geophys Res Lett 42:10573-10579, doi:10.1002/2015gl066726

Nemchin AA, Whitehouse MJ, Grange ML, Muhling JR (2011) On the elusive isotopic composition of lunar Pb. Geochim Cosmochim Acta 75:2940-2964, doi:10.1016/j.gca.2011.02.042

Newcombe ME, Brett A, Beckett JR, Baker MB, Newman S, Guan Y, Eiler JM, Stolper EM (2017) Solubility of water in lunar basalt at low pH_2O. Geochim Cosmochim Acta 200:330-352, doi:10.1016/j.gca.2016.12.026

Ni P, Zhang Y, Guan Y (2017) Volatile loss during homogenization of lunar melt inclusions. Earth Planet Sci Lett 478:214-224, doi:10.1016/j.epsl.2017.09.010

Ni P, Zhang Y, Chen S, Gagnon J (2019) A melt inclusion study on volatile abundances in the lunar mantle. Geochim Cosmochim Acta 249:17-41

Nie NX, Dauphas N (2019) Vapor drainage in the protolunar disk as the cause for the depletion in volatile elements of the Moon. Astrophys J 884:L48, doi:10.3847/2041-8213/ab4a16

Nier AO (1950) A redetermination of the relative abundances of the isotopes of carbon, nitrogen, oxygen, argon, and potassium. Phys Rev 77:789-793, doi:10.1103/PhysRev.77.789

Nittler LR, Starr RD, Weider SZ, McCoy TJ, Boynton WV, Ebel DS, Ernst CM, Evans LG, Goldsten JO, Hamara DK, Lawrence DJ, McNutt RL, Schlemm CE, Solomon SC, Sprague AL (2011) The major-element composition of Mercury's surface from MESSENGER X-ray spectrometry. Science 333:1847-1850, doi:10.1126/science.1211567

Norris CA, Wood BJ (2017) Earth's volatile contents established by melting and vaporization. Nature 549:507-510, doi:10.1038/nature23645

O'Leary JA, Gaetani GA, Hauri EH (2010) The effect of tetrahedral Al^{3+} on the partitioning of water between clinopyroxene and silicate melt. Earth Planet Sci Lett 297:111-120, doi:10.1016/j.epsl.2010.06.011

O'Neill HS (1991) The origin of the Moon and the early history of the Earth: A chemical model. Part 1: The Moon. Geochim Cosmochim Acta 55:1135-1157

O'Neill HSC, Palme H (2008) Collisional erosion and the non-chondritic composition of the terrestrial planets. Philos Trans R Soc London, Ser A 366:4205-4238, doi:10.1098/rsta.2008.0111

Ono SH, Keller NS, Rouxel O, Alt JC (2012) ^{33}S constraints on the origin of secondary pyrite in altered oceanic basement Geochim Cosmochim Acta 87:323-340, doi:10.1016/j.gca.2012.04.016

Osinski GR, Melosh HJ, Andrews-Hanna JC, Baker D, Denevi B, Dhingra D, Ghent R, Hayne PO, Hill P, James PB, Jaret S, Johnson B, Kenkmann T, Kring D, Mahanti P, Minton D, Neish CD, Neumann GA, Plescia J, Potter RWK, Richardson J, Silber EA, Soderblom JM, Zanetti M, Zellner N (2021) Lunar impact features & processes. Rev Mineral Geochem XX:xxx-xxx

Palme H., Lodders K. and Jones A. (2014) Solar System abundances of the elements. *In* Planets, Asteriods, Comets and The Solar System (ed. A. M. Davis). 15-36.

Palot M, Cartigny P, Harris JW, Kaminsky FV, Stachel T (2012) Evidence for deep mantle convection and primordial heterogeneity from nitrogen and carbon stable isotopes in diamond. Earth Planet Sci Lett 357:179-193, doi:10.1016/j.epsl.2012.09.015

Paniello RC, Day JMD, Moynier F (2012) Zinc isotopic evidence for the origin of the Moon. Nature 490:376-379, doi:10.1038/nature11507

Pernet-Fisher JF, Howarth GH, Liu Y, Chen Y, Taylor LA (2014) Estimating the lunar mantle water budget from phosphates: Complications associated with silicate-liquid-immiscibility. Geochim Cosmochim Acta 144:326-341, doi:10.1016/j.gca.2014.09.004

Peslier AH (2010) A review of water contents of nominally anhydrous natural minerals in the mantles of Earth, Mars and the Moon. J Volcanol Geotherm Res 197:239-258, doi:10.1016/j.jvolgeores.2009.10.006

Peslier AH, Woodland AB, Bell DR, Lazarov M, Lapen TJ (2012) Metasomatic control of water contents in the Kaapvaal cratonic mantle. Geochim Cosmochim Acta 97:213-246, doi:10.1016/j.gca.2012.08.028

Peslier AH, Schonbachler M, Busemann H, Karato S-I (2017) Water in the Earth's interior: Distribution and origin. Space Sci Rev 212:743-810, doi:10.1007/s11214-017-0387-z

Pieters CM, Goswami JN, Clark RN, Annadurai M, Boardman J, Buratti B, Combe JP, Dyar MD, Green R, Head JW, Hibbitts C, Hicks M, Isaacson P, Klima R, Kramer G, Kumar S, Livo E, Lundeen S, Malaret E, McCord T, Mustard J, Nettles J, Petro N, Runyon C, Staid M, Sunshine J, Taylor LA, Tompkins S, Varanasi P (2009) Character and spatial distribution of OH/H_2O on the surface of the Moon seen by M^3 on Chandrayaan-1. Science 326:568-572, doi:10.1126/science.1178658

Plescia JB, Cahill JTS, Greenhagen B, Hayne PO, Mahanti P, Robinson MS, Spudis PD, Siegler MA, Stickle A, Williams JP, Zanetti M, Zellner NEB (2021) Lunar Surface Processes. Rev Mineral Geochem XX:xxx-xxx

Pogge von Strandmann PAE, Elliott T, Marschall HR, Coath C, Lai YJ, Jeffcoate AB, Ionov DA (2011) Variations of Li and Mg isotope ratios in bulk chondrites and mantle xenoliths. Geochim Cosmochim Acta 75:5247-5268, doi:10.1016/j.gca.2011.06.026

Poitrasson F, Halliday AN, Lee DC, Levasseur S, Teutsch N (2004) Iron isotope differences between Earth, Moon, Mars and Vesta as possible records of contrasted accretion mechanisms. Earth Planet Sci Lett 223:253-266, doi:10.1016/j.epsl.2004.04.032

Portnyagin M, Almeev R, Matveev S, Holtz F (2008) Experimental evidence for rapid water exchange between melt inclusions in olivine and host magma. Earth Planet Sci Lett 272:541-552, doi:10.1016/.j.epsl.2008.05.020

Potts NJ, Barnes JJ, Tartèse R, Franchi IA, Anand M (2018) Chlorine isotopic compositions of apatite in Apollo 14 rocks: Evidence for widespread vapor-phase metasomatism on the lunar nearside similar to 4 billion years ago. Geochim Cosmochim Acta 230:46-59, doi:10.1016/j.gca.2018.03.022

Premo WR, Tatsumoto M, Misawa K, Nakamura N, Kita NI (1999) Pb-isotopic systematics of lunar highland rocks (> 3.9 Ga): Constraints on early lunar evolution. *In*: Planetary Petrology and Geochemistry: The Lawrence A Taylor 60th Birthday volume Snyder GA, Neal CR, Ernst WG, (eds). Bellwether Publishing, Columbia, MD, p 207-240

Prettyman TH, Hagerty JJ, Elphic RC, Feldman WC, Lawrence DJ, McKinney GW, Vaniman DT (2006) Elemental composition of the lunar surface: Analysis of gamma ray spectroscopy data from Lunar Prospector. J Geophys Res: Planets 111, doi:10.1029/2005je002656

Pringle EA, Moynier F (2017) Rubidium isotopic composition of the Earth, meteorites, and the Moon: Evidence for the origin of volatile loss during planetary accretion. Earth Planet Sci Lett 473:62-70, doi:10.1016/j.epsl.2017.05.033

Rapp JF, Draper DS (2018) Fractional crystallization of the lunar magma ocean: Updating the dominant paradigm. Meteorit Planet Sci 53:1432-1455, doi:10.1111/maps.13086

Reedy RC (1981) Cosmic-ray-produced deuterium, ^{13}C, and ^{15}N in meteorites. Meteoritics 16:381-381
Richet P, Bottinga Y, Javoy M (1977) Review of hydrogen, carbon, nitrogen, oxygen, sulfur, and chlorine stable isotope fractionation among gaseous molecules. Annu Rev Earth Planet Sci 5:65-110, doi:10.1146/annurev.ea.05.050177.000433
Righter K, Go BM, Pando KA, Danielson L, Ross DK, Rahman Z, Keller LP (2017) Phase equilibria of a low S and C lunar core: Implications for an early lunar dynamo and physical state of the current core. Earth Planet Sci Lett 463:323-332, doi:10.1016/j.epsl.2017.02.003
Riker J, Humphreys MCS, Brooker RA, De Hoog JCM, EIMF (2018) First measurements of OH-C exchange and temperature-dependent partitioning of OH and halogens in the system apatite – silicate melt. Am Mineral 103:260-270, doi:10.2138/am-2018-6187CCBY
Ringwood AE, Kesson SE (1977) Basaltic magmatism and the bulk composition of the Moon. The Moon 16:425-464
Robinson KL, Taylor GJ (2014) Heterogeneous distribution of water in the Moon. Nat Geosci 7:401-408, doi:10.1038/ngeo2173
Robinson KL, Barnes JJ, Nagashima K, Thomen A, Franchi IA, Huss GR, Anand M, Taylor GJ (2016) Water in evolved lunar rocks: Evidence for multiple reservoirs. Geochim Cosmochim Acta 188:244-260, doi:10.1016/j.gca.2016.05.030
Roedder E (1979) Origin and significance of magmatic inclusions. Bull Mineral 102:487-510
Roeder PL, Emslie RF (1970) Olivine-liquid equilibrium. Contrib Mineral Petrol 29:275-289, doi:10.1007/bf00371276
Roedder E, Weiblen PW (1970) Silicate liquid immiscibility in lunar magmas, evidenced by melt inclusions in lunar rocks. Science 167:641-644, doi:10.1126/science.167.3918.641
Ross CS, Smith RL (1955) Water and other volatiles in volcanic glasses. Am Mineral 40:1071-1089
Saal AE, Hauri EH, Langmuir CH, Perfit MR (2002) Vapour undersaturation in primitive mid-ocean-ridge basalt and the volatile content of Earth's upper mantle. Nature 419:451-455, doi:10.1038/nature01073
Saal AE, Hauri EH, Lo Cascio M, Van Orman JA, Rutherford MC, Cooper RF (2008) Volatile content of lunar volcanic glasses and the presence of water in the Moon's interior. Nature 454:192-195, doi:10.1038/nature07047
Saal AE, Hauri EH, Van Orman JA, Rutherford MJ (2013) Hydrogen isotopes in lunar volcanic glasses and melt inclusions reveal a carbonaceous chondrite heritage. Science 340:1317-1320, doi:10.1126/science.1235142
Sakai H, Desmarais DJ, Ueda A, Moore JG (1984) Concentrations and isotope ratios of carbon, nitrogen, and sulfur in ocean-floor basalts. Geochim Cosmochim Acta 48:2433-2441, doi:10.1016/0016-7037(84)90295-3
Salters VJM, Stracke A (2004) Composition of the depleted mantle. Geochem Geophys Geosyst 5, doi:10.1029/2003gc000597
Sarafian AR, Nielsen SG, Marschall HR, McCubbin FM, Monteleone BD (2014) Early accretion of water in the inner solar system from a carbonaceous chondrite-like source. Science 346:623-626, doi:10.1126/science.1256717
Sarafian AR, Hauri EH, McCubbin FM, Lapen TJ, Berger EL, Nielsen SG, Marschall HR, Gaetani GA, Righter K, Sarafian E (2017) Early accretion of water and volatile elements

to the inner Solar System: Evidence from angrites. Philos Trans R Soc London, Ser A 375, doi:10.1098/rsta.2016.0209
Sato M (1979) The driving mechanism for lunar pyroclastic eruptions inferred from the oxygen fugacity behavior of Apollo 17 orange glass. Proc 10th Lun Planet Sci Conf 10:311-325
Savage PS, Moynier F, Chen H, Shofner G, Siebert J, Badro J, Puchtel IS (2015) Copper isotope evidence for large-scale sulphide fractionation during Earth's differentiation. Geochem Perspect Lett 1:53-64, doi:http://dx.doi.org/10.7185/geochemlet.1506
Saxena P, Elkins-Tanton L, Petro N, Mandell A (2017) A model of the primordial lunar atmosphere. Earth Planet Sci Lett 474:198-205, doi:10.1016/j.epsl.2017.06.031
Schauble EA (2004) Applying stable isotope fractionation theory to new systems. Rev Mineral Geochem 55:65-111
Schilling JG, Bergeron MB, Evans R (1980) Halogens in the mantle beneath the north-Atlantic. Philos Trans R Soc London, Ser A 297:147-178
Schlichting HE, Mukhopadhyay S (2018) Atmosphere impact losses. Space Sci Rev 214, doi:10.1007/s11214-018-0471-z
Seitz H-M, Brey GP, Weyer S, Durali S, Ott U, Muenker C, Mezger K (2006) Lithium isotope compositions of Martian and lunar reservoirs. Earth Planet Sci Lett 245:6-18, doi:10.1016/j.epsl.2006.03.007
Seitz HM, Brey GP, Zipfel J, Ott U, Weyer S, Durali S, Weinbruch S (2007) Lithium isotope composition of ordinary and carbonaceous chondrites, and differentiated planetary bodies: Bulk solar system and solar reservoirs. Earth Planet Sci Lett 260:582-596, doi:10.1016/j.epsl.2007.06.019
Seitz HM, Zipfel J, Brey GP, Ott U (2012) Lithium isotope compositions of chondrules, CAI and a dark inclusion from Allende and ordinary chondrites. Earth Planet Sci Lett 329:51-59, doi:10.1016/j.epsl.2012.02.015
Sharp ZD, Draper DS (2013) The chlorine abundance of Earth: Implications for a habitable planet. Earth Planet Sci Lett 369-370:71-77, doi:https://doi.org/10.1016/j.epsl.2013.03.005
Sharp ZD, Barnes JD, Brearley AJ, Chaussidon M, Fischer TP, Kamenetsky VS (2007) Chlorine isotope homogeneity of the mantle, crust and carbonaceous chondrites. Nature 446:1062-1065, doi:10.1038/nature05748
Sharp ZD, Shearer CK, McKeegan KD, Barnes JD, Wang YQ (2010) The chlorine isotope composition of the Moon and implications for an anhydrous mantle. Science 329:1050-1053, doi:10.1126/science.1192606
Sharp ZD, McCubbin FM, Shearer CK (2013a) A hydrogen-based oxidation mechanism relevant to planetary formation. Earth Planet Sci Lett 380:88-97, doi:10.1016/j.epsl.2013.08.015
Sharp ZD, Mercer JA, Jones RH, Brearley AJ, Selverstone J, Bekker A, Stachel T (2013b) The chlorine isotope composition of chondrites and Earth. Geochim Cosmochim Acta 107:189-204, doi:10.1016/j.gca.2013.01.003
Sharp Z, Williams J, Shearer C, Agee C, McKeegan K (2016) The chlorine isotope composition of martian meteorites 2. Implications for the early solar system and the formation of Mars. Meteorit Planet Sci 51:2111-2126, doi:10.1111/maps.12591
Shearer CK, Papike JJ, Spilde MN (2001) Trace-element partitioning between immiscible lunar melts: An example from naturally occurring lunar melt inclusions. Am Mineral 86:238-246
Shearer CK, Hess PC, Wieczorek MA, Pritchard ME, Parmentier EM, Borg LE, Longhi J, Elkins-Tanton LT, Neal CR, Antonenko I, Canup RM, Halliday AN, Grove TL, Hager BH, Lee

DC, Wiechert U (2006) Thermal and magmatic evolution of the Moon. Rev Mineral Geochem 60:365-518, doi:10.2138/rmg.2006.60.4

Shearer CK, Burger PV, Guan Y, Papike JJ, Sutton SR, Atudorei NV (2012) Origin of sulfide replacement textures in lunar breccias. Implications for vapor element transport in the lunar crust. Geochim Cosmochim Acta 83:138-158, doi:10.1016/j.gca.2011.11.031

Shearer CK, Sharp ZD, Burger PV, McCubbin FM, Provencio PP, Brearley AJ, Steele A (2014) Chlorine distribution and its isotopic composition in "rusty rock" 66095. Implications for volatile element enrichments of "rusty rock" and lunar soils, origin of "rusty" alteration, and volatile element behavior on the Moon. Geochim Cosmochim Acta 139:411-433, doi:10.1016/j.gca.2014.04.029

Shearer CK, Elardo SM, Petro NE, Borg LE, McCubbin FM (2015) Origin of the lunar highlands Mg-suite: An integrated petrology, geochemistry, chronology, and remote sensing perspective. Am Mineral 100:294-325, doi:10.2138/am-2015-4817

Shearer CK, Neal CR, Glotch TD, Prissel TC, Bell AS, Fernandes VA, Gaddis LR, Jolliff BL, Laneuville M, Magna T, Simon JI (2021) Magmatic evolution 2: A new view of post-differentiation magmatism. Rev Mineral Geochem XX:xxx-xxx

Shields WR, Garner EL, Murphy TJ (1964) Absolute isotopic abundance ratio and the atomic weight of a reference sample of copper. J Res Nat Bur Stand 68:589-592, doi:10.6028/jres.068A.056

Siebert J, Sossi PA, Blanchard I, Mahan B, Badro J, Moynier F (2018) Chondritic Mn/Na ratio and limited post-nebular volatile loss of the Earth. Earth Planet Sci Lett 485:130-139, doi:https://doi.org/10.1016/j.epsl.2017.12.042

Simon JI, Christoffersen R, Wang J, Mouser MD, Mills RD, Ross DK, Rahman Z, Alexander CMOD (2020) Volatiles in lunar felsite clasts: Impact-related delivery of hydrous material to an ancient dry lunar crust. Geochim Cosmochim Acta 276:299-326, doi:https://doi.org/10.1016/j.gca.2020.02.008

Singer JA, Greenwood JP, Itoh S, Sakamoto N, Yurimoto H (2017) Evidence for the solar wind in lunar magmas: A study of slowly cooled samples of the Apollo 12 olivine basalt suite. Geochem J 51:95-104, doi:10.2343/geochemj.2.0462

Snape JF, Nemchin AA, Bellucci JJ, Whitehouse MJ, Tartèse R, Barnes JJ, Anand M, Crawford IA, Joy KH (2016) Lunar basalt chronology, mantle differentiation and implications for determining the age of the Moon. Earth Planet Sci Lett 451:149-158, doi:10.1016/j.epsl.2016.07.026

Snyder GA, Neal CR, Taylor LA, Halliday AN (1995) Processes involved in the formation of magnesian-suite plutonic rocks from the highlands of the Earth's Moon. J Geophys Res: Planets 100:9365-9388

Sossi PA, Moynier F (2017) Chemical and isotopic kinship of iron in the Earth and Moon deduced from the lunar Mg-suite. Earth Planet Sci Lett 471:125-135, doi:10.1016/j.epsl.2017.04.029

Sossi PA, Klemme S, O'Neill HSC, Berndt J, Moynier F (2019) Evaporation of moderately volatile elements from silicate melts: Experiments and theory. Geochim Cosmochim Acta 260:204-231, doi:https://doi.org/10.1016/j.gca.2019.06.021

Stacey JS, Kramers JD (1975) Approximation of terrestrial lead isotope evolution by a 2-stage model. Earth Planet Sci Lett 26:207-221, doi:10.1016/0012-821x(75)90088-6

Steele A, McCubbin FM, Fries M, Glamoclija M, Kater L, Nekvasil H (2010) Graphite in an Apollo 17 impact melt breccia. Science 329:51-51, doi:10.1126/science.1190541

Steenstra ES, Lin YH, Dankers D, Rai N, Berndt J, Matveev S, van Westrenen W (2017) The lunar core can be a major reservoir for volatile elements S, Se, Te, and Sb. Sci Rep 7, doi:10.1038/s41598-017-15203-0

Stephant A, Anand M, Zhao X, Chan QHS, Bonifacie M, Franchi IA (2019) The chlorine isotopic composition of the Moon: Insights from melt inclusions. Earth Planet Sci Lett 523:115715, doi:https://doi.org/10.1016/j.epsl.2019.115715

Stolper E (1982) Water in silicate glasses: An infrared spectroscopic study. Contrib Mineral Petrol 81:1-17, doi:10.1007/bf00371154

Sunshine JM, Farnham TL, Feaga LM, Groussin O, Merlin F, Milliken RE, A'Hearn MF (2009) Temporal and spatial variability of lunar hydration as observed by the Deep Impact spacecraft. Science 326:565-568, doi:10.1126/science.1179788

Tartèse R, Anand M (2013) Late delivery of chondritic hydrogen into the lunar mantle; insights from mare basalts. Earth Planet Sci Lett 361:480-486, doi:http://dx.doi.org/10.1016/j.epsl.2012.11.015

Tartèse R, Anand M, Barnes JJ, Starkey NA, Franchi IA, Sano Y (2013) The abundance, distribution, and isotopic composition of Hydrogen in the Moon as revealed by basaltic lunar samples: implications for the volatile inventory of the Moon. Geochim Cosmochim Acta 122:58-74

Tartèse R, Anand M, Joy KH, Franchi IA (2014a) H and Cl isotope systematics of apatite in brecciated lunar meteorites Northwest Africa 4472, Northwest Africa 773, Sayh al Uhaymir 169, and Kalahari 009. Meteorit Planet Sci 49:2266-2289, doi:10.1111/maps.12398

Tartèse R, Anand M, McCubbin FM, Elardo SM, Shearer CK, Franchi IA (2014b) Apatites in lunar KREEP basalts: The missing link to understanding the H isotope systematics of the Moon. Geology 42:363-366, doi:10.1130/g35288.1

Tatsumoto M (1970) Age of the moon: An isotopic study of U-Th-Pb systematics of Apollo 11 lunar samples- II. Proc Apollo 11 Lun Sci Conf 1:1595-1612

Tatsumoto M, Premo WR, Unruh DM (1987) Origin of lead from green glass of Apollo 15426: A search for primitive lunar lead. J Geophys Res 92:E361-E371

Taylor GJ, Wieczorek MA (2014) Lunar bulk chemical composition: A post-gravity recovery and interior laboratory reassessment. Philos Trans R Soc London, Ser A 372, doi:10.1098/rsta.2013.0242

Taylor LA, Patchen A, Mayne RG, Taylor DH (2004) The most reduced rock from the Moon, Apollo 14 basalt 14053: Its unique features and their origin. Am Mineral 89:1617-1624

Taylor SR, Pieters CM, MacPherson GJ (2006a) Earth-Moon system, planetary science, and lessons learned. Rev Mineral Geochem 60:657-704

Taylor SR, Taylor GJ, Taylor LA (2006b) The Moon: A Taylor perspective. Geochim Cosmochim Acta 70:5904-5918, doi:10.1016/j.gca.2006.06.262

Teng F-Z (2017) Magnesium isotope geochemistry. Rev Mineral Geochem 82:219-287

Tenner TJ, Hirschmann MM, Withers AC, Hervig RL (2009) Hydrogen partitioning between nominally anhydrous upper mantle minerals and melt between 3 and 5 GPa and applications to hydrous peridotite partial melting. Chem Geol 262:42-56, doi:10.1016/j.chemgeo.2008.12.006

Tera F, Wasserburg GJ (1972) U-Th-Pb systematics in 3 Apollo 14 basalts and problem of initial Pb in lunar rocks. Earth Planet Sci Lett 14:281-304, doi:10.1016/0012-821x(72)90128-8

Thode HG, Rees CE (1976) Sulphur isotopes in grain size fractions of lunar soils. Proc 7th Lun Sci Conf 7:459-468

Tian Z, Jolliff BL, Korotev RL, Fegley B, Lodders K, Day JMD, Chen H, Wang K (2020) Potassium isotopic composition of the Moon. Geochim Cosmochim Acta 280:263-280, doi:https://doi.org/10.1016/j.gca.2020.04.021

Tomascak PB, Langmuir CH, le Roux PJ, Shirey SB (2008) Lithium isotopes in global mid-ocean ridge basalts. Geochim Cosmochim Acta 72:1626-1637, doi:https://doi.org/10.1016/j.gca.2007.12.021

Tomascak PB, Magna T, Dohmen R (2016) Advances in lithium isotope geochemistry. Springer International Publishing, Switzerland

Treiman AH, Boyce JW, Gross J, Guan YB, Eiler JM, Stolper EM (2014) Phosphate-halogen metasomatism of lunar granulite 79215: Impact-induced fractionation of volatiles and incompatible elements. Am Mineral 99:1860-1870, doi:10.2138/am-2014-4822

Treiman AH, Boyce JW, Greenwood JP, Eiler JM, Gross J, Guan YB, Ma C, Stolper EM (2016) D-poor hydrogen in lunar mare basalts assimilated from lunar regolith. Am Mineral 101:1596-1603, doi:10.2138/am-2016-5582

Urey HC (1947) The thermodynamic properties of isotopic substances. J Chem Soc 562-581, doi:10.1039/jr9470000562

Ustunisik G, Nekvasil H, Lindsley DH (2011) Differential degassing of H_2O, Cl, F, and S: Potential effects on lunar apatite Am Mineral 96:1650-1653

Ustunisik G, Nekvasil H, Lindsley DH, McCubbin FM (2015) Degassing pathways of Cl-, F-, H-, and S-bearing magmas near the lunar surface: Implications for the composition and Cl isotopic values of lunar apatite. Am Mineral 100:1717-1727, doi:10.2138/am-2015-4883

Vacher LG, Piani L, Rigaudier T, Thomassin D, Florin G, Piralla M, Marrocchi Y (2020) Hydrogen in chondrites: Influence of parent body alteration and atmospheric contamination on primordial components. Geochim Cosmochim Acta 281:53-66, doi:https://doi.org/10.1016/j.gca.2020.05.007

Vander Kaaden KE, McCubbin FM (2015) Exotic crust formation on Mercury: Consequences of a shallow, FeO-poor mantle. J Geophys Res: Planets 120:195-209, doi:10.1002/2014je004733

Vander Kaaden KE, Agee CB, McCubbin FM (2015) Density and compressibility of the molten lunar picritic glasses: Implications for the roles of Ti and Fe in the structures of silicate melts. Geochim Cosmochim Acta 149:1-20.

Vasavada AR, Bandfield JL, Greenhagen BT, Hayne PO, Siegler MA, Williams J-P, Paige DA (2012) Lunar equatorial surface temperatures and regolith properties from the Diviner lunar radiometer experiment. J Geophys Res: Planets 117, doi:10.1029/2011je003987

Vollstaedt H, Mezger K, Leya I (2020) The selenium isotope composition of lunar rocks: Implications for the formation of the Moon and its volatile loss. Earth Planet Sci Lett 542:116289, doi:https://doi.org/10.1016/j.epsl.2020.116289

Wadhwa M (2008) Redox conditions on small bodies, the Moon, and Mars. Rev Mineral Geochem 68:493-510, doi:10.2138/rmg.2008.68.17

Wallace PJ (2005) Volatiles in subduction zone magmas: concentrations and fluxes based on melt inclusion and volcanic gas data. J Volcanol Geotherm Res 140:217-240, doi:10.1016/j.jvolgeores.2004.07.023

Wang K, Jacobsen SB (2016a) Potassium isotopic evidence for a high-energy giant impact origin of the Moon. Nature 538:487-490, doi:10.1038/nature19341

Wang K, Jacobsen SB (2016b) An estimate of the bulk silicate Earth potassium isotopic composition based on MC-ICPMS measurements of basalts. Geochim Cosmochim Acta 178:223-232, doi:10.1016/j.gca.2015.12.039
Wang X, Fitoussi C, Bourdon B, Fegley B, Charnoz S (2019a) Tin isotopes indicative of liquid–vapour equilibration and separation in the Moon-forming disk. Nat Geosci 12:707-711, doi:10.1038/s41561-019-0433-4
Wang Y, Hsu W, Guan Y (2019b) An extremely heavy chlorine reservoir in the Moon: Insights from the apatite in lunar meteorites. Sci Rep 9:5727, doi:10.1038/s41598-019-42224-8
Wänke H, Baddenhausen H, Dreibus G, Jagoutz E, Kruse H, Palme H, Spettel B, Teschke F (1973) Multielement analyses of Apollo 15, 16, and 17 samples and the bulk composition of the Moon. Proc 4th Lun Sci Conf 4:1461-1481
Warren JM, Hauri EH (2014) Pyroxenes as tracers of mantle water variations. J Geophys Res: Solid Earth 119:1851-1881, doi:10.1002/2013jb010328
Warren PH, Wasson JT (1979) Origin of KREEP. Rev Geophys 17:73-88
Wasson JT, Boynton WV, Kallemeyn GW, Sundberg LL, Wai CM (1976) Volatile compounds released during lunar fire fountaining. Proc 7th Lun Sci Conf 7:1583-1596
Watson EB (1994) Diffusion in volatile-bearing magmas. Rev Mineral Geochem 30:371-411
Webster JD (2006) Melt inclusions in plutonic rocks. Mineralogical Association of Canada, Montreal
Webster JD, Piccoli PM (2015) Magmatic apatite: A powerful, yet deceptive, mineral. Elements 11:177-182, doi:10.2113/gselements.11.3.177
Weill DF, Drake MJ (1973) Europium anomaly in plagioclase feldspar: Experimental results and semiquantitative model. Science 180:1059-1060, doi:10.1126/science.180.4090.1059
Wetzel DT, Hauri EH, Saal AE, Rutherford MJ (2015) Carbon content and degassing history of the lunar volcanic glasses. Nat Geosc 8:755-758, doi:10.1038/ngeo2511
Weyer S, Anbar AD, Brey GP, Munker C, Mezger K, Woodland AB (2005) Iron isotope fractionation during planetary differentiation. Earth Planet Sci Lett 240:251-264, doi:10.1016/j.epsl.2005.09.023
Wimpenny J, Marks N, Knight K, Rolison JM, Borg L, Eppich G, Badro J, Ryerson FJ, Sanborn M, Huyskens MH, Yin Q-z (2019) Experimental determination of Zn isotope fractionation during evaporative loss at extreme temperatures. Geochim Cosmochim Acta 259:391-411, doi:https://doi.org/10.1016/j.gca.2019.06.016
Wing BA, Farquhar J (2015) Sulfur isotope homogeneity of lunar mare basalts. Geochim Cosmochim Acta 170:266-280, doi:10.1016/j.gca.2015.09.003
Wöhler C, Grumpe A, Berezhnoy AA, Shevchenko VV (2017) Time-of-day-dependent global distribution of lunar surficial water/hydroxyl. Sci Adv 3, doi:10.1126/sciadv.1701286
Wood JA, Dickey JS, Marvin UB, Powell BN (1970) Lunar anorthosites Science 167:602-604
Young ED (2000) Assessing the implications of K isotope cosmochemistry for evaporation in the preplanetary solar nebula. Earth Planet Sci Lett 183:321-333, doi:10.1016/s0012-821x(00)00276-4
Yu Y, Hewins RH, Alexander CMO, Wang J (2003) Experimental study of evaporation and isotopic mass fractionation of potassium in silicate melts. Geochim Cosmochim Acta 67:773-786, doi:10.1016/s0016-7037(02)01176-6
Zartman RE, Doe BR (1981) Plumbotectonics: The model. Tectonophysics 75:135-162, doi:10.1016/0040-1951(81)90213-4

Zeigler RA, Mosie AB, Corrigan C, Costello LJ, Kent JJ, Krysher CH, Watts LA, McCubbin FM (2019) The Apollo sample collection: 50 years of Solar System insight. Elements 15:286-287, doi:10.2138/gselements.15.4.286

Zhai MZ, Nakamura E, Shaw DM, Nakano T (1996) Boron isotope ratios in meteorites and lunar rocks. Geochim Cosmochim Acta 60:4877-4881, doi:10.1016/s0016-7037(96)00338-9

Zhang Y (2008) Geochemical kinetics. Princeton University Press, Princeton, NJ

Zhang Y, Ni H (2010) Diffusion of H, C, and O components in silicate melts. Rev Mineral Geochem 72:171-225

Zhang YX, Ni HW, Chen Y (2010) Diffusion data in silicate melts. Rev Mineral Geochem 72:311-408

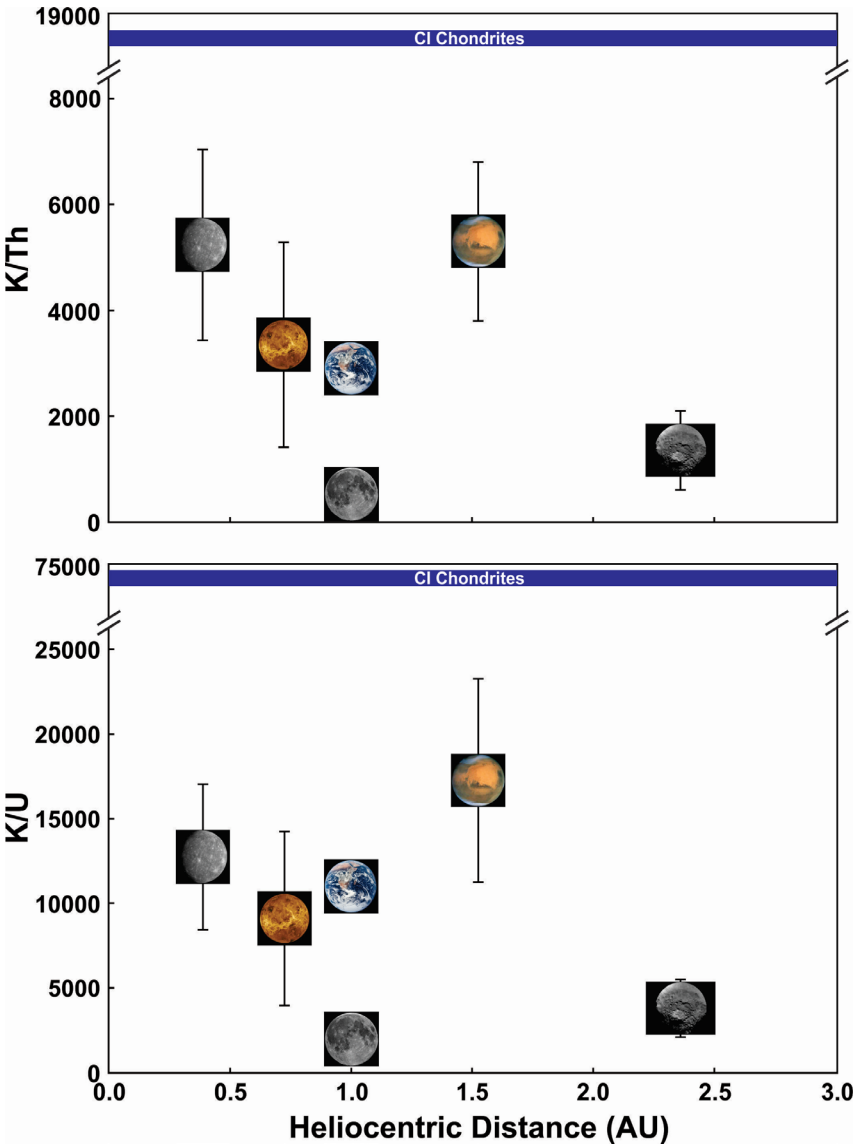

Figure 1. K/Th and K/U ratios of terrestrial bodies within the inner solar system plotted as a function of heliocentric distance. Data and error bars for K/Th and K/U from McCubbin et al. (2012) and references therein.

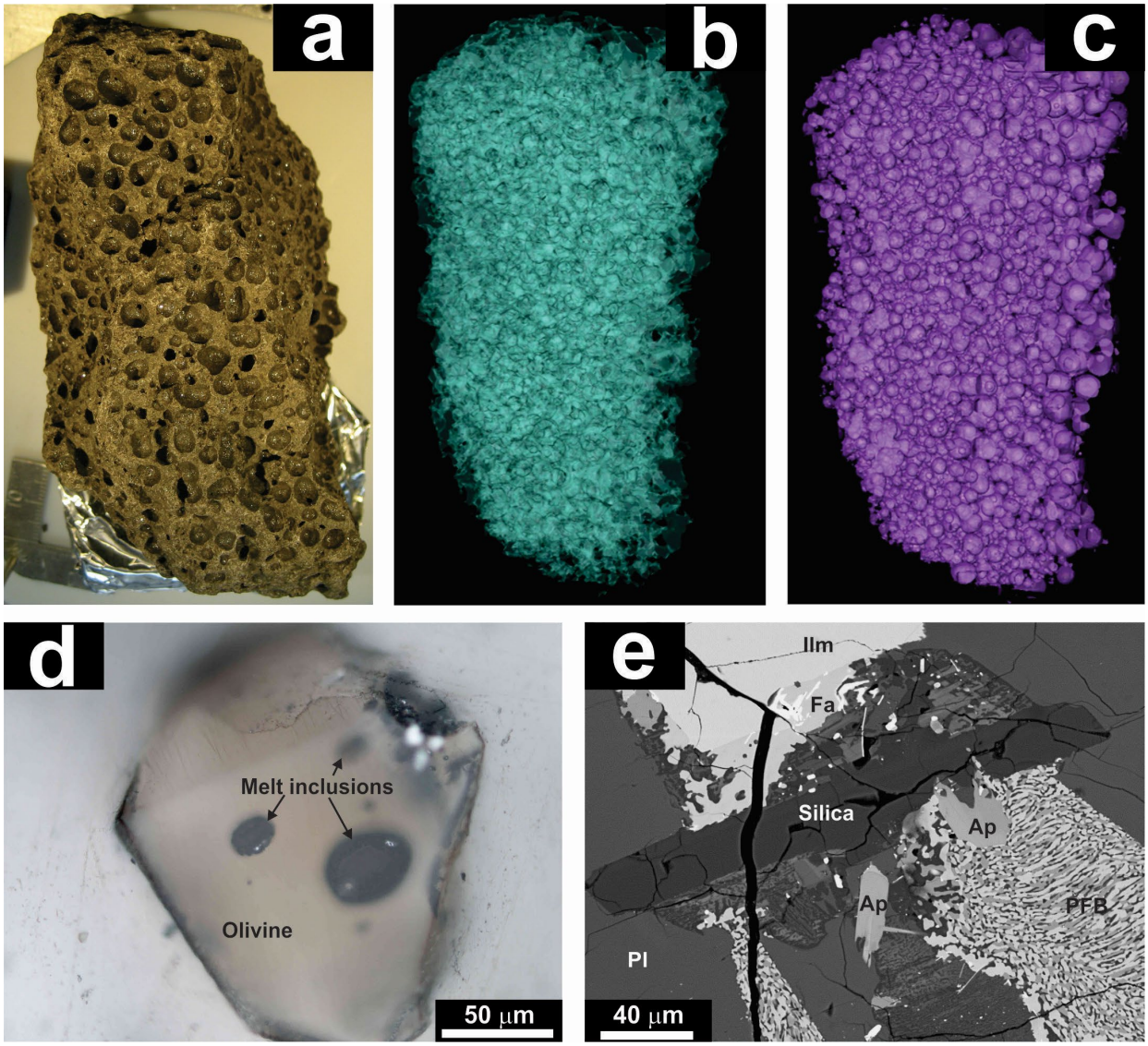

Figure 2. Evidence for volatiles in lunar samples. (a) Visible-light photomicrograph of olivine-hosted melt inclusions in 74220 after rehomogenization. (b) Back-scattered electron image of apatites within high-Ti mare basalt 10044,33. Phase abbreviations are as follows: Ap – apatite, Fa – fayalite, Ilm – ilmenite, PFB – pyroxferroite breakdown products, Pl – plagioclase. (c) Visible light image of Apollo sample 15556,215 (354 g; FOV = 10 cm long dimension), a vesicular lunar basalt sample from the Apollo 15 mission. (d-f) Three different images from an X-ray Computed Tomography (XCT) scan of vesicular lunar basalt sample 15556,215 (prepared by Scott Eckley). (d) An XCT isosurface view of the exterior of sample 15556,215. (e) An XCT image of both the isosurface view of the exterior (left side, in gold), as well as an isosurface view of void spaces within 15556,215 (right side, in white). (f) An XCT isosurface view of the void spaces within sample 15556,215.

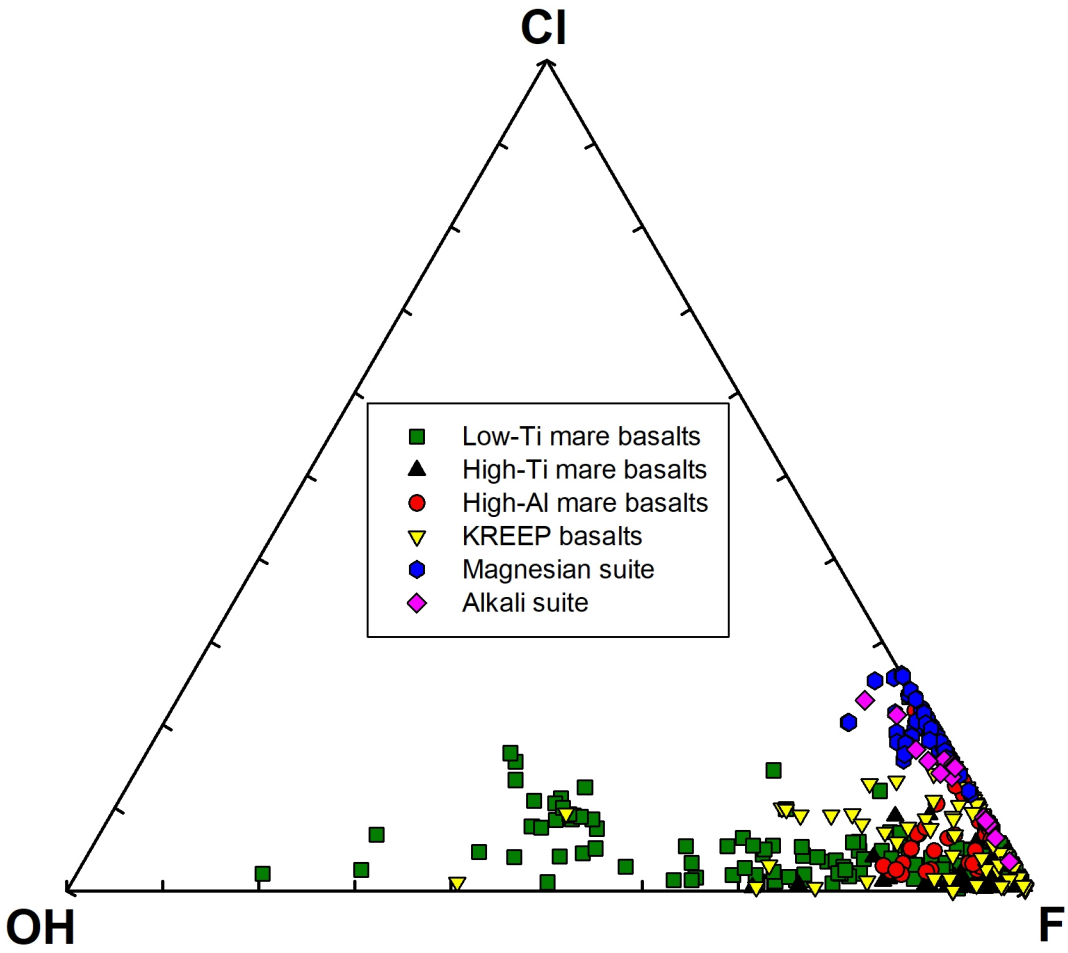

Figure 3. Ternary plots of apatite X-site occupancy (mol%) from mare basalts, KREEP basalts, magnesian-suite rocks, and alkali-suite rocks. Data yielding (F+Cl) > 1 atom are plotted along the OH-free join assuming 1 – Cl = F. Data used for plot are from Table S1. The ternary plot does not include X-site S abundances, although S occurs as sulfide in lunar apatite and ranges from 10's ppm to ~500 ppm S (e.g., Brounce et al. 2019).

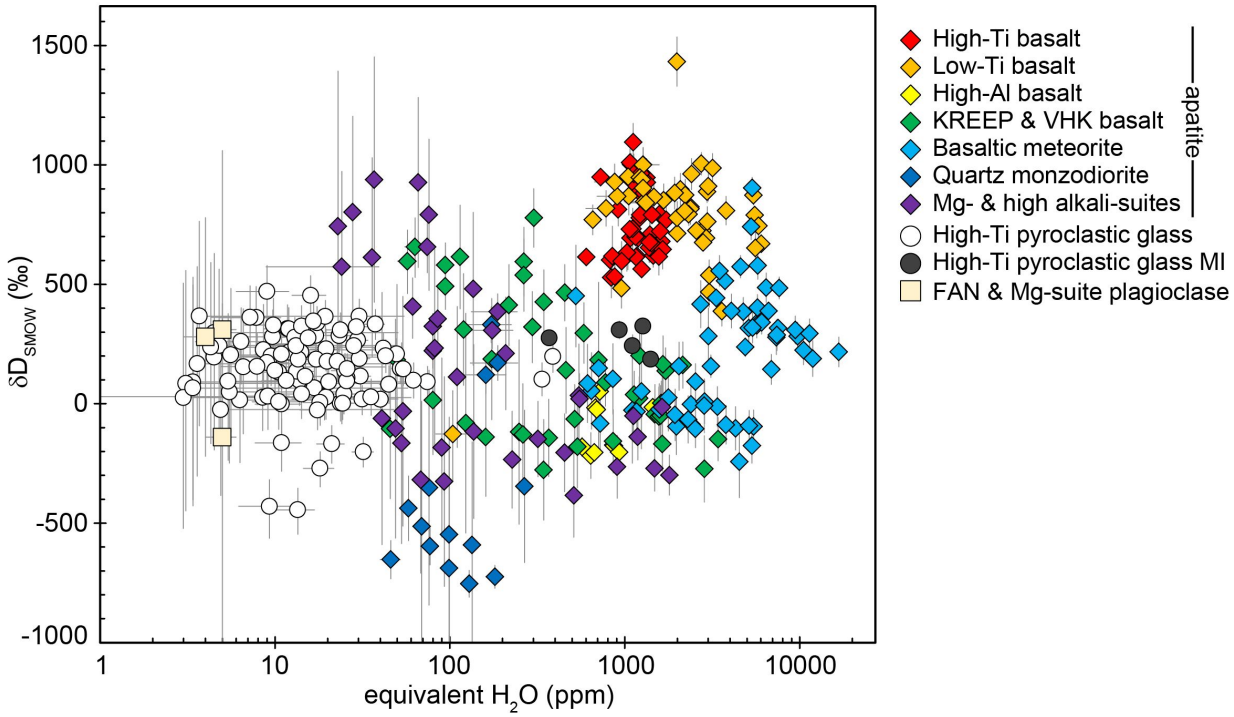

Figure 4. Hydrogen isotopic composition (permil) versus H_2O content (ppm) measured in lunar glasses (high-Ti), olivine-hosted melt inclusions, highlands plagioclase and apatite. All data sources are from the literature (Greenwood et al. 2011; Barnes et al. 2013; Saal et al. 2013; Tartèse et al. 2013; Barnes et al. 2014; Tartèse et al. 2014a; Tartèse et al. 2014b; Treiman et al. 2014; Boyce et al. 2015; Robinson et al. 2016; Treiman et al. 2016; Hui et al. 2017; Singer et al. 2017; Barnes et al. 2019; Wang et al. 2019b) and have been corrected for contributions from spallation reactions as explained in the main text. Errors are 2(σ).

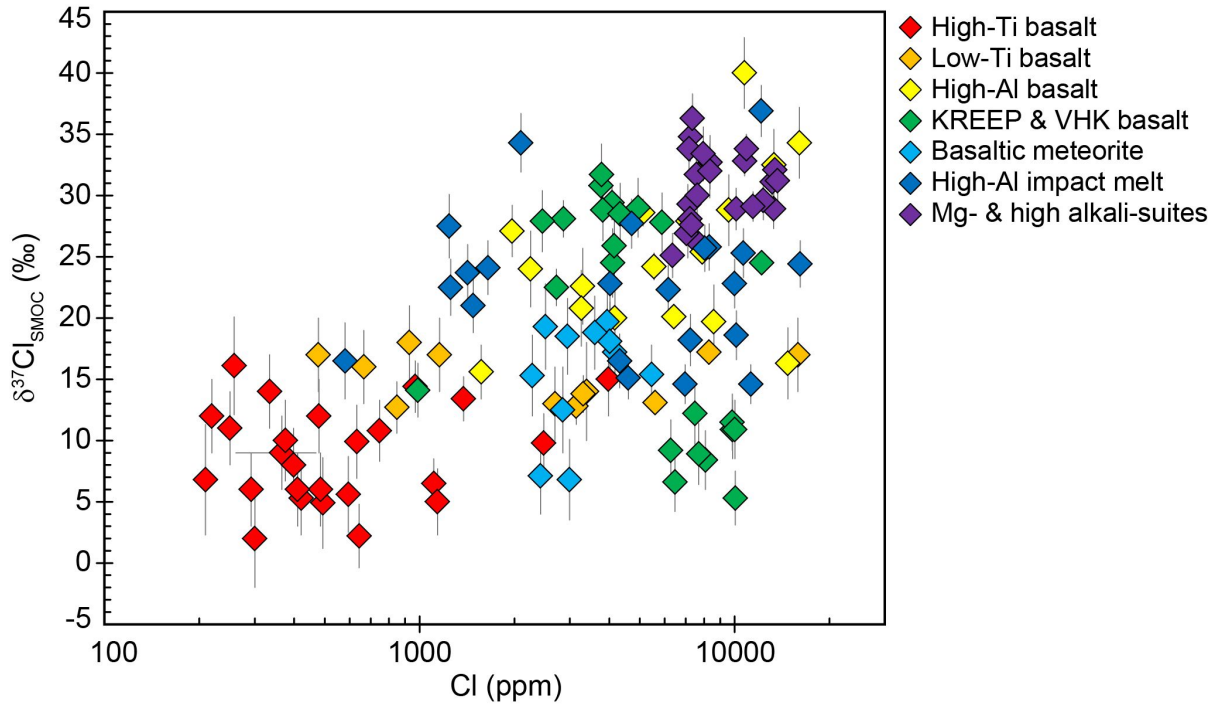

Figure 5. Cl isotopic composition versus Cl content (ppm) of apatite from lunar basalts, basaltic meteorites, impact melt, and highlands lithologies. All data sources are from the literature (Sharp et al. 2010; Tartèse et al. 2014a; Boyce et al. 2015; Barnes et al. 2016b; Potts et al. 2018; Barnes et al. 2019; Wang et al. 2019b). Errors are 2(σ).

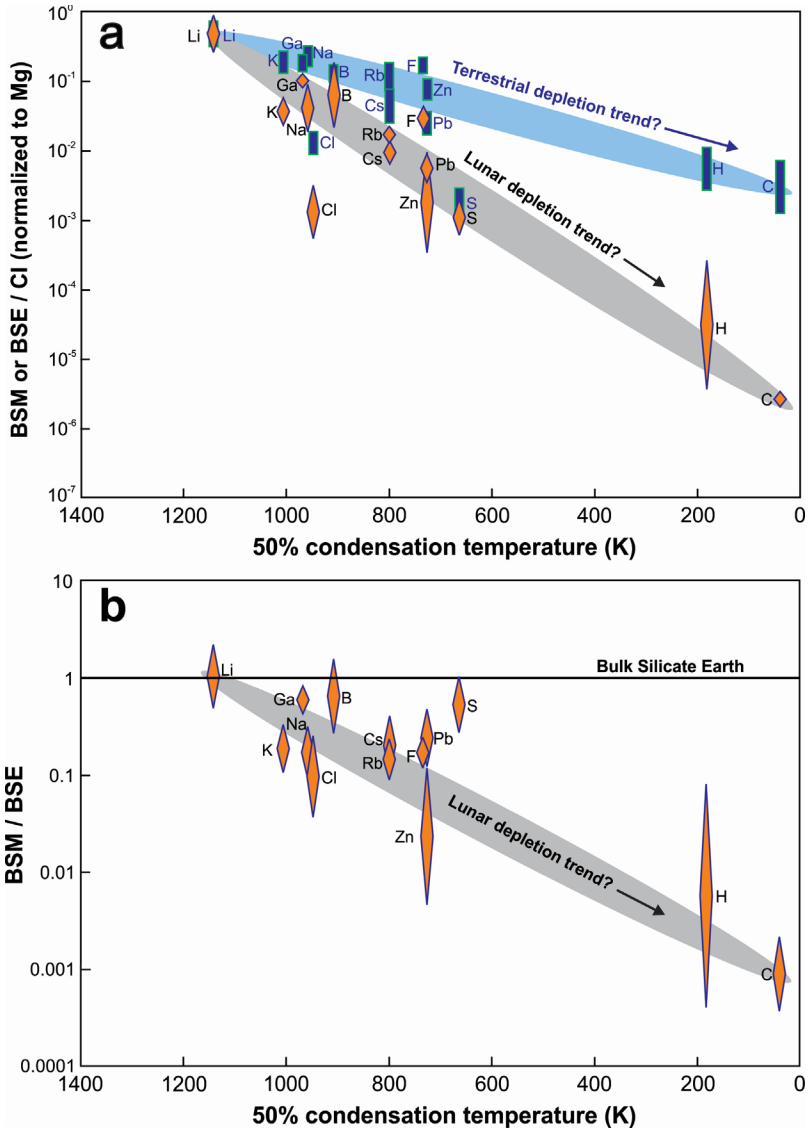

Figure 6. Abundances of select volatile elements in BSM, BSE, and CI chondrite as a function of 50% condensation temperature at 10^{-4} bars (Lodders 2003). Volatile depletion trends for the Earth (blue) and Moon (gray) are estimated with an envelope that has a slope defined by Li and C abundances (a) Abundances of select volatile elements in BSE (blue symbols) and BSM (orange symbols), normalized to Mg and CI chondrite (after McDonough and Sun 1995) using data from Table 2. (b) Abundances of select volatile elements in BSM normalized to BSE.

Figure 7: (top) A view of four large Apollo samples on display in the Pristine Apollo Sample Processing Laboratory at Johnson Space Center (left to right samples are 60015,1; 15016,0; 61016,7; and 15459,0). All pristine lunar samples are processed in stainless steel glove boxes using only stainless steel, aluminum, or Teflon tools in an ultra-pure dry N_2 gas environment. (bottom) A view of Apollo sample processors Andrea Mosie (right) and Charis Krysher (left) working in the Pristine Apollo Sample Processing Laboratory at NASA Johnson Space Center.

Table 1: Isotopic ratios discussed in the main text and information on the standards to which unknowns are commonly referenced

Isotopic ratio	Standard	Reference
$^{2}H/^{1}H$; δD	Vienna Standard Mean Ocean Water	De Wit et al., 1980
$^{7}Li/^{6}Li$; $\delta^{7}Li$	NIST SRM 8545 L-SVEC; IRMM-016	Flesch et al., 1973; Millot et al., 2004
$^{15}N/^{14}N$; $\delta^{15}N$	Atmospheric N_2	Nier, 1950
$^{33,34,36}S/^{32}S$; $\delta^{33,34,36}S$	Vienna-Canyon Diablo Troilite	Beaudoin et al., 1994
$^{37}Cl/^{35}Cl$; $\delta^{37}Cl$	Standard Mean Ocean Chloride	Kaufmann et al., 1984
$^{41}K/^{39}K$; $\delta^{41}K$	Bulk Silicate Earth through analyses of Merck KGaA Suprapur 99.995% purity KNO_3	Wang and Jacobsen., 2016
$^{65}Cu/^{63}Cu$; $\delta^{65}Cu$	NIST 976	Maréchal and Albarède, 2002; Shields et al., 1964
$^{66,67,68}Zn/^{64}Zn$; $\delta^{66,67,68}Zn$	JMC 3-0749L (Lyon standard)	Maréchal et al., 1999
$^{71}Ga/^{69}Ga$; $\delta^{71}Ga$	IPGP standard	Kato et al., 2017
$^{87}Rb/^{85}Rb$; $\delta^{87}Rb$	NIST SRM984 RbCl or BCR-2	Pringle and Moynier, 2017

Table 2. Abundances of select volatile elements in BSM, BSE, and CI chondrite. All values reported in μg/g.

Element	50% Condensation temperature at 10^{-4} bar (K)[a]	BSM_{Lo}	BSM_{Hi}	BSE_{Lo}	BSE_{Hi}	CI[b,g,h]
Li	1142	1.1	2.2	1.1[b]	2.1[b]	1.46
K	1006	33	58	192[b]	288[b]	530
Ga	968	2.0	2.6	3.6[b]	4.4[b]	9.51
Na	958	320	630	2270[b]	3071[b]	5010
Cl	948	1.0	4.1	17[b]	26[f]	698
B	908	0.06	0.26	0.17[c]	0.21[c]	0.713
Rb	800	0.075	0.086	0.42[b]	0.78[b]	2.13
Cs	799	0.0033	0.0045	0.0126[b]	0.0294[b]	0.185
F	734	3.1	4.9	23[d]	25[b]	60.6
Pb	727	0.025	0.05	0.12[b]	0.18[b]	2.56
Zn	726	0.28	5.5	47[b]	63[b]	310
S	664	88	202	200[b]	300[b]	54100
H[i]	182	1.2	74	1000[e]	3000[e]	138400
C	40	0.19	0.24	120[b]	500[e]	35180

[a]Values are from Lodders (2003)
[b]Values are from McDonough and Sun (1995)
[c]Values are from Marschall et al. (2017)
[d]Value is from Koga and Rose-Koga (2018)
[e]Values are from Marty (2012)
[f]Value is from Sharp and Draper (2013)
[g]Value for H_2O from Alexander et al. (2012)
[h]Value for Cl from Palme et al. (2014)
[i]All values reported pertain to H_2O